Modelling the drying kinetics of fresh-water and salt-water macroalgae

Craig Walker

in December, 2020

For the degree of Doctor of Philosophy

in the College of Science and Engineering

James Cook University

Townsville

Advisors: Dr Madoc Sheehan, Dr Andrew Cole

DECLARATION

I declare that this thesis is my own work and has not been submitted to elsewhere in whole or in part to obtain other degree award. The content of this thesis is the result of author work and the contribution of others has been acknowledged in the statement of contribution of others.

_____

Craig Walker

December, 2020

STATEMENT ON THE CONTRIBUTION OF OTHERS

This research was conducted under the supervision of Dr. Madoc Sheehan and he therefore has made academic guidance and editorial contributions to the thesis. The co-supervisor was Dr. Andrew Cole, who provided raw algae material access as a part of the Marine Aquaculture and Research Facility at James Cook University.

Financial support was provided from the School of Engineering and Physical Sciences for the components and build of the experimental equipment outlined in Chapter 4.

STATEMENT OF ACCESS TO THIS THESIS

I, the under-signed, the author of this research work, understand that James Cook University will make this thesis available for use within the University Library and via the Australian Digital Thesis Network, for use elsewhere.

I understand that an unpublished work, a thesis has significant protection under the Copyright Act. I do not wish to place any restriction on access to this thesis, but any use of its content must be acknowledged.

_____

Craig Walker

November, 2020

Acknowledgements

I would like to thank my supervisor Madoc Sheehan, for his support and inputs throughout the course of this thesis, and Andrew Cole and the other members of James Cook University's Marine Aquaculture and Research Facility for providing fresh algae material whenever it was sought and without forewarning or planning required. Finally, I would like to thank my family and friends for their support during my time at university.

Table of Contents

List of Figures

List of Tables

List of Symbols

A – surface area, m^2

A_t – surface area at time t

A_0 – surface area at $t = 0$

a – model fit variable

b – model fit variable

b_0 – model fit variable

C – concentration at time t

C_A – concentration of component A

C_p – heat capacity, $\frac{J}{kg.K}$

C_0 – initial concentration

C_∞ – concentration at $t = \infty$

c – model fit variable

c_0 – model fit variable

D – diffusivity, $\frac{m^2}{s}$

D_{AB} – diffusivity of component A through component B

D_e – effective diffusivity, $\frac{m^2}{s}$

D_0 – diffusion constant

$\frac{dm}{dt}$ – drying rate, $\frac{kg}{s}$

E_A – Activation energy, $\frac{J}{mol}$

F_c – correction factor

g – model fit variable

h – model fit variable

h_c – convective heat transfer coefficient

h_m – mass transfer coefficient

h_1 – model fit variable

h_2 – model fit variable

J_A – flux of component A through component B

k – thermal conductivity, $\frac{W}{m.K}$

k_0 – model fit variable

k_1 – model fit variable

k_2 – model fit variable

L – material slab width, m

L_D – dimensionless volume loss ratio

L_t – slab width at time t, m

L_0 – intial slab width, m

L_Δ – difference between initial and final slab width during drying

L_∞ – slab width at $t = \infty$, m

l – characteristic diffusion length, m

M – moisture content at time t, %d.b.

M_e – moisture content at $t = \infty$, %d.b.

$M_{e,exp}$ – moisture content at $t = \infty$ from experimental results, %d.b.

$M_{e,m}$ – moisture content at $t = \infty$ from model, %d.b.

M_0 – initial moisture content, %d.b.

m_D – dry mass of sample, g

m_t – sample mass at time t, g

MR – dimensionless moisture content at time t

MR_{exp} – dimensionless moisture content at time t from experimental data

MR_m – dimensionless moisture content at time t from model

n – model fit variable

Nu – Nusselt number

$p_{v,b}$ – vapour density in material bulk, $\frac{kg}{m^3}$

$p_{v,s}$ – vapour density at material surface, $\frac{kg}{m^3}$

$p_{v,sat}$ – saturation vapour density, $\frac{kg}{m^3}$

Q – heat, J

R – ideal gas constant, $\frac{J}{mol.K}$

Re – Reynolds number

RH – relative humidity, %

r – radius, m

Sc – Schmidt number

Sh – Sherwood number

T – temperature, K

T_g – temperature of drying gas, K

T_s – material surface temperature, K

T_t – material temperature at time t, K

T_0 – initial material temperature, K

t – time, seconds

t_h – material heating time, seconds

TR – temperature ratio

V_t – material volume at time t

V_0 – material volume at $t = 0$

v_g – drying gas velocity, $\frac{m}{s}$

x – position in material slab along 1-D diffusion direction

α – heat diffusivity, $\frac{m^2}{s}$

ΔE_v – activation energy of evaporation

ψ – fractionality coefficient

ρ – material bulk density, $\frac{kg}{m^3}$

Abstract

In this industry focused research, the drying kinetics of two commercially important macroalgae (*Ulva ohnoi* and *Oedogonium intermedium*) are determined experimentally for a range of temperatures, air flow rates and initial bulk densities representing typical conditions for industrial drying of biomaterials. The macroalgae species are compressible particulate materials and it has been noted that little research to date has covered the effect of material compression (i.e. bulk density) on drying. While the influence of temperature is well understood in literature, the response to other variables (air flow and density) is less understood and both influences are comprehensively addressed in this work.

The context and research aims of the work are stated in Chapter 1. The major aim is to develop an accurate and pragmatic model of drying rates, and demonstrate its ability to represent drying at larger scales. A review of the theory behind drying of biomaterials and the various approaches used to model drying is covered in Chapter 2. This includes a discussion on the best pragmatic approaches to representing drying for engineering design purposes, and reviews of drying kinetics studies that include the effects of drying gas temperature, drying gas flow rates and material bulk density. An analytical solution of Fick's Second Law (F2L) representing drying of an infinite slab is affirmed as the most suitable modelling approach for biomaterial drying in an equipment design context.

Chapter 3 presents experimental results determining the equilibrium moisture isotherms and thin layer drying kinetics as a function of temperature for both macroalgae. Equilibrium moisture contents for both species were determined between 35-55°C and 10-52% relative humidity, and were best represented using the Guggenheim-Anderson-deBoer model. Drying rates for radiative and convective heating methods were determined over 40-60°C, and the rates for each method and species are compared. Experimental results show that drying is always in a falling rate period for both heating methods, validating the model chosen for later test work. Convection drying was faster for both species and at all temperatures despite the single falling rate period. The results were used to determine the activation energy of drying for both species, and these values are used in further experimentation in Chapters 5 and 6. Experimental data in this Chapter was used to investigate numerical considerations associated with the application of the Fick's law drying model. High relative variance in the equilibrium moisture was found to have little effect on diffusivity estimation, and the effect of the number of terms used to represent the model infinite series is presented.

Chapter 4 describes the novel experimental apparatus and methodology which is used in Chapter 5 and 6 to determine algae drying kinetics as a function of air velocity and initial bulk density, with the

inclusion of image analysis to determine volume changes during drying. The setup was designed to measure both sample mass and volume loss in situ, removing errors typically associated with examples from the literature. Statistical experimental designs for the experimental work examining the effect of dryer operational variables (air velocity and material bulk density) on the effective diffusivity are outlined.

Chapter 5 presents experimental results obtained using the apparatus designed in Chapter 4, performed with the aim of determining any relationship between drying rates, drying gas velocity (between 0.4 and 2m/s) and material bulk density (between 33 and 100kg/m^3). Statistical analysis was used to prove that drying was in a single falling rate period during all conditions and therefore meets the assumptions of the Fick's law drying model. The results show diffusivity had a linear increase with increased gas velocity, and matches well with Chapter 3 radiative heating experiments as a zero air velocity point. Diffusivity had a linear decrease with increases in bulk density. Statistical analysis found there was no significant interaction between the two variables over the range of conditions tested. The effects of drying gas flow rate and material bulk density on diffusivity are provided as a correlation for both species. The likely theory and mechanisms by which these variables are affecting drying rates, and the effects on biomaterial slab geometry are discussed.

Chapter 6 analyses the differences between model assumptions and real phenomena that occurs during drying and develops model adjustments to include these effects, providing a better understanding of biomaterial drying. Volume losses measured in situ were found to be directly related to moisture losses and were most conveniently expressed as a non-dimensional value. This correlation between moisture and the extent of shrinkage was used to develop a model for slab width at any point from a known initial and final slab width. This relation was added to the Fick's law drying model, which was found to improve model fit at the initial and late stages of drying. An analytical solution for the average slab temperature was developed from the one-dimensional heat diffusion equation. Estimates of heating times from this solution align with the best fit heating time from a separate empirical approach. The inclusion of this heating period in the F2L model accounted well for initial deviations between experimental moisture content data and model predictions. The effects of this heating period was found to be especially relevant as drying scales increase. The final models developed in this thesis were tested using data collected from a pilot scale flighted rotary dryer. Drying rates were predicted from the equipment temperature, gas flow rate and material bulk density conditions using the relations developed at experimental scale. The predicted drying rates were found to well represent drying at pilot scale, with best fit occurring when exhaust gas temperatures were

used as an estimation of material temperature. The accurate fit to pilot scale drying indicates that the models developed are valid for industry use in prediction of drying times for the design of drying equipment. Finally, Chapter 7 outlines the conclusions and recommendations resulting from the research.

Chapter 1

1. Introduction

There is a growing focus on research into potential methods to reduce the use of non-renewable materials as a processing feedstock. Non-renewable materials are those such as coal and crude oil, where the natural processes that form them are too slow to replenish stocks compared to their current rate of consumption. The current use of many of these materials also contributes to climate change through the release of greenhouse gases such as carbon dioxide. The reduction of greenhouse gas emissions is the major component of governmental regulations aimed at minimizing the effects of climate change for future generations. As an example, the Paris Agreements (Paris Agreements 2015) are an international pact signed in 2016 by United Nations members aiming to limit the effects of global temperature increases to a maximum of 2°C above pre-industrial levels. These aims are reflected in national government regulations. For example, to achieve such aims the European Union in 2009 adopted a minimum target of a 10% share of biofuels used as transport fuel by 2020, and aims to more generally reduce their greenhouse gas emissions by 35% through the increased uptake of biofuel (Sorda *et al*., 2010). The United States of America adopted a Renewable Fuel Standard in 2005 (US Department of Energy 2005), which mandates an increasing amount of biofuels used per year with an aim of 36 billion gallons in 2022. Japan's energy policies also have a focus on renewable sources, particularly in waste woody biomass used in electricity co-generation with the aim of at least 4% of their national power supply from biomass by 2030 (Goh et al., 2019). Australia has adopted and met renewable energy targets of 33TW.hr by 2020, (Sorda et al., 2010) including the use of biomass as fuel by the sugar cane industry. Other nonfuel policies include the restrictions on single use plastics such as plastic bags. This has been implemented by Australia in several states (e.g. South Australia is in the process of legislating the banning of single use plastics like straws and stirrer rods by 2021 (Green Industries SA 2020)). Policies like these help drive renewable materials research in areas such as replacement biodegradable products. Biomaterials can be used as a part of circular economy designs that aim to create products from existing waste streams in other industries (e.g. biosolids conversion to biochar (Roberts et al., 2017)).

A potential method for reducing greenhouse gas emissions is by replacing non-renewable feedstock with renewable sources (Elshout et al., 2015). An example of renewable feedstock are biomaterials such as corn or sugar. These have a comparably short growth time to non-renewable materials, and reduce their overall emissions through consumption of carbon dioxide during photosynthetic growth

when compared to non-renewable materials for the same product or use. Biomaterials have the potential of being a renewable feedstock for a range of products, including but not limited to biofuels, health and nutrition supplements, CO_2 mitigation efforts, waste water treatment, fertilizers, high-value compounds, pigments and other biochemicals (Suganya et al., 2016). Biomaterials that have been studied for their use as a renewable feedstock can be broadly described in one of three groups.

The first generation of biomaterials include those traditionally grown as food, such as corn and sugar. An example of products manufactured form these biomaterials include several types of fuels (e.g. methanol, ethanol, biodiesel, methane) and other value added chemicals (Naik et al., 2010). The use of material that can be converted to food raises several issues. The conflict between product options can potentially lead to increased food prices and food security issues. The use of land specifically for growing these biomaterials as an energy feedstock would then use limited arable land and potable water resources.

Second generation biomaterials cover biomaterial sources not consumed as food, such as wood and plant lignocellulosic fibres. These materials encompass the majority of non-food biomaterial that is readily available (Gomez et al., 2008). This material source has the advantage of bypassing the 'food or fuel' issues associated with first generation sources. Growth of second generation material specifically for processing feedstock still uses arable land and water. Preventing competition with food resources limits this feedstock to waste material from other processes. Second generation materials can also be more complex to process – for example, wood fibres are heterogeneous and have several layers that are less useful for processing (e.g. lignins) that have to be separated out.

1.1 Third generation biomaterials - Macroalgae

Algae have been identified as a 3rd generation of renewable biomaterial that can be utilized for a range of products from fertilizers and animal feeds, human food supplements, nutraceuticals, specialty chemicals, and bioenergy (Angell et al., 2016, Mabeau and Fleurence, 1993, Garcia-Vaquero and Hayes, 2016). Algae are a plant-like organism that can grow in either fresh or salt water depending on species. They can be further classified as either microalgae or macroalgae, with microalgae growing as a mass of single cells and macroalgae growing as larger many-celled structures. Growth rates of algae are typically higher than those of terrestrial plants as they can absorb nutrients from all surfaces of the plant due to being submerged, and they do not use energy on developing bark or similar structural material. For example, the macroalgae *Ulva ohnoi* (Chlorophyta) can achieve specific growth

rates of up to 9.8%-12.5% fresh mass per day in optimal conditions (Lawton et al., 2013). The use of algae has some advantages over land-based biomass in that it can be grown on non-arable land, or for saltwater species, completely independent of potable water.

Microalgae have previously been the focus of research due to their higher theoretical growth rates. However, achievement of these rates on a large scale for products like biofuels is technically complex and expensive (Rawat et al., 2013) which currently limits their use to higher value applications such as food supplements. Macroalgae are a more recent focus of research as a lower cost biomaterial resource that has potential to help achieve sustainability and circular economy objectives. Potential applications for macroalgae include biofuels, food supplements for livestock, waste water treatment, fertilizers and extraction of high value compounds such as pigments, antioxidants and other compounds with potential health benefits (Raja et al., 2008, Suganya et al., 2016). There are many examples of studies of different macroalgae species to determine best growth rates and product yields for a range of processes. Neveux et al. (2014) found that a freshwater species of macroalgae, *Oedogonium intermedium* (Chlorophyta), had the highest biocrude yield (via hydrothermal liquefaction) of a range of species. Zeraatkar et al. (2016) performed a review of algae in bioremediation of heavy metals from wastewater, which concluded both macro- and micro-algae were suitable candidates. Castine et al. (2013) considered the use of macroalgae to treat wastewater from aquaculture, including obtaining added value from the resulting algae products. An assessment of the potential for algae in bioremediation was performed by Lawton et al. (2013), where the saltwater macroalgae *Ulva ohnoi* was found to have the highest growth rates of a range of local species. Several macroalgae species including *O. intermedium* and *Asparagopsis taxiformis* (Rhodophyta) have potential for use as supplement to livestock feed, leading to improved growth rates and reduced livestock methane emissions (Machado et al., 2015, Machado et al., 2016).

1.1.1 Case study species

The algal biomass used in this study was obtained from stock cultures locally sourced from the Marine and Aquaculture Research Facilities Unit (MARFU) at James Cook University in Townsville, Australia. The two species selected for use in the study were *U. ohnoi* and *O. intermedium*. *U. ohnoi* is a saltwater alga that forms thin, roughly rectangular blades up to 10cm wide, with the thickness of each blade being two cells wide. It was selected from a range of saltwater species based on its high growth rates and high biocrude yield as well as high resistance to bacterial ingress (Neveux et al., 2014, Lawton et al., 2013). *O. intermedium* is a freshwater alga that forms single filaments one cell wide, which can

significantly clump together when harvested. Both species have potential for use as livestock feed supplement (Machado et al., 2015, Vucko et al., 2017). *U. ohnoi* is currently being grown on a commercial scale as a potential source of fertilizer by Pacific Biotechnologies. The initial samples of *O. intermedium* were obtained by MARFU from Barramundi Fishing Farm, Townsville, and Fortune Bay Fisheries Ltd, Kelso. Initial *U. ohnoi* samples were obtained from the Australian coastline at 19°S 147°E. Samples were grown from lab-scale cultures up to 2000L tanks with water conditions simulating those in fisheries by the addition nitrogen and phosphorus. Water temperature averaged around 28°C, and air flow at 2L/min or higher was used during growth to ensure continuous motion. The algae material used throughout this study was obtained from these tanks. The approximate dry composition of the two macroalgae is shown in Table 1.1. Images of both species are shown in Figure 1.1.

Table 1.1; Approximate composition of the two macroalgae species. Solids composition from Neveux et al. (2014).

	U. ohnoi (% weight)	*O. intermedium* (% weight)
Dry solids	20	15
Moisture	80	85
Solids composition	*U. ohnoi* (% of dry mass)	*O. intermedium* (% of dry mass)
Lipids	2	10
Proteins	17.6	24.1
Carbohydrates	47.3	43.9
Ash	33.1	22

a) b)

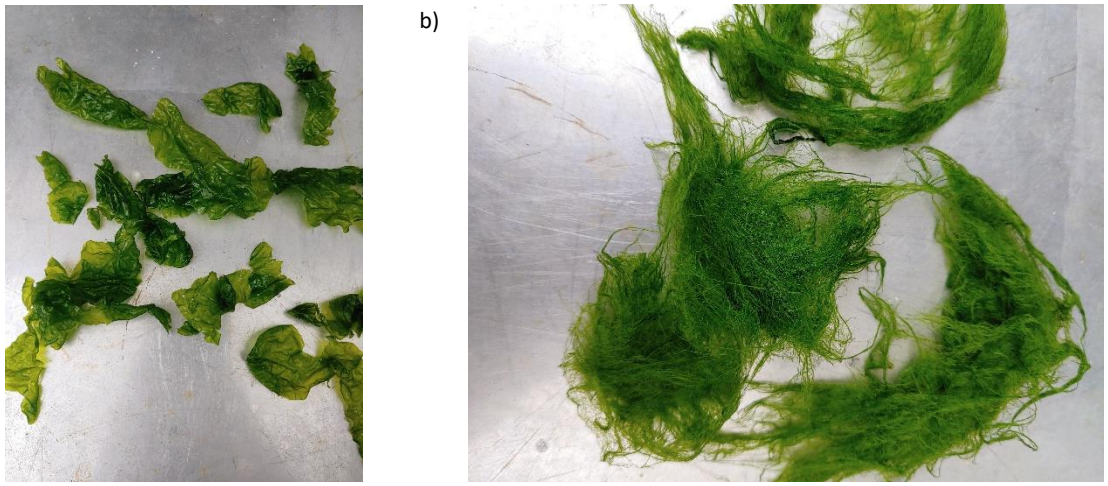

Figure 1.1; a) *U. ohnoi* b) *O. intermedium*

1.2 Pre-processing

A wide range of potential products and growth methods for specific species of macroalgae (e.g. use of waste water streams as a nutrient source) have been studied. However, there has been comparatively little attention on optimization of the pre-processing steps between macroalgae growth and final product processing. These pre-processing steps will be similar for most products, but are glossed over or covered with broad generalizations in macroalgae processing reviews (Ghadiryanfar et al., 2016). Most studied products from macroalgae are considered to be relatively low-value, and would require optimization of all processing steps for economic viability. Pre-processing of macroalgae can be energy intensive - Show et al. (2013) state pre-processing can take up to 75% of all processing energy costs for microalgae, and at a similar magnitude for macroalgae. It follows that a major hurdle for the implementation of macroalgae as a renewable biomaterial feedstock is the design and evaluation of pre-processing equipment, specifically for macroalgae.

The high water content of the macroalgae is an issue for many of the potential production pathways. High moisture content can cause several issues in biodiesel production (Sudakar et al., 2018), and conventional pyrolysis for the production of biogases or biochar requires little to no moisture in the material to achieve efficient processing (Milledge et al., 2014). The very high ratio of moisture to dry mass also incentivises drying of the material to reduce its weight and volume for any further transport. Furthermore, it reduces the size and volume required in further processing steps. For example, reducing moisture contents of *U. ohnoi* from 80% to 10% can result in around 30% reduction of conveying equipment costs (Peters and Timmerhaus, 1991). Finally, the removal of moisture increases the storage life of the material through the inhibition of spoilage due to microorganism growth and enzymatic reactions (Milledge et al., 2014). A focus of this pre-processing review is thus on the removal of moisture from the macroalgae.

The pre-processing stages to convert macroalgae to a typical feedstock are generally applicable to most potential products and therefore their optimization would provide benefits irrespective of the final processing method. The general stages of an algal bioprocess are growth of the macroalgae, removal of the macroalgae from the bulk of the tank water (dewatering), and drying of the macroalgae for long term stabilization. Figure 1.1 shows the important growth and pre-processing stages in the production of a dried macroalgae product.

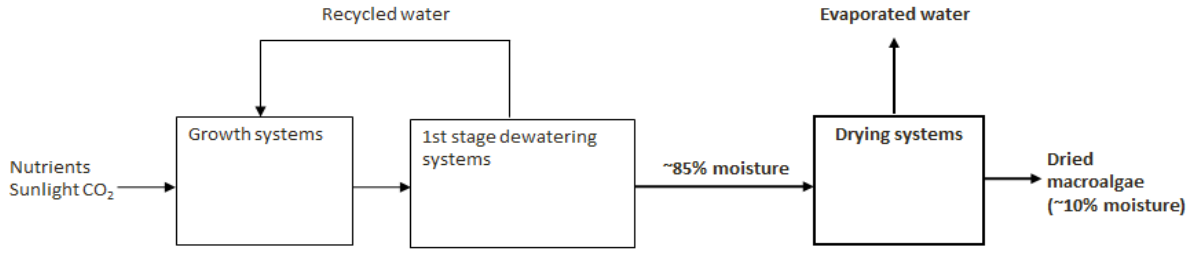

Figure 1.2; Block flow diagram of pre-processing stages for macroalgae.

1.2.1 Growth system

Algae are grown in tanks called bioreactors. There are two main types of bioreactors, differentiated by whether the tank is open or closed to the surrounding environment. Macroalgae are better suited to open bioreactor systems due to large particle sizes. The open system bioreactor is typically a large shallow pond called a raceway, shown in Figure 1.2 below. This consists of a track, where pumping forces nutrient solution and algae to circulate around the track. This helps to prevent stagnation of the water, and also ensures an even distribution of nutrients throughout the system. Typical concentrations of algae in raceway ponds are 0.5 to 1 kg fresh weight/m^3 for microalgae (Murphy and Allen 2011) and 2 to 6 kg fresh weight/m^3 for macroalgae (Lawton et al., 2013). The benefits of the open system are that it is easily scaled up to a larger size, and there are relatively low energy costs in the growth phase of operation. The problems associated with the open system are the risk of contamination of the tank by competing species, which could limit or stop the growth of the desired algae. As such, this method is best suited for robust algae species resistant to contamination or predation from other sources. Growth systems are relatively well understood for macroalgae, and most current research has been on optimization for specific applications. For example, the use of waste water streams from other industries as the nutrient source for macroalgae growth has been well described (Castine et al., 2013, Cole et al., 2013, Roberts et al., 2013).

Figure 1.3; Algae raceway pond at Pacific Biotechnologies, Queensland, Australia.

1.2.2 Harvesting and Dewatering

The dewatering stage involves separation of the algae mass from the growth medium liquid. This is required because the mass concentration of the algae in growth systems, as mentioned above, are too low for processing (typically below 1%wt for macroalgae (Lawton et al., 2013)). Dewatering reduces the overall mass and volume of material in further mass transport and processing stages, and allows for recycle of water and nutrients. Dewatering is typically performed by physical separation of the macroalgae from the growth system via filtration or similar methods. Further removal of the remaining surface moisture can then be achieved by methods such as centrifugation. These technologies are well established in industry practice and it is perceived that there is little room for enhancement in design or in our collective understanding of these processes. Moisture contents of algae after this stage are around 70 to 90% by weight depending on species. This moisture is inside the material and cannot be removed via the physical separation methods described above.

1.2.3 Drying

As mentioned above, the removal of most or all moisture from the material is desirable for many processing paths, and reduces material volume and weight significantly in further stages. Drying of

the material is required to remove the internal moisture remaining after dewatering. The drying stage typically involves the application of heat to the material which drives moisture transfer toward the material surface, which then can be removed via bulk convective transfer. Drying is an energy intensive process – a review of algae pre-processing by Show et al. (2013) recognised the drying step as the single biggest energy cost in an algae production process. Optimization of the drying stage is therefore a priority for developing the future viability of macroalgae bioresources.

There are many different methods of drying in operation or currently being tested (Inyang et al., 2017). The common drying methods that are applicable to the two macroalgae species being considered are solar drying and heated air drying. Current examples of aquaculture of macroalgae use solar drying of the material (Ghadiryanfar et al., 2016). This involves spreading the material as a thin layer and heating via direct sunlight. Although manual labour is substantial there are minimal costs in both required equipment and ongoing energy costs. However, solar drying can be limited by space for the material volumes that would be required for industrial scale production. Solar drying is dependent on weather and drying conditions cannot be controlled. As such, drying times and end product composition can be inconsistent. Finally, the material can be prone to contamination from outside sources such as insects or dust (Inyang et al., 2017).

Heated air drying is a common approach for drying at industrial scale and has been successfully applied to many biomass material types, for example flighted rotary drying and pneumatic flash drying of sugar cane bagasse. There are different methods using heated air that are applicable to different materials. Examples that are applicable to macroalgae would include belt and rotary drying equipment. These methods use heated air to heat the material and also to transport liberated moisture from the material. The advantages of these devices are that the rate of drying is easily controlled through variance of drying conditions such as gas temperature and humidity. These devices facilitate drying at much faster rates than solar drying leading to higher throughput.

The key design data for all drying equipment is the time required to remove the desired amount of moisture for the material. This can be determined from first principles by solving simultaneous heat, mass and momentum transfer equations, but this is only possible with thorough characterisation of the material and its changes during drying. The level of characterisation is rarely undertaken in practice, and does not exist for the target macroalgae species. It is more common to determine drying design data by obtaining experimental drying rates for new materials. Variables that are known to affect the rate of drying for biomass are the temperature, velocity and relative humidity of the surrounding medium, the bulk thickness of the material and internal properties of the material. This

has to be determined experimentally for new materials due to the effects of individual material properties on the effective drying rate of the material. Furthermore, there is very little data describing these drying kinetics for macro- or micro-algae species in the literature. Also, when this data is reported, it is often with a low level of sophistication, without considering and quantifying all of the independent variables that can affect the rate limiting its validity in scaling up. Control of drying rates to enable or predict design specifications can be difficult or impossible without understanding the effects of all relevant variables on macroalgae drying.

1.3 Conclusion

Renewable resources are an emerging and important research focus, driven by national and international policies and agreements. Examples of these policies include the Paris Agreements to reduce GHG emissions, the mandated use of biofuels as an additive to transportation fuel (implemented by US, AUS, EU and Japan among others) and bans on single use non-degradable plastics such as shopping bags and drinking straws. In all these examples and in others, biomaterials can be used as a renewable processing feedstock, and are an integral component of the many methods currently being investigated to help achieve these goals.

Algae have been identified as a source of renewable biomaterial that can be utilized for a range of products from fertilizers and animal feeds, human food supplements, nutraceuticals, specialty chemicals, and bioenergy (Ghadiryanfar et al., 2016). More recently, research effort in bioprocessing has broadened to include macroalgae, which are large multicellular alga found in both marine and freshwater environments. Due to their larger size and ease of harvesting, macroalgae are well suited to large-scale outdoor cultivation. Macroalgae have the capacity to complement existing industries and drive sustainability and circular economy objectives by utilizing their waste nutrients and water, effectively creating a sustainable source of high protein biomass from waste inputs (Cole et al., 2016, Lawton et al., 2017). Macroalgae have the advantages of not requiring the use of arable land, or even potable water, in the case of saltwater species, compared to other biomaterials. The case study species of macroalgae used in this work are *Ulva ohnoi*, a saltwater macroalgae, and *Oedogonium intermedium*, a freshwater macroalgae. Both are local species that have previously been considered as a promising biomaterial for commercial processing.

Research on macroalgae as a processing feedstock is mostly limited to experimentation to determine yields for different species and optimization of macroalgae growth, but there is currently little

consensus on the best processing pathways. Despite this uncertainty, most product paths will require similar pre-processing stages, including drying and dewatering, to ensure a consistent and stable feed material. Any insights gained into these processing steps could also be extended to inform our understanding of other similar biomaterials and their pre-processing stages. A significant barrier to the development of industry based around macroalgae production is the design of energy efficient and well-controlled drying systems that can transition freshly harvested biomass into a product suitable for storage and transport.

Drying is a required step for macroalgae; they contain a high percentage by mass of water even after removal of all surface moisture (*U. ohnoi* is up to 80% moisture by mass, while *O. intermedium* is up to 85% moisture by mass). Furthermore, this introduction identified that the drying step of a bioprocess was the single biggest energy demand for the processing of algal biomass, due to the large amounts of moisture requiring removal. The drying step was estimated as constituting up to 75% of processing costs in some cases. As such optimization of this step would both lead to significant gains in efficiency for the overall process, and would contribute to the development of viable product pathways for macroalgae to assist in addressing current climate challenges.

The design and optimization of industrial scale drying equipment requires a good understanding of the drying kinetics of the material and the influence of equipment design variables such as drying gas temperature and flow rates. This would allow for accurate prediction of drying times to a desired moisture content and therefore the equipment residence times and unit size required. Drying models and associated theoretical understanding of macroalgae drying does not exist in literature for the target species and such knowledge is extremely limited for any macroalgae species. In an effort to address this knowledge gap and provide pragmatic solutions for future industry, the following chapter includes a review of drying kinetics theory and outlines our current understanding of macro algae drying. Modelling and other biomaterial examples are reviewed in order to choose an appropriate modelling framework and to facilitate the development of a pragmatic model for macroalgae drying which includes the influence of typical equipment design variables.

Chapter 2

2. Drying Theory and Literature Review

The optimized design of drying equipment involves the choice of multiple design parameters to best fit desired specifications while minimizing operational (energy) and equipment costs. These base parameters are generally the throughput of material required to be processed and the time required for the material to be dried to the required moisture content (i.e. the residence time in the equipment). These values then affect the size of drying equipment required.

The residence time is dependent on a materials drying rate. Material drying rates are dependent on the properties of the material, the equipment drying conditions, and these are again influenced by the material loading. For convective drying equipment operational conditions include the drying gas temperature and flow rates. An understanding of how these parameters affect the rate of drying for the material is therefore a requirement for the design of drying equipment.

A review of the theory and literature for drying kinetics is performed in this chapter to provide a basis for the development of experimentation and methods to provide this understanding. The theory of drying pertaining to biomaterials is covered and the main types of moisture removal prevalent in biomaterials are identified. The common methods and models used to represent drying are identified, with a focus on pragmatic models that are relevant for industrial applications. Other material properties that are required as a part of these models (such as the equilibrium moisture content of the material) are investigated. Finally, the main variables affecting drying (which are also design variables for industrial drying equipment) are identified.

A review of the experimental data trends and conclusions from relevant drying kinetics studies that investigate the effects of the identified design variables for macroalgae and other similar biomaterials, as well as for determination of equilibrium moisture, is performed. Equilibrium moisture was identified as a function of the drying gas temperature and humidity, and common experimental methods for its determination are discussed. For drying kinetics the relevant variables identified and discussed are the drying gas temperature and flow rate, and the bulk density and loading of the material (represented as material slab thickness) being dried. This review is used to determine the experimental and modelling methodologies used in further chapters.

2.1 Drying Theory

The drying process involves simultaneous heat and mass transfer to and from the material being dried (Richardson et al. (2002)). When moisture is internal, such as for biomass, the movement of moisture within the material is typically modelled as mass transfer via diffusion driven by a moisture concentration gradient between the material and surrounding gas. Heat transfer from the surrounding drying gas acts to increase material temperature and also the effective diffusion of moisture through the material. Convective mass transfer describes the actual removal of moisture from the surface and into the drying gas.

Moisture is considered to be attached to a material via one of two methods (Richardson et al. (2002)). Unbound, or free, moisture is situated on the surface of the material, for example water on the surface of sand particles. It is not chemically or physically bonded to the material surface, and as such free moisture is easier to remove from the material. Physical methods such as filtration or centrifugation are often used to remove 'free' moisture.

The other type of moisture is bound or internal moisture. This is moisture chemically bound to the solid, or otherwise trapped internally in the material. An example of bound moisture is liquid water in cells of biological material such as wood and algae, or water attached to a hydrated crystal structure. Bound moisture is harder to remove than free moisture as the binding must first be overcome, and then the bound moisture must diffuse to the material surface before being removed, typically via convection.

The drying rate (the amount of moisture removed from the material per unit time) typically shows one of two trends depending on the type of moisture being removed (Richardson et al. (2002)). The removal of unbound moisture from a material surface will generally show a constant or unchanging rate of drying and can be represented by convective mass transfer and a partial pressure driving force. The rate does not change because the concentration of surface moisture (or partial pressure at the material temperature) does not change until all moisture is removed. Removal of bound or internal moisture from a material shows a falling rate of drying over time. This occurs because the average moisture concentration in the material is reduced as it is removed, which in turn reduces the concentration gradient with the surrounding gas and therefore the overall rate of transfer. A theoretical example of drying showing both a constant rate period (where excess surface moisture is removed) and a falling rate period (where no surface moisture remains, and the drying rate is limited by internal diffusive transfer) is shown below in Figure 2.1.

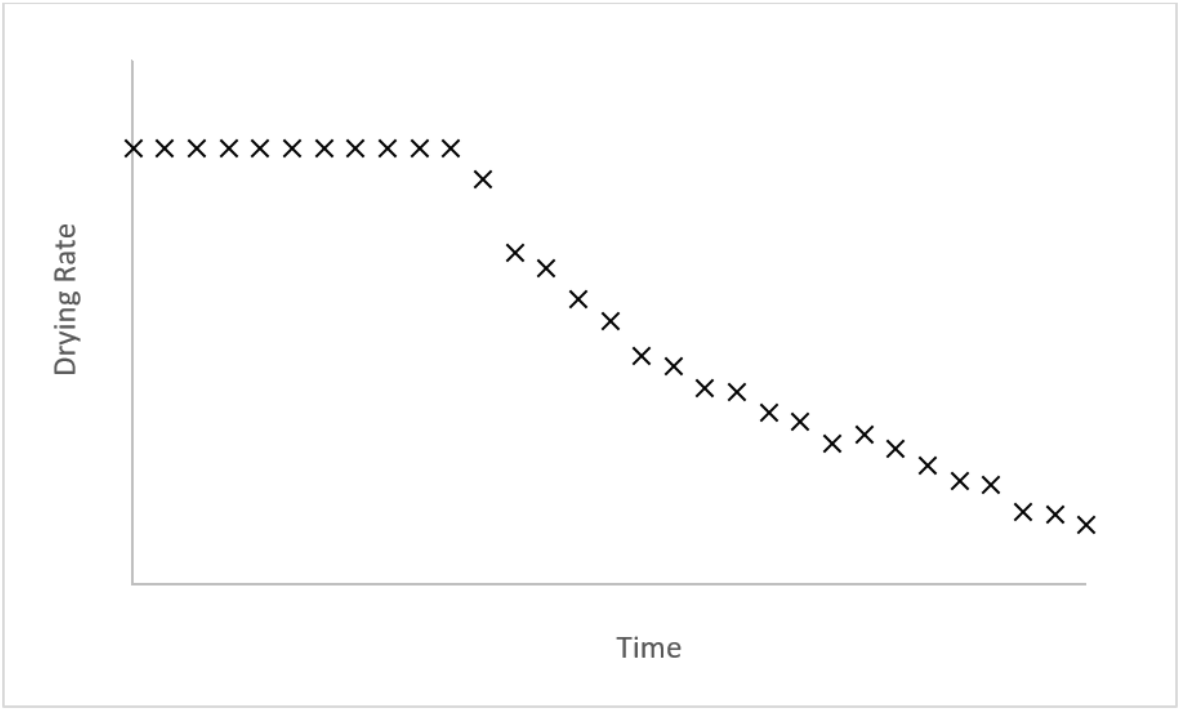

Figure 2.1; Theoretical example of a material showing both constant drying rate (horizontal trend) and falling rate (decreasing trend) periods.

The drying rate of a material is affected by both the surrounding conditions and the properties of the material itself. External variables that affect drying include the surrounding temperature, the capacity of the surrounding medium to hold the removed moisture (i.e. relative humidity), and movement/velocity of the surrounding drying medium (Sherwood 1932). Increases in temperature cause an increase in the rate of diffusion of moisture through the material, as well as an increase in the rate of removal of surface moisture. Lower relative humidity increases the rate of diffusion due to the increase in the concentration gradient of moisture. Gas velocity affects the rate of convection mass transfer from the material surface, with increases in gas velocity increasing the surface transfer rate.

The specific properties of the material will also affect the rate of diffusion within the material being dried. These properties include, but are not limited to, variables such as material slab thickness, pore size, moisture bonding type and strength (e.g. chemically bound, inside cells or in pores/capillaries). These internal properties affect the overall drying rate of the material, but apart from thickness there is no unified theory available to represent and predict the impacts of these internal properties on drying rates. Slab thickness changes the distance required for moisture to travel to the material surface and come into contact with the drying medium. Increased thickness then decreases the

effective rate of drying. Thus, new kinetics experimentation is required for each new material to account for these differences in material properties.

Drying is generally modelled via one of two overarching methods. The first is a mechanistic approach that numerically solves the simultaneous heat and mass transfer differential equations across the material volume. This approach requires a good understanding of material properties and the boundary conditions of the drying geometry and system used. This method is infrequently used to specifically model the drying rate of a material. It is considered to be a more accurate method for representing or predicting material effects that occur during drying, such as pore formation and changes on a microbial scale (Katekawa and Silva 2006) but is less viable for representation of industrial scale drying. The alternative method uses analytical models (lumping effects on drying rate into a single parameter) developed from diffusion equations for specific geometries. These models are much more commonly used to describe the drying of biomaterials. These models are discussed in greater detail in the following section.

2.1.1 Lumped Parameter Models

2.1.1.1 Empirical Models

Empirical models derive a direct link between the moisture content and drying time. Parameters from empirical equations have no physical meaning, and as such cannot be used to predict the impacts of changing material properties or to predict drying outside of those conditions used to develop the empirical relations themselves.

A list of common empirical equations used to model drying rates of material from literature is shown in Table 2.1 below (collated from Vijayaraj et al. (2006) and Tello-Ireland et al. (2011)).

Table 2.2; Empirical drying rate models.

Empirical models	Equation	
Lewis	$MR = \exp(-k_0 t)$	(2.1)
Page	$MR = \exp(-k_0 t^n)$	(2.2)
Modified Page	$MR = \exp(-k_0 t)^n$	(2.3)
Henderson and Pabis	$MR = a.\exp(-k_0 t)$	(2.4)
Logarithmic	$MR = a.\exp(-k_0 t) + c$	(2.5)
Two-term	$MR = a.\exp(-k_1 t) + b.\exp(-k_2 t)$	(2.6)
Two-term exponential	$MR = a.\exp(-k_0 t) + (1-a)\exp(-k_0 a t)$	(2.7)
Wang-Singh	$MR = 1 + at + bt^2$	(2.8)
Diffusion approach	$MR = a.\exp(-k_0 t) + (1-a)\exp(-k_0 b t)$	(2.9)
Modified Henderson and Pabis	$MR = a.\exp(-k_0 t) + b.\exp(-gt) + c.\exp(-ht)$	(2.10)
Verma et al.	$MR = a.\exp(-k_0 t) + (1-a)\exp(-gt)$	(2.11)
Midilli and Kuck	$MR = a.\exp(-k_0 t^n) + bt$	(2.12)
Weibull	$MR = \exp\left(-\left(\frac{t}{b}\right)^a\right)$	(2.13)

The variables $a, b, c,\ k_0, k_1, k_2, g, h$ and n are empirical model parameters, and t is the drying time. The value MR is the ratio between the current (at time t) amount of removable moisture in the material, to the initial amount of removable moisture. Its most general description is given by;

$$MR = \frac{M}{M_0} \tag{2.14}$$

Where M is the average moisture concentration in the material, and M_0 is the initial moisture concentration. The amount of moisture is usually expressed as the ratio of moisture mass to the dry solids mass, called the moisture content on a dry basis (%db). This description assumes that all moisture in the material can be removed at the drying conditions. MR is a dimensionless value that ranges between 1 and 0. It is equal to 1 at $t = 0$, where no drying has occurred and therefore $M = M_0$. It is equal to zero at $t = \infty$, where all the removable moisture has left the material.

In reality, biomaterials adsorb moisture from the surrounding air at some constant rate. This rate is dependent on the temperature and humidity of the surroundings. As the concentration of moisture in the material decreases, the rate of moisture transfer out of the material also decreases. At some specific concentration the rate of desorption and adsorption become equal, and therefore any further drying cannot take place. This limit is referred to as the equilibrium moisture content (M_e). The definition of MR must then be adjusted to account for this non-zero endpoint;

$$MR = \frac{M - M_e}{M_0 - M_e} \tag{2.15}$$

Where M_e is the moisture content at the equilibrium. The equilibrium moisture content is discussed further below in Section 2.1.3.1. The equations presented in Table 2.1 and later in this thesis are valid for both definitions of MR (equations 2.14 and 2.15).

2.1.1.2 Reaction Engineering Approach

The reaction engineering approach (REA) model (Chen and Xie 1997) is a semi-empirical model that considers evaporation of moisture in the same way that chemical reactions are described. In the REA model, evaporation is assumed to work as an activation process in that moisture removal must overcome an energy barrier to proceed. The model has previously been used to describe drying for droplets and thin layer slabs of biomasses (Fu et al. 2011). It is intended to model drying of materials with purely external moisture. For example, this approach has been used to describe spray drying of milk where the material is considered as a solid core surrounded by a layer of moisture or raw sugar crystal drying where a film of surface moisture surrounds the solid crystal.

The drying rate of a system is defined by assuming surface convection is the rate limiting step and taking a classical approach as shown below;

$$\frac{dm}{dt} = -h_m A(\rho_{v,s} - \rho_{v,b}) \tag{2.16}$$

Where $\frac{dm}{dt}$ is the drying rate (kg/s), h_m is the mass transfer coefficient (m/s), A is the material surface area (m^2), and $\rho_{v,s}$ and $\rho_{v,b}$ are the vapour density (kg/m^3) at the material surface and in the drying medium bulk respectively.

The surface vapour density can be related to the saturated vapour density at the surface temperature (T_s) by a fractionality coefficient ψ, shown below. The coefficient can be interpreted as the relative humidity at the surface conditions.

$$\rho_{v,s} = \psi \rho_{v,sat} \tag{2.17}$$

The fractionality constant is defined in terms of the activation energy of evaporation (ΔE_v) and the surface temperature using an Arrenhius-type equation, where R is the ideal gas constant;

$$\psi = \exp\left(-\frac{\Delta E_v}{RT_s}\right) \tag{2.18}$$

Combining above equations gives the following;

$$\frac{dm}{dt} = -h_m A\left(\rho_{v,sat}\exp\left(-\frac{\Delta E_v}{RT_s}\right) - \rho_{v,b}\right) \tag{2.19}$$

The mass transfer coefficient, h_m, can either be determined experimentally for the drying conditions or via established Sherwood number correlations. The Sherwood number (Sh) represents the ratio of convective to diffusive mass transfer, as defined below;

$$Sh = \frac{h_m L}{D} = \frac{\text{convective mass transfer coefficient}}{\text{diffusion mass transfer coefficient}} \tag{2.20}$$

Where l is the characteristic diffusion length (m), and D is the mass diffusivity (m^2/s). The correlation used to previously determine the Sherwood number for REA calculations in literature is the Modified Ranz and Marshall correlation (Ranz and Marshall 1952), originally derived for water droplets, shown below;

$$Sh = 1.63 + 0.54 Re^{\frac{1}{2}} Sc^{\frac{1}{3}} \tag{2.21}$$

Where Re is the Reynolds number and Sc is the Schmidt number.

2.1.1.3 Fick's Law analytical drying model

Diffusion of one material through another is described by Fick's Laws of diffusion (Fick 1855). These laws were originally defined for the diffusion of dissolved solids through liquid media but have also been used to model moisture diffusion through solids during drying (Sherwood 1932, Crank 1975). Diffusion describes movement of one component through another via random molecular movement. The overall direction of travel is from areas of high concentration to lower concentration. Fick's first law is given below, which describes the flux of a component A (J_A) through another component B under steady state conditions for a single direction x. Material geometry for the model is shown in Figure 2.2.

$$J_A = -D_{AB}\frac{\partial C_A}{\partial x} \tag{2.22}$$

The diffusion of mass causes changes in the concentration gradient over time. This time dependent (dynamic) behaviour is described by Fick's second law, which is written for a single dimension as

$$\frac{\delta C}{\delta t} = D\frac{\delta^2 C}{\delta x^2} \tag{2.23}$$

Where $C = f(x,t)$ is the concentration at a given point and time, x is the distance of the point from the boundary surface, t is time and D is the diffusion constant.

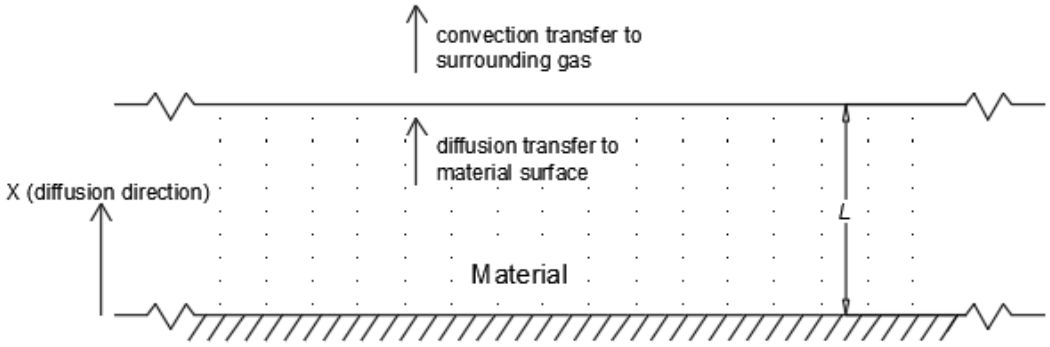

Figure 2.2; Diagram of material geometry assumed in the development of the Fick's law analytical drying model.

Sherwood (1932) developed an analytical (mechanistic) solution to Fick's second law when applied to the drying of solids. The analytical solution was derived by using the known similarities between models used to describe heat diffusion and that used to describe mass diffusion. The differential equations describing heat diffusion for a single direction is shown in Equation 2.24, where T is the temperature at point x and time t, and α is the heat diffusivity in the material. This is essentially the same as Equation 2.23, with temperature replaced by concentration.

$$\frac{\delta T}{\delta t} = \alpha\frac{\delta^2 T}{\delta x^2} \tag{2.24}$$

A known solution of Equation 2.24 for T as a function of position and time for material in an infinite slab geometry with width L was modified to become a function of concentration using the above similarities. This is shown in Equation 2.25. This equation generates a curve of moisture concentration across the slab at a given time. Refer to Figure 2.3 for examples of the theoretical moisture distribution resulting from this model across an arbitrarily defined slab at differing times.

$$\Delta = \frac{C}{C_0} = \frac{4}{\pi}\sum_{n=0}^{\infty}\frac{1}{(2n+1)}\sin\left(\frac{(2n+1)\pi x}{2L}\right)exp\left(-\frac{(2n+1)^2\pi^2 Dt}{4L^2}\right) \quad (2.25)$$

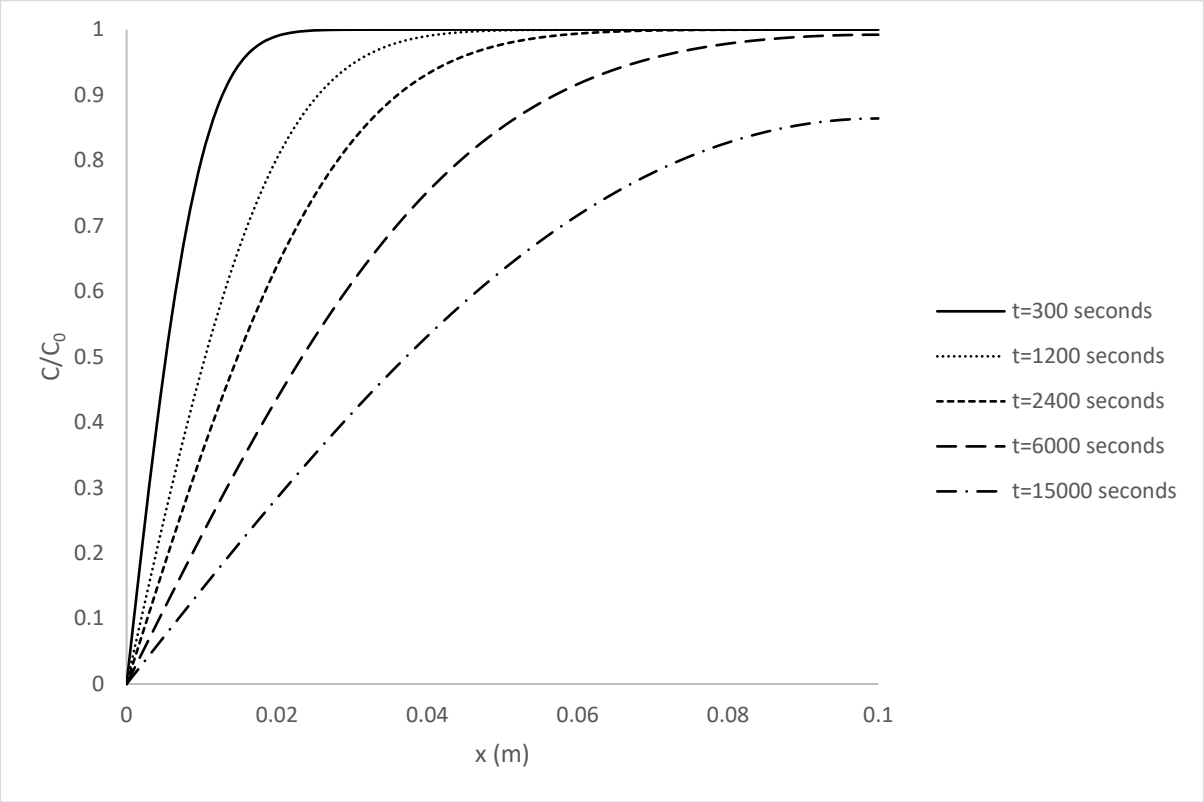

Figure 2.3; concentration ratio as a function of position across a 0.1m wide slab over time (arbitrary diffusivity value of $1e^{-7}$ m^2/s).

It was noted by Sherwood that an equation for the average moisture content across the slab width is more useful for describing drying of material. This was obtained by integrating $\frac{C}{C_0}$ across the slab width L along with the following assumptions and associated boundary conditions;

- Diffusion can well represent the overall drying mechanism, and drying rate is limited by diffusive transfer.
- Uniform initial distribution of moisture throughout the sheet.
- Drying direction is one-directional and directly out of the sheet surface.
- Moisture on the sheet surface is immediately removed via bulk transfer, ensuring the surface concentration is constant at the equilibrium concentration and therefore diffusion is the rate limiting step.
- The diffusion coefficient is a constant.
- Sheet geometry is constant throughout drying.

Boundary conditions are;

- $C = C_\infty$ (or zero) at $x = L, t > 0$ (material surfaces are at equilibrium concentration).
- $C = C_0$ at $t = 0$ for all x (initial concentration distribution is uniform).
- $\frac{\delta C}{\delta x} = 0$ at impermeable surfaces or centreline of sheet (defined as $x = 0$) (no moisture transfer at these points).

The full derivation of the drying kinetics model is not readily available in identified literature, and a full derivation of the analytical solution from the Fick's second law differential equation for a slab geometry can be found in Appendix 1 (compiled from Crank (1975) and Sherwood (1929)). The final equation for drying of material in an infinite slab is;

$$MR = \frac{8}{\pi^2} \sum_{n=0}^{\infty} \frac{1}{(2n+1)^2} exp\left(\frac{-(2n+1)^2 \pi^2 Dt}{4L^2}\right) \tag{2.26}$$

Similar solutions have been developed for other standard geometries. For an infinite length cylinder with a radius of r, the analytical solution is;

$$MR = 4 \sum_{n=1}^{\infty} \frac{1}{(\varepsilon_n)^2} exp\left(\frac{(-D(\varepsilon_n)^2 t)}{r^2}\right) \tag{2.27}$$

Where ε_n is the nth root of the zeroth order Bessel function. All drying is assumed to be directly outward from the centre line of the cylinder.

Finally, for a sphere of radius r;

$$MR = \frac{6}{\pi^2} \sum_{n=1}^{\infty} \frac{1}{n^2} exp\left(\frac{(-Dn^2 \pi^2 t)}{r^2}\right) \tag{2.28}$$

All drying is assumed directly outward from the centre point of the sphere.

The diffusion constant D is usually instead written as D_e, or the effective diffusivity. This is used to indicate that it is incorporating all variables that effect the drying of the material, both external (e.g. drying temperature, air velocity, pack density) and internal (e.g. pore size, average pathway lengths, layer resistances to diffusion). This is referred to as a lumped parameter model and is a common method to pragmatically account for complexity in material behaviour. This approach makes this model semi-empirical in practice.

The relationship between temperature and effective diffusivity is typically shown to fit an Arrenhius-type relationship, written as;

$$D_e = D_0 \exp\left(-\frac{E_a}{RT}\right) \tag{2.29}$$

Where E_a is the activation energy (J/mol), R is the ideal gas constant (J/mol.K), T is drying temperature in Kelvin, and D_0 is the diffusion pre-exponential (m^2/s). It should be noted that in this application, the values of E_a and D_0 are determined empirically from experimental data by plotting $\frac{1}{T}$ against $ln(D_e)$, and fitting a linear relationship. The slope of the fitted line is then equivalent to $-\frac{E_a}{R}$ and the y-intercept is equivalent to $ln(D_0)$.

This Arrenhius-type model is primarily used to represent the relationship between chemical reaction rates and temperature. For chemical reactions E_a is related to the specific reaction independent of external conditions, and the pre-exponent (D_0) is the reaction rate at an infinitely high temperature. Assuming these can be translated to the diffusivity relationship use of the equation, E_a should be a constant related to the specific material (likely encompassing the material property effects on diffusivity) and D_0 should be the effective diffusivity at infinitely high temperature.

2.1.2 Equilibrium Moisture Content

Part of the drying kinetics models is the equilibrium moisture content of the material, defined as the minimum moisture content achievable when exposed to drying gas with a given set condition. Drying of the material cannot be pushed further than the equilibrium point for those conditions. If a material has been dried beyond the equilibrium moisture content for its surroundings, it will re-absorb moisture from the surroundings instead of drying further.

The equilibrium moisture content depends on the material properties and the relative humidity and temperature of the surroundings. The equilibrium moisture content is usually represented as sorption isotherm lines on a relative humidity versus temperature graph. Like drying kinetics, the equilibrium moisture content data has to be determined experimentally because of the influence of internal properties. From the literature reviewed, a list of equations used for the equilibrium moisture content are shown in Table 2.2 below (collated from Mohamed et al. 2005 and Akin 2009);

Table 2.2; Equilibrium moisture content models.

Model	Equation(s)	
Chung-Pfost	$E_{RH} = \exp\left(\frac{-a}{T+b}\exp(-cM_e)\right)$	(2.30)
Halsey	$E_{RH} = \exp\left(\frac{-\exp(a+bT)}{{M_e}^c}\right)$	(2.31)
Oswin	$M_e = (a+bT)\left(\frac{E_{RH}}{1-E_{RH}}\right)^c$	(2.32)
Henderson	$1 - E_{RH} = \exp[-a(T+b){M_e}^c]$	(2.33)
Brunauer-Emmett-Teller	$M_e = \frac{(a+Bb)cE_{RH}}{(1-E_{RH})(1-E_{RH}+cE_{RH})}$	(2.34)
Guggenheim-Anderson-de Boer	$M_e = \frac{abcE_{RH}}{(1-bE_{RH})(1-bE_{RH}+bcE_{RH})}$	(2.35)
	$b = b_0\exp\left(\frac{h_1}{RT}\right)$	(2.36)
	$c = c_0\exp\left(\frac{h_2}{RT}\right)$	(2.37)

Where a, b and c are model coefficients, M_e is the equilibrium moisture content of the material expressed as a % dry basis, E_{RH} is the equilibrium relative humidity of the surroundings (in kg H_2O/kg H_2O at saturation), and T is the temperature of the surroundings in °C. For the Guggenheim-Anderson-deBoer model b_0, c_0, h_1 and h_2 are coefficients, R is the universal gas constant and T is the temperature in Kelvin.

The models in Table 3 are empirical relations based on the Freundlich Adsorption model, modified to account for multilayer adsorption of molecules to the material surface, and to use relevant variables for equilibrium moisture. The Freundlich model itself is an empirical modification to the Langmuir model that considers effects of rough surfaces and differences in adsorption sites. The Modified BET model is accurate for relative humidity below 0.5 (Al-Muhtaseb et al. 2002). The GAB model has provisions for estimation of equilibrium moisture outside of experimental temperature ranges. This estimation does not account for the effects of material properties and assumes all materials respond similarly to changes in temperature outside of experimental conditions.

The drying and adsorption of moisture to and from a material can be affected by hysteresis. That is, the output, in this case the equilibrium moisture content, is affected by whether the material is initially

above or below the equilibrium point. In practice this means that the determined equilibrium moisture content for a material could be different if the material is dried to equilibrium compared to when moisture is adsorbed toward the equilibrium point. The cause of these phenomena is linked to permanent changes of water-filled pores and capillaries. As such, for drying applications the material should always begin with high moisture and be dried to equilibrium.

2.1.2.1 Equilibrium moisture of biomaterials – Literature

The following is a review of some equilibrium moisture studies of biomaterials (either macroalgae or those with similar properties when possible), focusing on the methodologies used.

A common approach to determining moisture equilibrium is to use saturated salt solutions to create an air space with a known and predictable humidity in an enclosed container. In short, the saturated solution forms a moisture transfer equilibrium with air above the solution, giving a fixed humidity. A review of saturated salt solution relative humidity at given temperatures was completed by Greenspan (Greenspan 1976). They provided tables of temperature versus relative humidity for a large range of saturated salts, and the measured uncertainty in the relative humidity. Equations to predict the relative humidity at a given temperature for a solution were also provided.

Akin (Akın 2009) studied the water activity, equilibrium moisture content and sorption isotherms of *Capsicum annuum*. The equilibrium moisture content of samples was determined for temperatures of 30, 45 and 60°C, with a range of relative humidity from 10 to 98%. Different saturated salt solutions were used to fix the relative humidity. The sample was placed in a sealed sorption container along with the salt solution. The containers were placed in a heated water bath to fix the temperature. The time taken to reach equilibrium was approximately 14 days. The data was fitted to five different models (Oswin, GAB, Modified Henderson, Halsey, and Modified Halsey) to determine the best equation for prediction. The Modified Henderson model was found to be the best fit for the 30°C data, while the GAB model was the best fit for the 45 and 60°C data. Another equation was developed in an attempt to have a single model that fit the entire range of conditions.

Mohamed, (Mohamed et al. 2005) studied the equilibrium moisture content and heat of sorption for *Gelidium sesquipedale*, a species of red macroalgae. The equilibrium moisture content of the algae was determined experimentally at 30, 40 and 50°C, and for six relative humidity points between 5 and 90%. The samples were placed into sealed jars with a range of saturated salt solutions used to fix the internal relative humidity. A thermostatic bath was used to fix the temperature, and the samples were

weighed daily. Equilibrium was recognised as when three consecutive weight measurements showed a difference of less than 0.001g. Their results showed hysteresis effects, where drying to equilibrium and resorption of moisture to equilibrium produced differing values. Six models (Modified Henderson, modified Chung-Pfost, modified Oswin, modified Halsey, modified BET and GAB) were fitted to the data, and all predicted the experimental data fairly accurately. The modified BET model was the most accurate in its valid range of relative humidity (<0.5), and the GAB model was the best fit for the whole range of data.

Rastikian (Rastikian et al. 1999) performed modelling of sugar drying using experimental conditions to imitate the conditions inside a countercurrent cascading rotary dryer. Initial experiments to determine moisture content and sorption isotherms for other required data for drying where also performed. The initial moisture content of the sample was determined using heating in an oven at 105°C over three hours. The sorption isotherms (equilibrium moisture content) of the sugar sample was experimentally determined by placing 10g samples in closed glass vessels, with the air humidity in the vessels fixed by sulphuric acid solution of defined concentration. Sorption values at the used temperatures of 22 and 35°C showed a negligible effect from temperature, and humidity had little effect until 82-83% humidity. No models were fitted to the sorption data.

(Moreira et al 2017) determined the water sorption isotherms and drying kinetics of the brown macroalgae *Fucus vesiculosus*. Equilibrium moisture was determined using saturated salt solution to generate fixed humidity atmosphere in sealed jars at temperatures between 5 and 65°C, with humidity between 5 and 95% relative. The BET and Halsey models were used to represent the sorption isotherms, with the Halsey model found to best fit over the condition range. Drying kinetics experiments were performed with a hot air convective dryer, with air temperature between 35 and 75°C, with constant air velocity (2 m/s) and relative humidity (30%). Measurement of mass during the drying experiments was performed by removing the material from the dryer and measuring mass, frequently during the initial period and every hour at late stages. Equilibrium moisture showed a crossover point at higher humidity values (70+%), where increasing temperature caused increase in equilibrium moisture (opposite to the expected effect). This effect was explained as caused by the high polysaccharides content of the macroalgae and has also been shown to occur for other macroalgae (Lemus et al 2008, Mohamed et al 2005, Vega-Galvez et al 2008).

2.2 Variables Affecting Drying Rates

A review of biomass drying kinetics studies in literature was performed to gain an understanding of the variables that can affect drying rates for biomaterials as well as the condition ranges typically used. Journal articles were found using the Google Scholar, ScienceDirect and Scopus directories, using 'drying kinetics' as the search term. Those studying drying kinetics of biomaterials were then checked further for relevance. Unfortunately, there are very limited studies quantifying the drying rates of macroalgae species in literature, and none using the two target species. Therefore, the studies reviewed were chosen because they used biomaterials with similar properties to the species of macroalgae chosen for this thesis. The properties that characterise the key macroalgae species are compressibility and porosity, and they have been observed to undergo volume losses during drying (Hammond et al 2018). Where possible drying kinetics studies of other macroalgae species were used for the review. However, given the limited number of macroalgae studies examining the effects of variables other than temperature on drying rates, other biomaterials with similar characteristics were included to better understand the potential impact of these variables.

2.2.1 Temperature

The relationship between drying kinetics and temperature is well understood, with virtually all drying studies in literature varying temperature. An increase in drying temperature is observed in many studies to correspond with an increase in effective diffusivity and therefore drying rate. Temperature increases diffusive movement and ability to 'free' bound internal moisture. The following review aims to collate typical methodologies used to characterise the impact of temperature on the drying rate of biomaterials. Furthermore, temperature ranges used in drying of biomaterials are identified. Finally, this review is also used to identify the typical models used and their success in representing the drying of biomaterials.

2.2.1.1 Macroalgae

Vega-Galvez (Vega-Galvez et al 2008) determined sorption isotherms and modelled drying kinetics of the brown macroalgae *Macrocystis pyrifera*. Sorption isotherms were determined using saturated salt solutions to generate a fixed humidity, but only determined at 50°C. A convective tray dryer was used for the drying kinetics experiments. Air velocity at the sample was held constant at 2.1 m/s. The load

density of material was kept constants at 10.5±0.2 kg/m^2. Drying temperatures used were 50, 60, 70 and 80°C. Sample mass was measured in situ. A range of empirical equations were used to represent the drying kinetics, with the Midilli and Kuck and logarithmic model chosen as the best fit. The first term of the Fick's law analytical model (functionally equivalent to the Lewis empirical model) was used to calculate effective diffusivity (between 5 to 10x10^{-10} m^2/s) and to calculate the drying activation energy (19.9 kJ/mol).

Gupta (Gupta el al 2010) studied the effects of drying temperature on the drying kinetics, as well as phytochemical constituents on the edible macroalgae *Himanthalia enlongata*. A hot air convection oven was used for the drying experiments. The temperature range used was 25, 30, 35 and 40°C. The air velocity was held constant at 2.0 m/s. Measurement of sample mass was performed by periodically removing the material from the oven and directly measuring. The Newton, logarithmic, and Henderson and Pabis models were used to represent drying, with the Newton model found to be the best fit to data. The first term of the Fick's law analytical model, which is functionally equivalent to the Lewis model, was used to determine effective diffusivity for comparison with other material (5.6 to 12.2 x$10^{-7}$$m^2$/s) and calculation of activation energy (37.2 kJ/mol).

Uribe (Uribe et al 2017) studied desorption isotherms and drying kinetics for the brown macroalgae *Durvillaea antarctica*, using a wide range of models to represent the drying data. Equilibrium moisture was determined using saturated salt solutions to generate fixed humidities between 10 and 90%. The GAB, BET, Halsey and Caurie models were used to represent the sorption isotherms, with the Halsey chosen as the best fit to the experimental data. Drying was performed in a convective dryer. Temperatures used were 40, 50, 60, 70 and 80°C, with air velocity constant at 1.5 m/s passed upwards through the sample. Sample mass was measured in situ by suspending the sample from a digital balance on a tray. The Midilli-Kucuk model provided the best fit to the experimental data. The first term of the analytical drying model for cylinder geometry was used to estimate the effective diffusivity (0.74x10^{-9} to 2.37x10^{-9} m^2/s) and activation energy (27.9 kJ/mol) of the material.

Lemus (Lemus et al 2008) determined the desorption isotherms and drying kinetics of the red macroalgae *Gracilaria chilensis*. Desorption was performed at 5, 25 and 40°C with fixed humidities generated by saturated salt solution. The Halsey model was found to best fit the desorption data. The equilibrium moisture for each drying temperature was assumed to be represented by the Halsey model at 40°C, because the drying air outlet temperature was 45°C+-5°C. Drying temperatures were 40, 50, 60 and 70°C, with air flow rate of 2m/s. Material mass was measured by removal from heating

source and measurement via mass balance. The drying rate of the alga increased as temperature was increased. The Page model was found to fit the drying data best.

Tello-Ireland (Tello-Ireland et al 2011) studied the influence of air temperature during drying on the desirable characteristics of the alga *Gracilaria chilensis*. Characteristics tested were the drying kinetics, functional properties, colour, protein and antioxidant content, texture and agar yield. A laboratory convective oven was used to dry the samples, with air temperatures ranging from 40 to 70°C and a constant air flow of 2 m/s. The results from drying kinetics were fitted to the Weibull model. The other material quality parameters were tested experimentally using the dried material. Generally, the quality parameters decreased with increasing temperature due to protein denaturation at the higher temperatures. The highest temperature tested corresponded with the highest agar yield, but also caused degradation of the algae quality.

2.2.1.2 Other biomaterials

Krokida (Krokida et al. 2002) researched the design of rotary dryers for olive cake, a fibrous by-product of olive oil production which is directly burned for energy. The diffusion constant for drying olive cake was determined experimentally on a laboratory scale by passing hot air through the material. Controlled variables in their lab scale experiments were air humidity (1 and 3% relative humidity), velocity (2, 3 and 5m/s) and temperature (50 and 70°C). The range of variables used for dryer design were air temperature (50 to 135°C), initial air humidity (0.01 to 0.09 kg H_2O/kg db), and air velocities (0.5 to 3 m/s). An empirical equation ($K_m = K_0 T^{k_1 k_2 k_3}$, where k_m is the drying constant) was fit to the experimental data to represent drying rates, and the drying rate model was used to help design a rotary dryer. The economics of the dryer were also considered, and a sensitivity analysis was conducted on the effects of process variables (heating air velocity and temperature) on the process unit costs. Temperature had the largest effect on the product cost, while the effect of velocity on costs was less significant.

Langrish (Langrish 2008) experimentally determined drying curves for cellulosic fibres sourced from citrus fruits. Air was used as the drying medium and was heated to the desired temperature in a heat exchanger. Steam from a small boiler was used as the heating medium. The dry bulb and wet bulb temperature of the air were controlled through heating the air and the injection of steam respectively. The wet bulb temperature was set to 40°C, and dry bulb temperatures of 50, 60 and 80°C were used. It is important to note that the wet bulb temperature is an indirect measure of the relative humidity

of the air. Air velocity through the sample was kept constant at 1.3 m/s. The normalized drying rate curve for the citrus fibres was found to be very similar to previously determined curves for sugar beet fibres.

2.2.1.3 Summary

The drying kinetics studies reviewed predominately use some type of empirical model to represent drying rates. However, the first term of the Fick's law analytical model was commonly used to represent or calculate the relationship between drying rates and temperature by calculating D_e and then using the Arrenhius-type model to obtain E_a and D_0. This is usually performed without consideration of any impact from the use of only one term of an infinite series, which makes it functionally equivalent to the Henderson and Pabis empirical model (Equation 2.4) where $a = \frac{8}{\pi^2}$ and $k = \frac{\pi^2 D_e}{4L^2}$. Using only one term of Equation 2.26 is justified by stating that it is sufficient for long drying time but without description of what a 'long drying time' is or why this is the case. This is an uncertainty in model application that should be considered.

As mentioned above, a common methodology is to represent the drying kinetics with an empirical model but then applying the semi-empirical analytical solution model to calculate diffusivity. Direct application of the F2L model to represent drying would be advantageous if it can accurately represent experimental data. The model has been used directly to model drying by some authors (some examples are Friere et al 2001, Slogrove et al 2017, Bezzina et al 2018). This approach would remove the need to use two different models for representation of experimental data and to investigate drying response to temperature. The F2L model (as a semi-theoretical model) can also be directly used to represent drying as a function of drying conditions. The implications of the number of terms used in modelling is not widely considered in literature and should also be investigated.

The drying rate is noted to increase with drying temperature in all studies reviewed. This relationship is well known and temperature is considered to be the highest impact variable for drying rates. The effect of temperature was found to fit the Arrenhius-type relationship well in all studies that tested for it. E_a and D_0 were determined from experimental data in all cases via an empirical method. Temperatures used in the drying of algal biomaterials are typically limited to a maximum of 60 to 70°C to prevent degradation of proteins and charring or discoloration.

2.2.2 Drying Gas Velocity

Drying air or gas flow rate is a design variable for most drying equipment. The gas flow rate directly affects convective mass transfer rate. The F2L analytical model assumes that diffusion transfer is the limiting step in drying, and that convective transfer occurs at a much higher rate such that any surface moisture is removed from the system immediately. The validity of this assumption can be evaluated with the mass transfer Biot number Bi_m. Its definition is shown in Equation 2.38 below;

$$Bi_m = \frac{h}{D}L$$

Where h is the convective mass transfer coefficient. A value of Bi_m below 0.1 indicates that the system in question is limited by convective transfer from the surface, whereas a value of Bi_m above 0.1 indicates a system limited by diffusive transfer to the surface (as assumed by the F2L drying model).

Values for the convective transfer coefficient for water over a range of conditions relevant to biomass drying (18.5 to 60.2°C, and 0.27 to 2.04 m/s gas velocity) have been evaluated by Poor et al (2020) as between 0.0029 and 0.108 m/s, while diffusivity is typically found to be between $1e^{-6}$ and $1e^{-10}$ m^2/s in drying kinetics studies. Taking h=0.0029 m/s and D=$1e^{-6}$ m^2/s as a worst case example, $Bi_m = 2900L$. This shows that it is reasonable to assume that drying is limited by diffusion, and gives weight to the related assumption that any surface moisture is immediately removed from the system.

If surface moisture is being immediately removed from the system, it is logical to then conclude that an increase in the convective transfer rate (e.g. from increased gas velocity) should not have any effect on the overall drying rate for the system. There is no physical contact between internal moisture and drying gas, so there should be no effect on diffusion rate either. However, several studies of biomass drying show some type of dependence between drying rates and gas velocity despite their use of similar conditions as those described above. The following is a review of several drying kinetics studies that included experimentation of whether drying gas velocity affected drying rates when using the F2L model to represent drying. Given the limited number of macroalgae drying studies that have examined the impacts of gas velocity, studies of other biomaterials were also examined.

Freire (Freire et al. 2001) studied thin layer drying kinetics of olive bagasse, a fibrous biomaterial. They used a laboratory scale dryer for experimentation, which used flue gases resulting from combustion of propane as the drying gas medium. The sample was placed in the hot gas stream on top of piezoelectric sensors, which allowed in situ measurement of mass versus time. The fluctuations in the sample mass and weight measurements brought about by gas drag were minimized by periodically

directing the hot air stream through a bypass of the drying chamber. The variables that were tested for their effects on drying kinetics were gas velocity (from 0.5 to 2m/s), gas temperature (125-250°C) and slab thickness (0.002 to 0.004m). Thickness was varied by sieving the olive bagasse and drying separate fractions. The material was laid out as a single layer of particles with minimal touching between particles to ensure maximised exposure to the drying gas. Temperatures above 250°C were tested but were found to cause pyrolysis in the sample.

Drying was found to occur mostly under falling rate conditions. All variables tested were found to have some effect on the drying kinetics, with gas temperature having the greatest influence. While increases in gas velocity led to increased drying rates, Friere et al. observed a critical value at 1.5 m/s, where further increases in velocity had no significant effect on drying rate. It was suggested that above this point, the drying kinetics became limited by internal mass transfer and the F2L model assumptions were met. The experimental data was fitted to a two-term approximation of the analytical Fick's Law solution for spherical geometry, where drying of a single grain was modelled with the assumption that drying is even across all grains. The analytical drying model was found to have a high accuracy in predicting drying kinetics for the conditions studied. Deviation in the initial drying stage was adjusted for using a correction factor as shown in Equation 2.38, where F_c is the correction factor. They mention it is only translating the line upward, but no data was shown to prove this didn't affect the model in some other way. It is proven in later chapters in this work that this initial deviation is minimised with the use of additional series terms. This reinforces the need for a clear understanding of series terms implications.

$$MR_c = \frac{MR}{F_c} = \frac{6}{\pi^2 F_c}\ exp\left(\frac{(-D_e\pi^2 t)}{r^2}\right) + \frac{6}{4\pi^2 F_c}\ exp\left(\frac{(-4D_e\pi^2 t)}{r^2}\right) \quad (2.38)$$

The critical point found in this study was expected by Friere et al. to correspond with a sufficient convective mass transfer rate to meet the assumption of a sufficiently high gas flow such that diffusive transfer is rate limiting at all times during drying. It is suspected that they had a critical point occurring because of their geometry choices. The material was set up as a single layer of small, regularly sized particles without touching. This ensures all particles have full and even surface area exposure to drying gas, which closely represents geometry in the F2L model derivation for a sphere of material. This closeness of geometry is then why air velocity is acting as theoretically expected. This geometry is easy to define for a separated material, but is difficult for clumping or irregularly size material. The geometry choice is fine for representing specific systems such as the initial curtain of falling material in an FRD. However, it is not a good representation of many other real systems; for example, there

will be gas channelling around falling curtains in a real FRD and therefore this may not well represent all material.

Several other studies show a dependency between air velocity and diffusivity without evidence of a critical velocity point (Djaeni and Sari 2015, Chkir et al 2015, Santacatalina et al 2016). This point could still exist for those materials but at a higher value than those tested. This would place the critical velocity well above the typical ranges used in industrial drying equipment (0.5 to 2m/s) for those materials and therefore of limited use for equipment design. These studies are reviewed below.

2.2.2.1 Macroalgae

Mohamed (Mohamed et al 2007) experimentally determined the convective thin layer drying kinetics of the macroalga *Gelidium sesquipedale* with a convective solar heated air drying system. Drying temperatures used were 40, 50 and 60°C, and air flow of 0.0227, 0.0556 and 0.0833 m^3/s (corresponding to about 0.04 to 0.15m/s air flow rate across the material trays). Their results show purely falling rate drying, with no constant rate period. Increasing drying temperature caused an increase in drying rate, while no significant change in rate was found when air flow was increased. Their range and magnitude of air velocities tested is was very low suggesting that drying may well have been non-convective in nature, leading to difficulty in determining an impact of gas velocity.

Djaeni (Djaeni and Sari 2015) tested convection drying kinetics of the macroalga *Eucheuma cottonii* and determined whether dehumidification of the air had an effect on the drying rate. Temperatures used were 40, 50, 60 and 70°C, and air flow rates were very high, at 5 and 7m/s. Their results show an increase in drying rate both with increasing temperature and air flow. The addition of dehumidification had an inconsistent effect, showing some increase in rate at 50°C but no change at 60°C.

Studies of air velocity effects on drying of other macroalgae are limited in the literature. In specific, there have been no studies identified that consider the effect of drying gas velocity on macroalgae drying using ranges that are represent those typically used in industrial equipment design i.e. 0.5 to 2 m/s.

2.2.2.2 Other biomaterials

Chkir (Chkir et al 2015) tested effects of air velocity and temperature on drying kinetics and properties of brewers grain. A convective drying system was used, with air temperature of 40, 50 and 60°C and

velocities of 0.7, 1 and 1.3 m/s. Their results show an increase in drying rate as temperature and air velocity increased, with no apparent critical velocity point found for the tested range.

Santacatalina (Santacatalina et al 2016) determined the drying kinetics of eggplant at a range of air flow rates and low temperature. A convective drying system was used for the experiments. Temperatures used were -10, 0 and 10°C. Air flow rates used were 1, 2, 4, and 6m/s. Sample mass was measured in situ at intervals. The drying rate increased with the air flow rate across the range used.

2.2.2.3 Summary

There have been several studies that do show an apparent relation between drying gas velocity and drying kinetics for a wide range of biomaterials, where increases to gas velocity cause an apparent increase in drying rate. These observations of the effect of air velocity is at odds with the model assumptions of drying purely limited by internal moisture transport. Some of these studies show a relation up to a 'critical' velocity point, with no further increase in drying rate as gas velocity is increased past this point. The expectation is that studies that show a critical velocity are using geometries that can closely mimic the theoretical geometry conditions – they explicitly state they use separate very small particles with one particle wide or extremely thin layers. This ensures all particles have full and even surface area exposure to drying gas.

Drying studies with more complex material geometry (i.e. multiple layers of particles) do not appear to show a critical velocity for air flow ranges relevant to industrial drying equipment design. Complex particle geometries are more applicable to a wider range of drying equipment than the ideal case described above. Furthermore, no studies were identified that provide insight as to what causes this apparent relationship – no conclusions can be made from material properties or drying conditions as to whether that material will exhibit a relationship with air velocity. Some effect caused by particle geometries may be causing the apparent relation between drying gas velocity and drying rates. Finally, an understanding of the effect of air velocity below any possible critical velocity point is still relevant for equipment design purposes – critical velocities that were identified in literature are at the upper end of typical drying equipment air velocity ranges.

2.2.3 Material Bulk Density

The density of compressible materials can be used as a design variable for several types of drying equipment, including solar and belt fed convective dryers. Compressible materials are those with irregularly shaped particles that result in a large void fraction when unconstrained (e.g. cotton, bagasse and other fibrous materials). Compression forces the material to take up more of the void fraction, and results in a higher bulk density for a given volume. The bulk density of material can vary in drying systems. For example, in a flighted rotary dryer material in a falling curtain will exhibit a low density compared to material that is constrained within the flights or on the base of the drum for. Material compression can be a design variable for systems with a confined bed of material, and increased density would allow for more material to be dried per area or batch. The macroalgae used in this study are highly compressible. As an example, the loose bulk density of the material is around 30-50kg/m^3, but the true density is far higher (the macroalgae are neutrally buoyant in water). The material can be compressed by hand up to at least 500-600 kg/m^3. This is caused by flexible and irregularly folding particles that in turn result in large void fractions unless compressed.

The theoretical drying model described in Section 2.1.3 was developed to be independent of material mass, representing the material as an infinite slab of a defined thickness L. However, the model was not developed with consideration for compressible materials; a varying bulk density means that there can be differing mass of material for a given slab width. It makes logical sense that an increased amount of material for a given slab width and given drying conditions should result in a slower drying rate, due to a combination of increased mass of moisture and an increase in physical resistance to moisture transfer to the interaction surface. However, studies of the effect of bulk density on drying kinetics are exceptionally limited in the literature. Only two studies were identified that consider material bulk density effects on drying rates (Slogrove et al., 2017, Bezzina et al., 2018). Both were focused on drying of sugar cane bagasse and were undertaken under the supervision of the author of this thesis, including one study using an experimental apparatus developed by the author and described in chapter 4.

Slogrove (Slogrove et al 2017) studied the drying kinetics of sugar cane bagasse over a range of temperatures and bulk density, using radiative heating (i.e. with zero drying gas velocity). A lab scale oven was used for the drying kinetics experiments. Bulk density of the material was controlled by use of a fixed volume container, with differing loading of the container corresponding to different density. Densities used were 90, 110, 130 and 150 kg/m^3, and temperatures used were 120, 140 and 160°C.

The Fick's law analytical solution was used to model the drying kinetics data and had a generally high model fit. An example from this work is shown in Figure 2.4 for varying density of bagasse at 140°C. Effective diffusivity was found to be inversely related to the initial bulk density, where increases to the density caused a decrease in drying rate. An Arrenhius-type relation was applied to represent temperature and diffusivity relationship, where E_a was assumed to be constant, and D_0 changed with density. The relationship between D_0 and bulk density is reproduced in Figure 2.5.

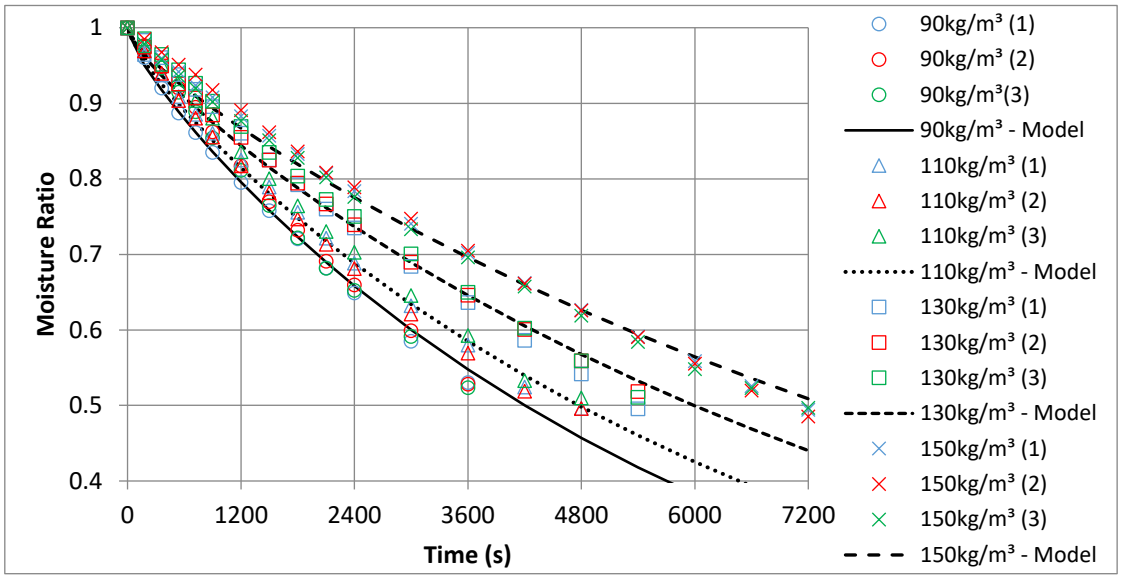

Figure 2.4; Experimental triplicate data and model fit at varying density for sugar cane bagasse; drying at 140°C. Reproduced from Slogrove et al. (2017).

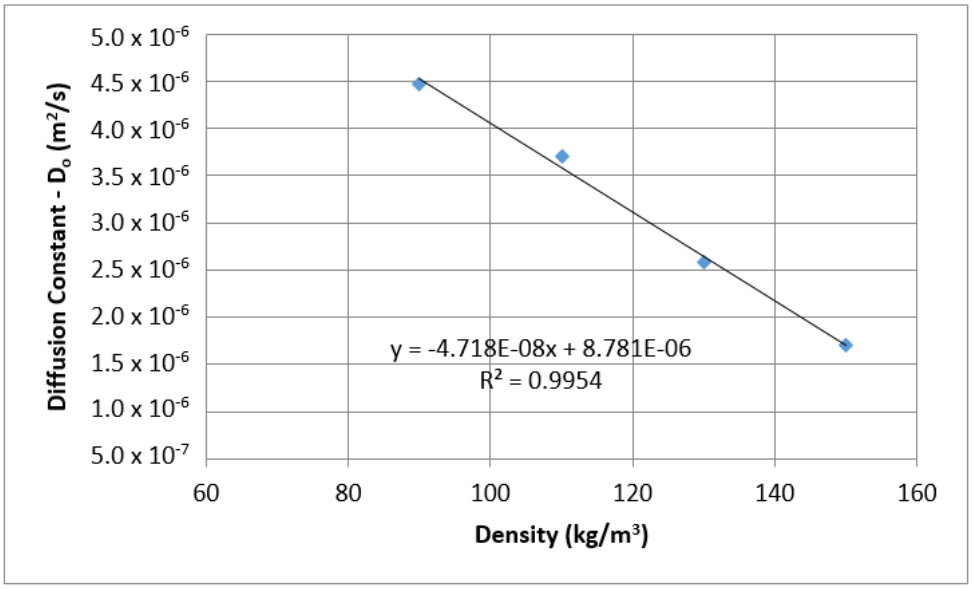

Figure 2.5; Relationship between diffusion constant D_0 and bulk density for sugar cane bagasse. Reproduced from Slogrove et al. (2017).

Bezzina (Bezzina et al 2018) further studied convective drying kinetics for sugar cane bagasse and studied the effects of both air velocity and material pack density. These variables were tested together to identify whether any interaction effects on diffusivity occurred. The equipment used in their study is the same equipment described in Chapter 4. The air velocities tested were 0.6, 1.0, 1.3, 1.7 and 1.9 m/s, and densities were 110, 130 and 150 kg/m^3. Statistical analysis of the experimental data showed that both air velocity and density had an effect on diffusivity. Relationships between D_0 and material density were provided for each air velocity tested.

2.2.3.1 Summary

Studies of the effect of material bulk density on drying rates are very limited in literature. The only literature studying this relationship identified in this review are those co-written by the author using the apparatus described in Chapter 4, characterising density effects for sugar cane bagasse. It is not known whether the material density has a significant impact on drying rates for other compressible biomaterials like *U. ohnoi* and *O. intermedium*. Any possible relationship between bulk density and drying rates for the target macroalgae is unknown and should be experimentally determined.

The Fick's law analytical model is universally applied with a lumped parameter approach which results in any difference in properties (other than temperature and slab width) being considered as a 'new' material. Thus, a different bulk density for a material results in a new value for D_e and would therefore be considered a 'new' material under this approach. This is not useful for an equipment design approach, as it results in a different equation for diffusivity as a function of temperature for every density and gas velocity combination tested or required. A better approach for the purposes of developing a drying rate for design would be to include the effects of the variables in an expression for D_e while retaining the theoretically sound Arrenhius-type representation of the impacts of temperature (Equation 2.29). Of the two variables in this relation, E_a is considered to be related to the internal moisture binding 'strength' that has to be overcome for drying to begin, and should therefore be independent of external conditions such as material bulk density. It is expected that these external variables should be considered to cause changes in D_0 as shown in the approach used by Slogrove et al (2017) and Bezzina et al (2018).

The approach used in Slogrove et al (2017) and Bezzina et al (2018) was to consider D_0 as a function of external variables that affect drying (i.e. gas velocity and material bulk density). These studies show

that air velocity and bulk density are able to be considered as separate non-interacting effects in this approach, confirmed by statistical analysis. It is not currently realistic to consider both D_0 and E_a varying with external conditions; this would be possible if either or both had a theoretical basis or were directly measurable, but they are both semi-empirical values and have only ever been determined in literature via an empirical approach. The addition of new terms is similarly arbitrary without a full and clear understanding of the mechanisms behind why these variables have an apparent effect on drying rates.

2.3 Conclusions

An accurate understanding of material drying kinetics, particularly as a function of dryer design variables, is required to produce an optimized design of industrial scale drying equipment. Modelling of drying kinetics for new materials typically requires experimental determination because the effect of internal material properties on drying is not well understood and there is an absence of unifying theory. Furthermore, a first principles approach is prohibitively complex to quantify because it requires several undefined coefficients, adding to uncertainty and generally being too mathematically complex to be useful or broadly utilised in industry for the design of dryers. In the search for a more pragmatic but accurate approach the literature review identified several empirical and theoretical modelling approaches used to represent drying of biomaterials.

A theoretical model developed from an analytical solution of Fick's law of diffusion was identified as a pragmatic compromise between accuracy and industry usability, but its validity in modelling macroalgae has not been confirmed. Furthermore, it was noted that the number of terms chosen in studies that have utilized the Fick's law drying model appears arbitrary. One aim for this work is then to determine if it can well represent drying of the two macroalgae *Oedogonium intermedium* and *Ulva ohnoi*. Empirical models described in this review were considered less useful in that they cannot be relied upon for accurate predictions outside of the experimental conditions used, and there is no direct link or theoretical basis for relationships between model parameters and drying conditions to drying rates. Any effects of the number of series terms used on modelling results should be investigated. The equilibrium moisture content of macroalgae needs to be determined as a part of the Fick's law analytical model and is a function of drying temperature and gas humidity. A promising method for the control of humidity in equilibrium moisture via the use of saturated salt solutions as per Greenspan (1976) was identified and will be used in the following chapter. The review identified

specific temperature and drying gas velocity ranges suitable for preserving algae quality and in line with typical industrial drying equipment.

The review of drying theory and literature identified drying gas temperature, drying gas flow rate, and material bulk density as important equipment design variables that have been observed to affect drying kinetics of biomaterials. Material bulk density was noted to affect drying for another compressible particulate biomaterial, but otherwise has not been comprehensively reported in the literature. It was concluded that dependence on air velocity may be related to material geometry choices in experimental design, with studies that used a simple geometry with very thin layer (<0.01m) showing no dependence. Studies with thicker slab widths have shown dependency between drying rates and gas velocity. It is expected that layer sizes more representative of industrial scales are likely to show some relationship with drying gas velocity. In order to provide useful relations that are applicable to industry drying systems it is essential to study whether any dependence between gas velocity and drying rate exists, particularly in algae drying where no such studies are available.

The core aim of this research is then to develop an accurate and pragmatic model of drying rates for the two specific macroalgae, investigating the effects of drying temperature, drying gas flow and material bulk density. Finally, there is a need to prove this type of drying kinetics model can be used to represent drying at larger scales – modelling is performed at laboratory scale (often with unrealistic material thickness or gas velocity) in almost all literature, but little was identified that proves its accuracy at representing scaled up systems.

Chapter 3

Sections 3.1 and 3.2 in this chapter have been published in 'Walker, C.; Cole, A.; Antunes, E.; Sheehan, M. Equilibrium Moisture and Drying Kinetics Modelling of Macroalgae Species *Ulva ohnoi* and *Oedogonium intermedium*. *Clean Technol.* **2020**, *2*, 225-239.' The article and its experimental work were performed in their entirety by myself, with the other authors providing academic and editorial input. These sections are presented as published, except for changes in formatting to match that of the rest of the thesis.

3. Material Properties and Initial Parameters

The previous chapter has covered the literature, theory and analysis methods used to characterize the drying kinetics of biomaterials. For materials experiencing falling rate drying, the Fick's law analytical model was found to be an effective modelling approach. However, several parameters must be determined to enable moisture drying data to be modelled via this method. This includes the equilibrium moisture content isotherms, initial moisture content of material and determination of the activation energy of drying.

In this chapter, lab scale experimental work is presented that determines these identified parameters for a thin layer of macroalgae. The equilibrium moisture contents of salt- and fresh-water macroalgae species are experimentally determined as a function of relative humidity and temperature. The best fit of a range of isotherm models is presented. Thin layer drying kinetics are performed for typical biomass drying temperatures under both convective and radiative heating. The presence of falling rate drying periods and validity of the Fick's law analytical model is examined. The effectiveness of the two heating methods (ie. with and without air flow) are compared. Drying via radiative heating is used to determine diffusivity as a function of temperature, and extract activation energies of drying for both materials. Finally, numerical considerations in the application of Fick's law analytical model, such as the number of terms of the infinite series, and variance in the equilibrium moistures are examined.

3.1 Methodology

3.1.1. Materials

As outlined in Section 1.2, the algae species used in this study are *U. ohnoi* and *O. intermedium*. In both kinetic and equilibrium tests, surface moisture was removed from the algae samples via use of lab scale centrifuge (Koh-I-Noor Engineering Works, Punjab, Pakistan) at 2800 RPM. Algae samples

were dewatered in the centrifuge until outlet moisture flow completely stopped, which provided a consistent starting point for the drying and equilibrium moisture trials. Nine dewatered subsamples of the algae were used to determine the initial moisture content (M_0) and to evaluate consistency in the determination of moisture content following the dewatering step. Dry weights were obtained using a moisture analyser (MA-45, Sartorius AG, 37075 Goettingen, Germany) drying at 110°C to ensure complete moisture removal. Average initial moisture content (following dewatering) and 95% confidence interval for *U. onhoi* was 81.73% weight ± 1.4% (relative), and 83.54% weight ± 1.1% (relative) for *O. intermedium*. The low variance in these starting-point (dewatered) moisture contents demonstrated both consistency in dewatering process and in the use of the MA-45 to obtain moisture content and dry basis algae mass values.

3.1.2 Equilibrium Moisture experiments

The equilibrium moisture content is the final moisture content that can be achieved by drying material at a given set of conditions below 100°C. A non-zero final moisture content occurs because the material also adsorbs moisture from the surroundings. Equilibrium occurs when the drying rate falls to where it is equal to the rate of adsorption. This equilibrium moisture content depends on the air temperature, air relative humidity and material properties.

The setup used for the equilibrium moisture experiments consists of fifteen sealed containers (see Figure 3.1 for an example) fully immersed in a hot water bath to control internal temperature. Each container was 500mL in volume and had a mesh platform suspended above a saturated salt solution filling a third of the container volume. At a given temperature, a saturated salt solution will achieve equilibrium with the air inside the container, giving a fixed humidity (Greenspan 1976). Temperature (T) and humidity (E_{RH}) inside the sample containers were measured using a humidity probe (Center 313, Center Technology Corporation, Taipei, Taiwan). Fresh centrifuged algae samples, weighing approximately 4g each were placed on the mesh platforms inside each container. Excess salts were used as a visual indicator to ensure saturated solutions during each experiment. The solutions used (and their respective relative humidity) at equilibrium were lithium chloride (11%); sodium acetate (20%); magnesium chloride (31%); sodium carbonate (43%); and sodium bromide (52%). Three containers of each solution were used to obtain triplicate results for each temperature and humidity.

The mass of the algae samples was measured daily after being left for a week to reach equilibrium. Three consecutive and constant measurements were obtained to ensure equilibrium. The measured equilibrium masses were converted to moisture content in % dry basis, via Equation 3.1;

$$M_e(\%db) = \left(\frac{M_{e,g} - D}{D}\right) \tag{3.1}$$

Where $M_{e,g}$ is the equilibrium mass of the algae in grams, and D is the dry weight of the algae in grams. Algae dry weight was determined using the Sartorius MA-45 through fully drying the material at 110°C. Refer to Table 2.2 for the equilibrium isotherm models that were fit to the experimental data.

Figure 3.1; Example of equilibrium moisture experimental set-up.

3.1.3 Drying Kinetics experiments

Freshly centrifuged algae was used to experimentally investigate drying kinetics. Given proteins in algae are prone to denaturation at high temperature, and characteristics such as colour also deteriorate (changing from green to brown) at high temperature, temperatures used for the

experimental runs were 40, 45, 50, 55 and 60°C. Three repeats were performed for each temperature. The initial material thickness (L=0.01m) and the initial fresh mass was kept constant between runs.

A Sartorius MA-45 moisture analyser (Figure 3.3) was used for the radiation drying experiments. Relevant technical details for the moisture analyser are as follows; frequency 48-60Hz, temperature range 40-230°C in 1°C increments, mass measurement accuracy of 0.2%, balance resolution 1mg. Initial fresh masses were set at 1.5g. Triplicates of moisture ratio versus time show excellent consistency in experimental moisture profiles obtained under radiative drying conditions (Figure 3.2).

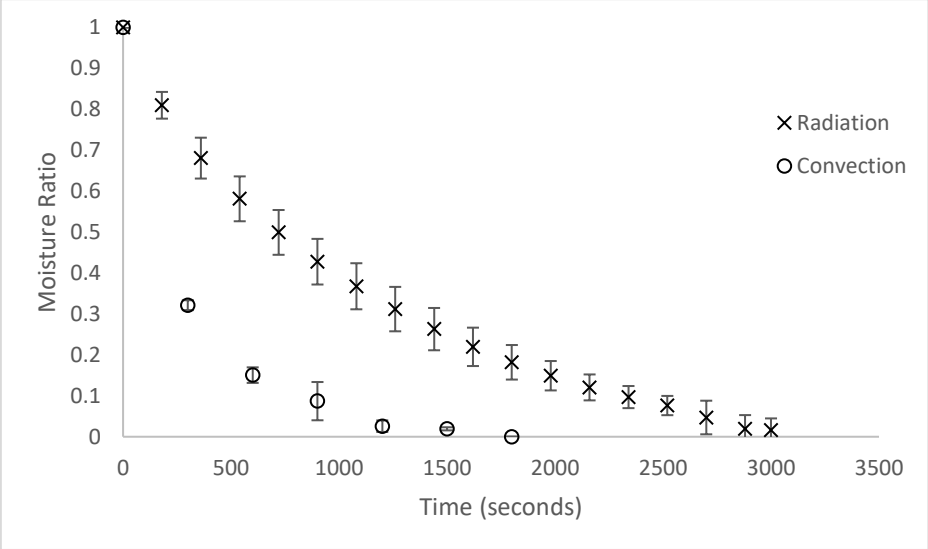

Figure 3.2; Triplicate moisture profiles for U. ohnoi at 40°C for a) radiative and b) convective drying.

Figure 3.3; Sartorius MA-45 moisture analyser.

A convective food desiccator (Ezi-Dri FD-1000, Hydraflow Industries Limited, Upper Hutt, New Zealand) (Figure 3.4) was used for the convection drying experiments. The equipment passes heated air through vertically stacked trays on which the algal material is placed. Gas temperature (40, 50, 60°C) and flow rate (0.7m/s) were confirmed from measurement of outlet conditions via hot-wire anemometer (AM-4214SD, Lutron Electronics Enterprise, Taipei, Taiwan). Initial biomass weight was measured before placement in the stacked trays. Trays were removed in a randomised order at discrete time intervals and material weight was obtained at each interval. Randomisation was chosen to reduce any potential effects of tray positions on the drying kinetics. Humidity of the exhaust air was measured directly using a handheld humidity meter and probe (Center 313, Center Technology Corp., Taipei, Taiwan). Initial fresh masses on each tray were set at 7g.

Figure 3.4; Convective food dryer.

3.2 Results and Discussion

3.2.1 Analysis Methods

3.2.1.1 Equilibrium Moisture

For each algae type, two equilibrium moisture content models (BET and GAB) were fit to the experimentally determined equilibrium moisture content at each temperature and relative humidity. Model fitting was performed by adjusting model parameter values to minimize the total sum of square errors between the model and the triplicate experimental data sets. Initial guess values for the model fit process were chosen to represent the expected parameter range for the equations, and a wide range of different initial parameter values were tested to ensure the global minimum was found. These calculations were performed using Microsoft Excel using the solver function with GRG nonlinear

solver method. The objective function is summarised in Equation 3.7, where m corresponds to a given data set, and the objective function (Obj) minimized by varying the model constants.

$$Obj = \sum_{m=1}^{3} \left(\sum (M_{e,m} - M_{e,exp})^2 \right) \tag{3.7}$$

3.2.1.2 Drying Kinetics

The raw experimental data of mass against time in the convective and radiative drying experiments were converted to moisture ratio versus time. The analytical solution to the Fick's second law model for drying with infinite slab geometry was fit to moisture ratio versus time data sets. Model fitting was performed by minimization of the total sum of square errors between the model and experimental data, with the model representing the best fit to all three sets of data at a given condition. Ten terms of the infinite series were used in modelling to ensure convergence in the infinite series solution (analysis of this choice and its effects are shown in Section 3.3.2). These calculations were performed using Microsoft Excel with the solver function and GRG nonlinear solver method, assuming constant relative variance in the experimental data. The objective function is summarised in Equation 3.8, where m corresponds to the number of data sets. The objective function (Obj) was minimized by varying the magnitude of the effective diffusivity parameter (D_e).

$$Obj = \sum_{m=1}^{3} \left(\sum (MR_m - MR_{exp})^2 \right) \tag{3.8}$$

3.2.2 Equilibrium Moisture Modelling

Of the models used, the best fit (i.e. demonstrating the highest R2 value) for both species over the conditions tested was the GAB model. This model is recommended to be adopted for both species. The model constants and the goodness of fit (R2) for the GAB equation are summarised in Table 3.1. Graphs of the experimental equilibrium moisture compared with the GAB model predictions are shown in Figure 3.5 for both species.

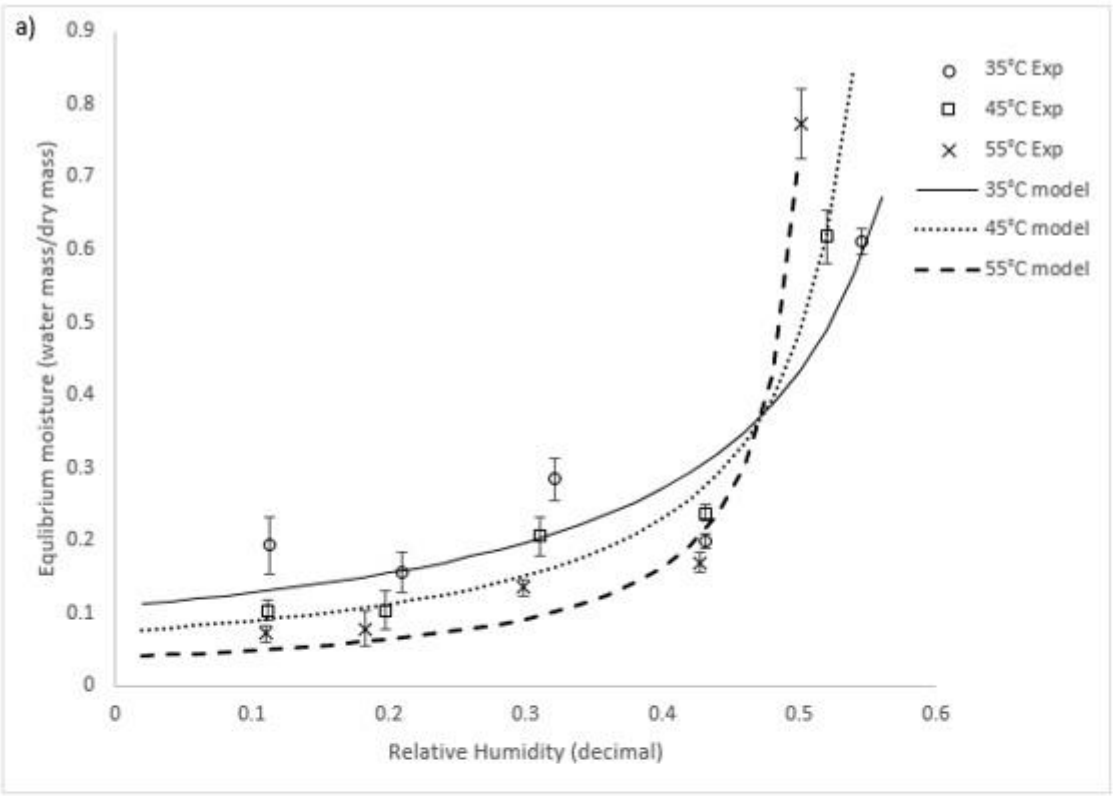

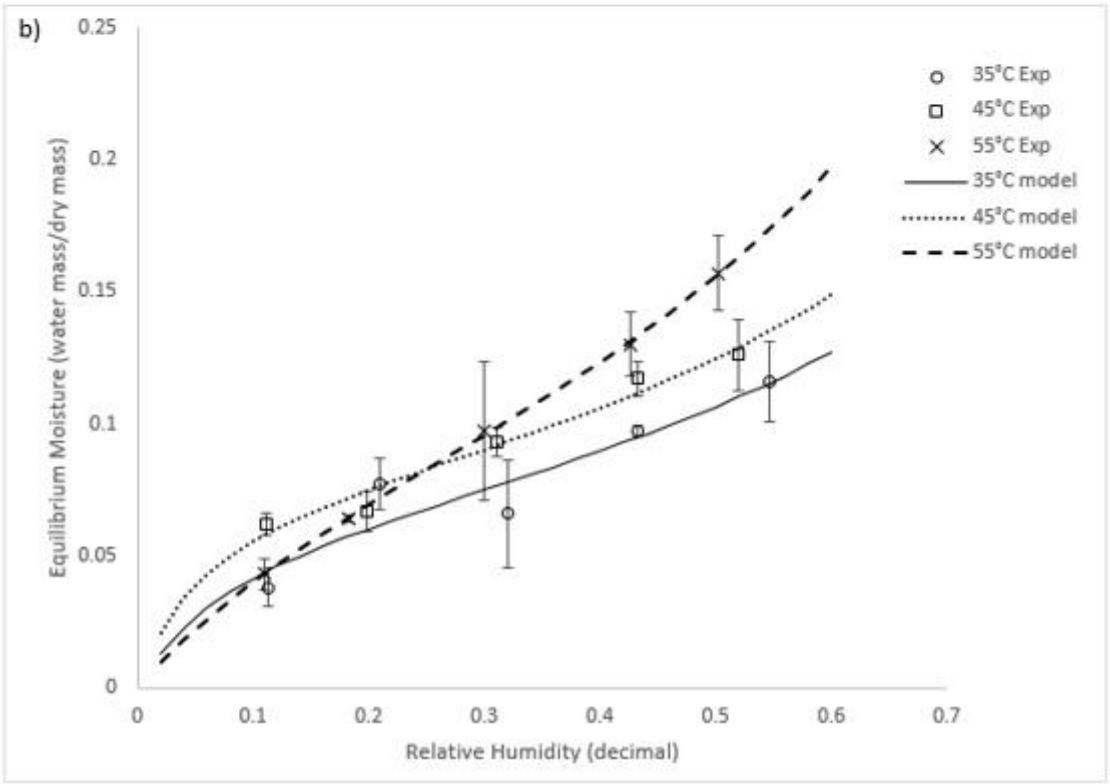

Figure 3.5; GAB model and experimental data for a) U. ohnoi b) O. Intermedium.

Table 3.1; GAB model coefficients and fit.

Algae	Temperature (°C)		
	35	45	55
U. ohnoi			
A	0.109	0.075	0.040
B	1.496	1.689	1.889
C	2.68×10^5	2.847×10^5	2.38×10^5
R^2	0.844	0.977	0.989
O. intermedium			
A	0.069	0.077	0.106
B	0.824	0.845	0.894
C	13.39	21.04	5.29
R^2	0.881	0.967	0.999

A statistical analysis was performed using SPSS software to determine the significance of temperature and relative humidity for determining the equilibrium moisture. A general linear univariate model analysis was used, which provided regression and variance analysis of the equilibrium moisture as the dependent variable against temperature and relative humidity. The analysis showed that both temperature and relative humidity are statistically significant in their ability to predict changes in the equilibrium value for both species (significance<0.05 for all variables for both species). F-tests (a measure of the relative predictive ability) showed that, of the two variables, relative humidity is the best single predictor of the equilibrium moisture content. Comparing between the two types of algae, U. ohnoi exhibits a significantly higher equilibrium moisture content than O. intermedium. It is assumed that this is because U. ohnoi has reduced surface area (algal sheets are two cells thick rather than the single cell strings of O. intermedium) and is a salt-water alga.

At around 50% humidity for Ulva and 30% humidity for O. intermedium, there is a crossover point where higher temperatures result in higher equilibrium moisture than those observed at lower temperatures. Lemus et al (2008) had a similar crossover effect at higher humidities in their study of the red macroalgae *Agarophyton chilense*, as did Moreira et al (2017) for *Fucus vesiculosus*. They reasoned that this is due to solubility effects of polysaccharides and proteins that make up much of the alga solids mass. The crossover point would then be where these solubility effects on the equilibrium point become larger than effects of the surrounding atmospheric conditions. Similar results have been shown for other algae biomass, including *Gelidium corneum*, as well as other biomaterial with soluble components (Mohamed et al 2005, Al-Muhtaseb et al 2002). Both *U. ohnoi*

and *O. intermedium* have polysaccharide and protein content totalling about 60% of dry mass (Neveux et al 2014). It should be noted that the GAB equation is not designed to represent these interactions. As such, it follows that the parameters of the GAB equation are semi-empirical or empirical in this application, reinforcing the importance of experimental characterisation of algal species.

In general, equilibrium moisture isotherms and equilibrium moisture magnitudes for both species are similar to those for other macroalgae and biomaterials. Table 3.2 provides equilibrium moisture content values for this work and also for a variety of biomass types.

Table 3.2; Examples of equilibrium moisture contents for various biomaterials and algae.

Material	Temperature (°C)	Relative humidity (%)	M_e (%db)
Apple [34]	45	20-90	4-81
Pear [34]	45	19-93	2-73
Argan (leaves) [35]	40	7-90	3-30
Canola [36]	40	10-90	4-10
O. intermedium [this study]	45	10-50	6-12
U. ohnoi [this study]	45	10-50	10-60
Arthrospira platensis [20]	30	5-90	4-40
Fucus vesiculosus [15]	45	10-70	2-70
Macrocystis pyrifera [16]	50	10-70	5-200
Agarophyton chilense [24]	40	10-80	0.5-100
Gelidium corneum [32]	40	10-90	5-40

3.2.3 Drying Kinetics Modelling

During the parameter estimation for drying kinetics the empirical models were noted to have very similar parameters and R^2 values. An example of this is shown in Table 3.3 for *U. ohnoi* radiative drying at 40°C.

Table 3.3; Results of empirical model fitting for U. ohnoi drying at 40°C.

Model	Equation with parameters	R^2
Lewis	$MR = \exp(-0.001t)$	0.974
Page	$MR = \exp(-0.001t^{0.99})$	0.974
Henderson and Pabis	$MR = 0.98\exp(-0.001t)$	0.974
Two-term exponential	$MR = 0.026\exp(-0.04t) + 0.974\exp(-(0.04 \times 0.026)t)$	0.974
Diffusion approach	$MR = 0.026\exp(-0.024t) + 0.974\exp(-(0.39 \times 0.024)t)$	0.974
Logarithmic	$MR = 0.98\exp(-0.001t) + 0$	0.974
Midilli and Kuck	$MR = 0.96\exp(-0.001t^{1.04}) + 0t$	0.974

This appears to be occurring because the models can all be simplified to the Lewis model. Because the Lewis model finds an accurate fit (high R^2) the other models are converging to that same fit, with parameters that make them collapse to the same as the Lewis model.

The model predicted effective diffusivities for both *U. ohnoi* and *O. intermedium* at each temperature were determined by including the GAB modelled equilibrium moisture contents (M_e). The parameter estimated effective diffusivities are shown in Table 3.4 for both species. The effective diffusivity is lower for *O. intermedium* than *U. ohnoi* and this is likely due to the tendency for *O. intermedium* to clump together when harvested, which reduces overall contact area for drying compared with individual blades of *U. ohnoi*.

Diffusivity values for the two species are similar to those of other macroalgae, summarized in Table 3.5. However, diffusivities for both algae species are high compared to those determined for microalgae drying. For example, effective diffusivities for spirulina drying under convective conditions were in the range 3x10-10 to 7x10-10 m2/s (Dissa et al 2014). Both species of macroalgae have relatively high effective diffusivities compared to other biomaterials, such as wood and fruit slices, which indicates a lower internal resistance to diffusion for macroalgae. This is likely due to the comparative simplicity of the algae material combined with the large discrete particles giving a high void fraction. The algae cells also use diffusion across cell walls to transfer water and nutrients from their surroundings. This predisposition could be enhancing the drying rate in comparison to material like wood and fruits. Generally, biomaterials with comparatively lower effective diffusivities have outer solid surfaces (eg. bark) that do not facilitate moisture transfer (to the same extent that algae

does), as well as being materials with more complex structures (e.g. lignin, fibres) that include multiple different internal layers.

Table 3.4; Effective diffusivity from radiative and convective drying.

Temperature (°C)	Radiative heating: D_e (m^2/s)		Convective heating (0.7m/s): D_e (m^2/s)	
	U. ohnoi	*O. intermedium*	*U. ohnoi*	*O. intermedium*
40	$3.18x10^{-8}$	$2.32x10^{-8}$	$1.17x10^{-7}$	$5.66x10^{-8}$
45	$3.96x10^{-8}$	$2.45x10^{-8}$	-	-
50	$5.47x10^{-8}$	$3.63x10^{-8}$	$1.40x10^{-7}$	$6.66x10^{-8}$
55	$5.87x10^{-8}$	$4.02x10^{-8}$	-	-
60	$8.75x10^{-8}$	$4.82x10^{-8}$	$1.48x10^{-7}$	$8.94x10^{-8}$

Table 3.5; Examples of effective diffusivity values for various macroalga during convective drying.

Biomaterial	Temperature (°C)	Air velocity (m/s)	Diffusivity (m^2/s)
Fig (Xanthopoulos et al., 2009)	45-65	1-5	$3\text{-}16\ x10^{-10}$
Persimmon (Carcel et al., 2007)	50	0-12	$2.4\text{-}6\ x10^{-10}$
O. intermedium [this study]	40-60	0.7	$5.7\text{-}8.9x10^{-8}$
U. ohnoi [this study]	40-60	0.7	$1.2\text{-}1.5x10^{-7}$
Arthrospira platensis (Dissa et al., 2014)	40-60	0-1.2	$3.1\text{-}6.7x10^{-10}$
Durvillaea antarctica (Uribe et al., 2017)	40-80	1.5	$0.7\text{-}2.4x10^{-9}$
Fucus vesiculosus (Moreira et al., 2017)	35-75	2	$1\text{-}3x10^{-10}$
Himanthalia elongata (Gupta et al., 2011)	25-40	2	$5.6\text{-}12.2x10^{-7}$
Macrocystis pyrifera (Vega-Galvez et al., (2008)	50-80	2.1	$5.6\text{-}10.2x10^{-9}$

Graphs of the experimental data for radiative and convective drying of both algae species are compared to each fitted model in Figures 3.6 and 3.7. The general fit of the Fick's second law model to the experimental data is excellent and comparable to the empirical models tested (R^2 values in all runs except for 40°C radiative heating for O. intermedium were between 0.945 and 0.99). As such, the F2L model will be used for drying kinetics modelling in the thesis for the advantage of directly

modelling drying as a function of equipment design variables. However, the F2L model has a tendency to under predict the experimental data for moisture ratios between one and 0.3, then over predict as the moisture ratio approaches zero. Worst fit was O. intermedium at 40°C under radiation drying, where the tendency of the algal biomass to clump unevenly caused an increase in the variance of the experimental data. Convection drying rates were higher than for radiation, with increased heat transfer and slab penetration likely to be the cause.

The assumptions made in the derivation of this analytical solution are: initial moisture distribution is even; internal moisture transport is by diffusion only; drying gas volumes are large enough that surrounding environmental conditions are not changed by moisture transfer; slab thickness is constant throughout the drying process; temperature of the slab is isothermal and equal to the temperature of the surroundings; and bulk transfer of moisture (by convection) to the surroundings is sufficiently fast that drying is only limited by the internal rate of diffusion. These conditions are rarely if ever fully satisfied, and D_e is used in drying kinetics to pragmatically represent a global effective diffusivity, which accounts for these deviations. In this way, the diffusion coefficient consolidates the effects of deviations from these assumptions into a single (lumped) parameter model. This covers internal effects such as resistance to diffusion from material layers and a biomaterial's binding strength holding moisture internally, as well as external effects of temperature gradients, drying gas velocity and humidity. The effective diffusivity approach requires new experimental results for new materials, due to the influence of material properties. In the case of biomaterial drying there is typically some volume loss or material shrinkage that occurs, and there is also an initial heating period required to bring the biomaterial up to the gas temperature. Despite these physical and mechanistic deviations from ideal behaviour, model accuracy remains typically high and any errors introduced by using this modelling approach are widely considered to be acceptable. Both materials undergo significant shrinkage during drying, which is not accounted for in the analytical model. This shrinking would reduce the effective slab thickness as the material dries, which would lead to increased effective diffusivity values as drying progresses. A solution of the original Fick's second law partial differential equations by including time variant boundary conditions would be required to account for this effect. However, the complexity of this approach would limit its utility for industry practitioners seeking to use model equations to design drying operations.

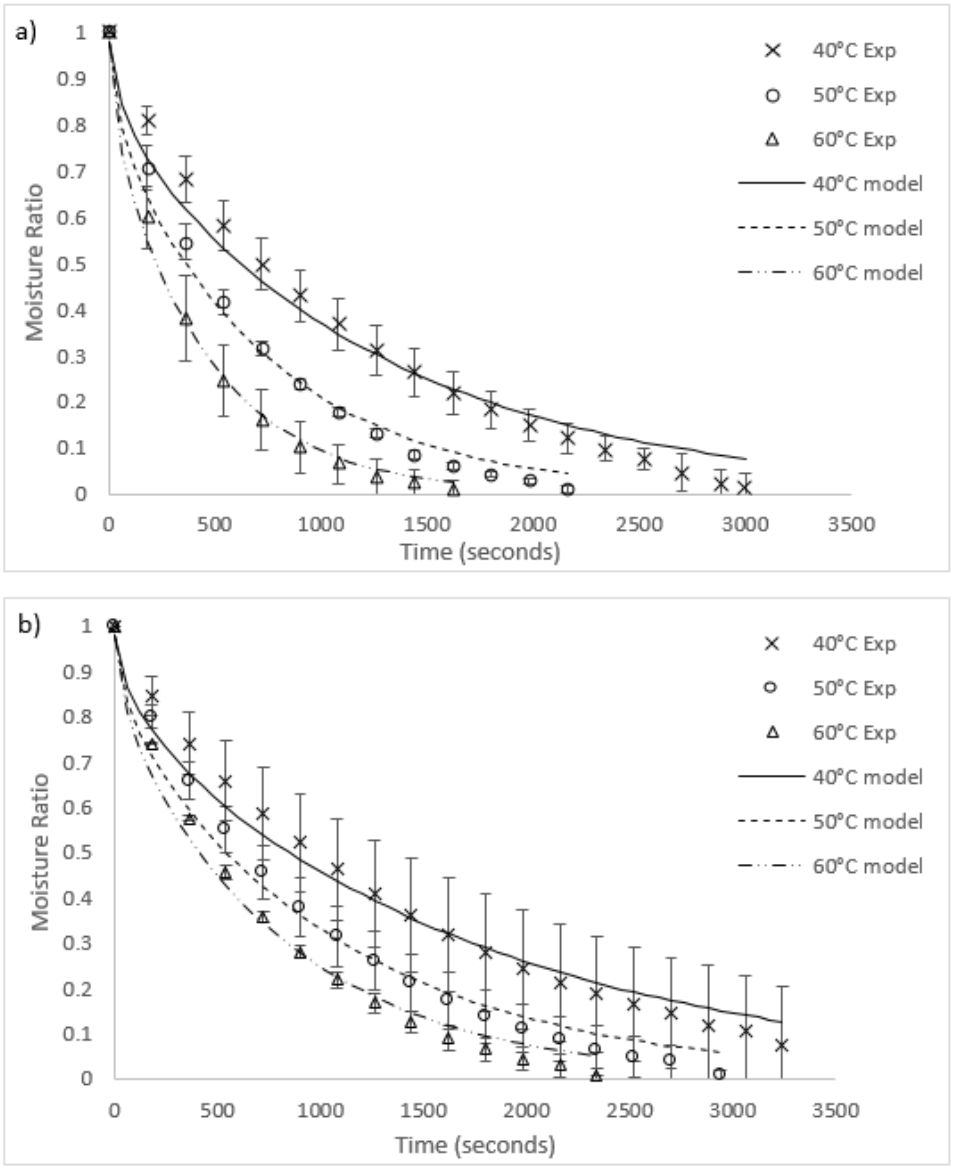

Figure 3.6; Comparison of radiation drying results and model for a) U. ohnoi; b) O. intermedium. (Exp = experimental; model = modelling outcome).

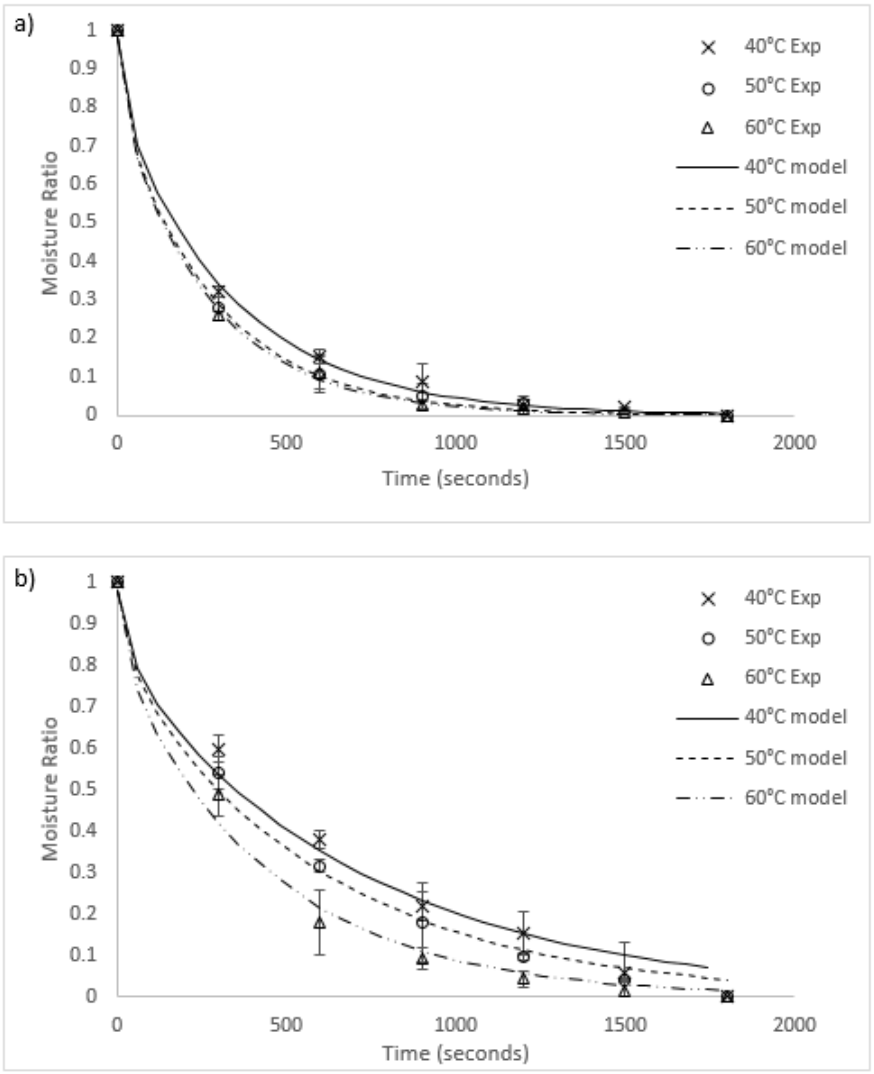

Figure 3.7; Comparison of convection drying results and model for a) U. ohnoi; b) O. intermedium. (Exp = experimental; model = modelling outcome).

Radiative drying was measured as slower than convection drying. There are two potential explanations as to why this could be the case. The first is that drying was not a diffusion limited process and was instead controlled by surface transport of moisture. This is not expected to be the case as per the evaluation of Bi_m in section 2.2.2, but is tested via a secondary method below. Drying limited by surface moisture removal would lead to accumulation of moisture on the surface, which would result in a constant rate drying period. This was investigated by numerically calculating the drying rate using second order Taylor approximation (shown in Equation 3.9). Figure 3.8 includes graphs of the rate of change of drying for both alga species, shown as absolute values. In these graphs, a constant rate drying period (and therefore drying limited by surface moisture transport) would show as a horizontal trend in the initial drying stage. The graphs in Figure 3.8 show that drying is in a single falling rate period for both species and all temperatures. The shape is the same as the expected rate of change from the Fick's law model. This shows the assumption of diffusion limited drying is correct.

$$\frac{dMR_t}{dt} = \frac{(4MR_{t+1} - 3MR_t - MR_{t+2})}{2\Delta t} \tag{3.9}$$

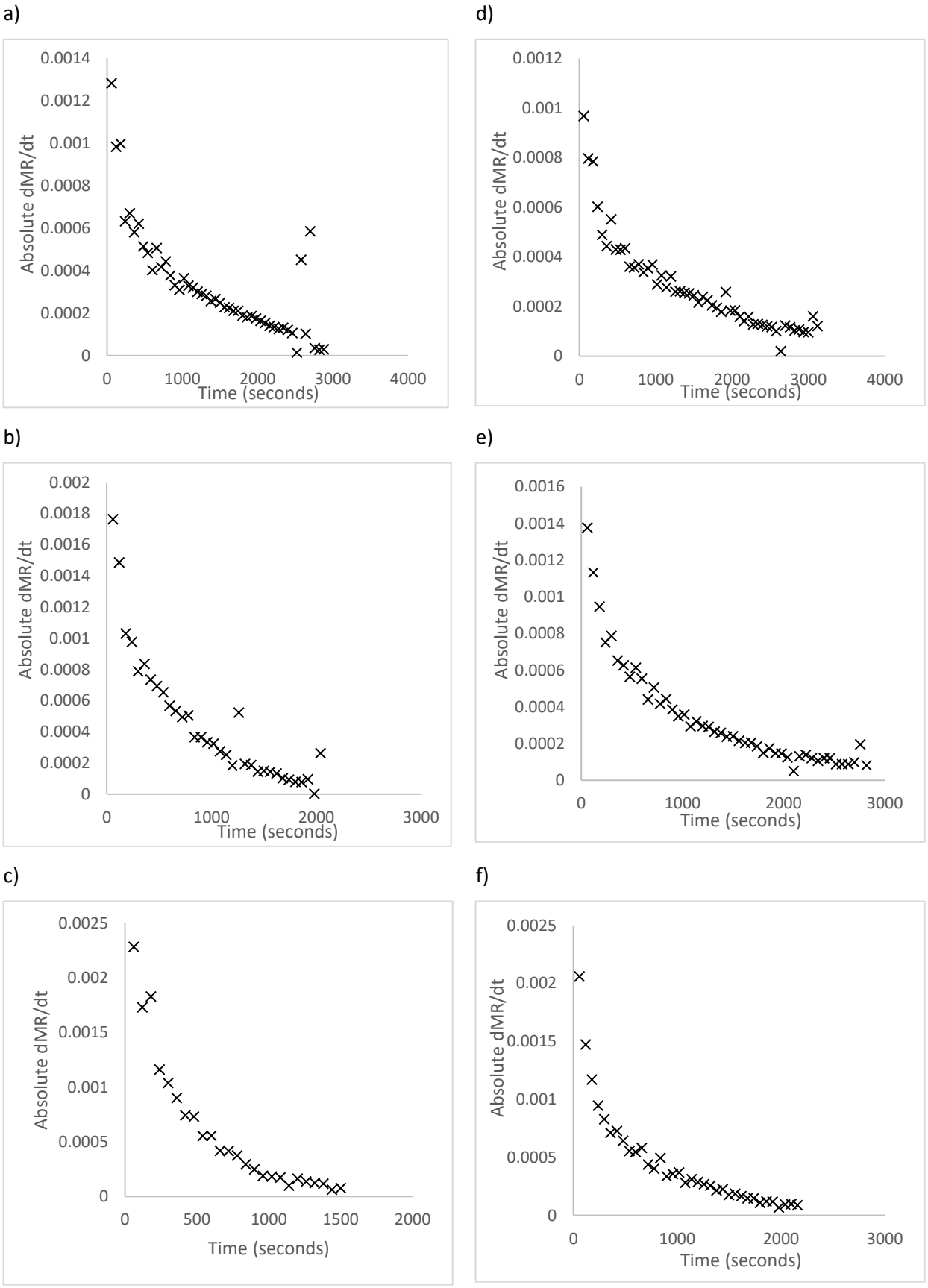

Figure 3.8; MR rate of change vs time; U. ohnoi a) 40°C b) 50°C c) 60°C O. intermedium d) 40°C e) 50°C f) 60°C.

Given that diffusion limited drying is occurring, the addition of air flow must then be affecting the material in a way that lead to an apparent increase in effective diffusivity. Several other studies have shown increases in air velocity cause an increase in effective diffusivity, including for eggplant, potato slices and other macroalgae (Djaeni and Sari, 2015, Santacatalina et al., 2016, Hassini et al., 2007). Other materials have studies showing little to no effect with flow rate changes, including a selection of vegetables and a differently structured macroalgae (Mohamed et. al., 2005, Krokida et. al. 2006). There is little discussion on possible mechanisms for this in literature. The most likely explanation is that airflow causes an increase in penetration through the material slab, which results in a reduction of the average distance moisture is required to diffuse through (ie the parameter L, the slab width reduces with increasing gas velocity). At this point a pragmatic approach was chosen, leaving L as the initial slab width and representing the effect as an increase in the effective diffusivity.

3.2.4 Diffusivity temperature model

The Fick's law analytical model enables a mechanistic or theoretical description of the influence of temperature, through the determination of activation energy of drying. Studies of drying kinetics typically show temperature has an Arrenhius-type relationship to the effective diffusivity, shown in Equation 3.10;

$$D_e = D_0 \exp\left(-\frac{E_a}{RT}\right) \tag{3.10}$$

Where D_0 is the diffusion pre-exponential factor (m^2/s), E_a is the activation energy (J/mol), R is the ideal gas constant (8.314 J/mol.K) and T is temperature in Kelvin. D_0 and E_a are not well defined in that they do not directly represent any measured quantity, but the relationship tends to hold. These values can be estimated from effective diffusivity at different temperatures through plotting $\frac{1}{T}$ against $ln(D_e)$, and fitting a linear relationship. The slope of the fitted line is then equivalent to $-\frac{E_a}{R}$ and the y-intercept is equivalent to $ln(D_0)$. Graphs of the fitting process are shown in Figure 3.9. The determined values of E_a and D_0 can be found in Table 3.6, and a comparison of these values with literature results for other macroalga and biomaterial is shown in Table 3.7.

Table 3.6; Activation energy and diffusion pre-exponent.

Algae	E_a (kJ/mol)	D_0 (m^2/s)	R^2
U. ohnoi	41.3	0.24	0.968
O. intermedium	34.1	0.011	0.948

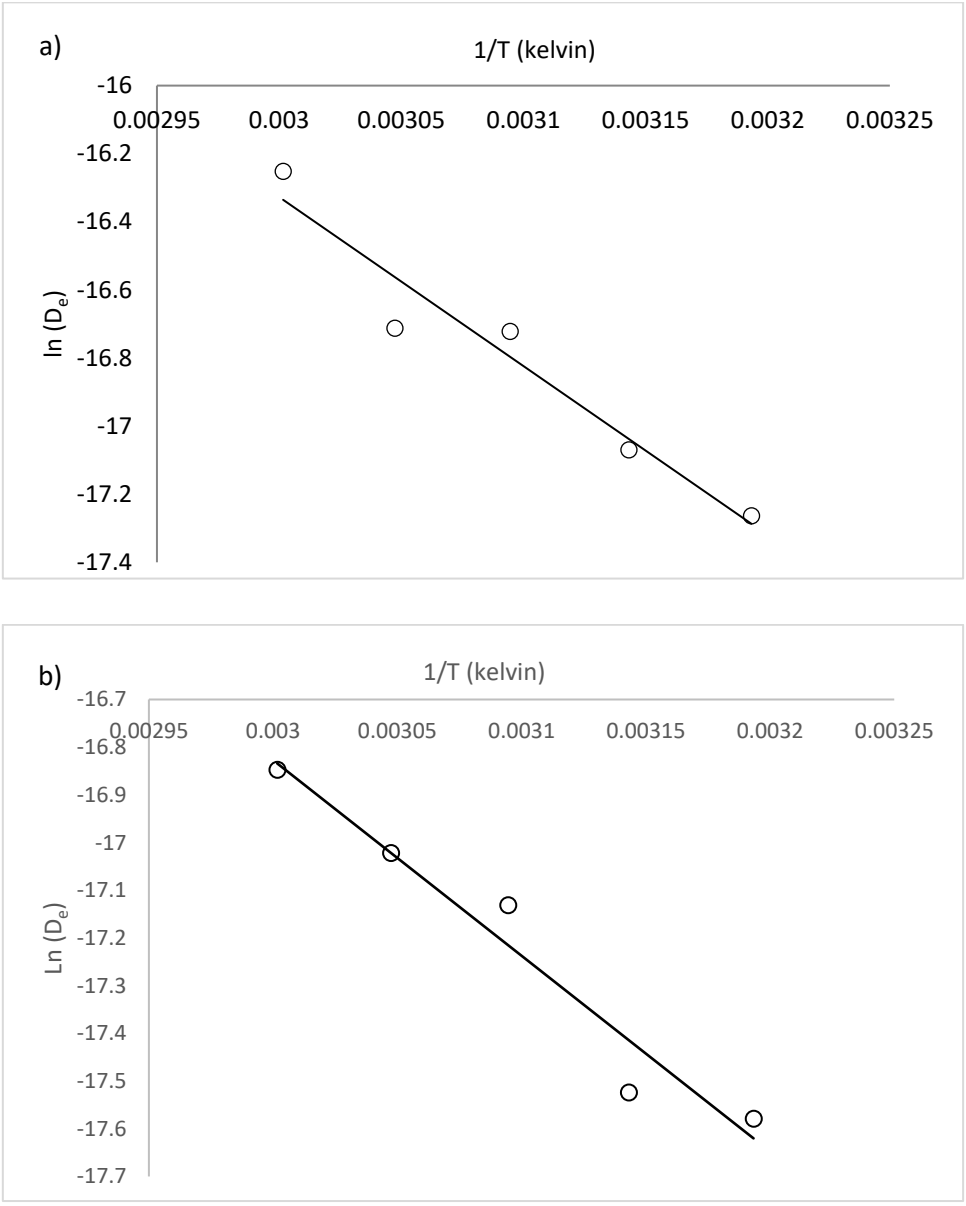

Figure 3.9; Graphical solution method for calculation of activation energy and diffusion pre-exponent; a) *U. ohnoi* b*) O. intermedium*.

Table 3.7; examples of activation energy for other biomaterials.

Material	Activation energy (kJ/mol)	Reference
Macrocystis pyrifera	25.31	Vega-Gálvez et al 2010
Fucus vesiculosus	22.1	Moreira et al 2017
Gracilaria chilensis	39.9	Vega-Gálvez et al 2008
Himanthalia elongata	37.2	Gupta et al 2010
Red pepper	23.35	Scala and Craptiste 2007
Orange seeds	16.5	Rosa et al 2015

3.3 Numerical Considerations

3.3.1 - Equilibrium variance effect on diffusivity estimation

Testing was performed to determine whether the uncertainty in the value for M_e had a significant effect on diffusivity parameter estimation. The upper and lower values for the 95% confidence interval in M_e (as calculated from experimental data) was used to estimate the average relative variance in M_e. This was used to calculate an upper and lower value for M_e, then calculate MR values at each time step for the radiative drying data, for both species and at all temperatures tested. The MR vs time data was then used in parameter estimation for diffusivity as outlined in Section 3.2.1.2. The estimated diffusivity for each data set (including results from Section 3.2.3 for comparison) are shown in Table 3.8.

The results show that despite the large relative variance in the equilibrium moisture data, it has a negligible effect on the parameter estimated value for D_e and can be disregarded. The minimal change in D_e is due to the high initial moisture content of the material (up to ~500%db for *O. intermedium,* and ~450%db for *U. ohnoi*) and comparatively small change in the absolute value for M_e, minimizing any impact on MR values and therefore on D_e.

Table 3.8; Variance effects on calculated effective diffusion.

Ulva ohnoi	Low M_e	Mean M_e	High M_e	Relative variance (D_e) (%)
	Effective diffusivity (10^{-8} m^2/s)			
40°C	3.11	3.18	3.24	2.2
50°C	5.33	5.47	5.62	2.6
60°C	8.56	8.75	8.99	2.7
Oedogonium sp.				
40°C	2.30	2.32	2.34	0.9
50°C	3.60	3.63	3.67	1.1
60°C	4.77	4.82	4.87	1.0

3.3.2 – Model series terms analysis

The analytical Fick's law drying model is represented as an infinite series of terms. The number of terms required for accurate modelling and/or any effects from the number of terms used is not clearly explained in literature. The choice often appears arbitrary or unexplained, with the most common choice to be using the first series term only. The justification (if any) is that it is valid for 'long drying times', but there is often no reference for the choice, or explanation of what constitutes 'long' drying. The most likely origin of this is from Perry et al. (1997), where the same wording is used, again without clear explanation of what constitutes a 'long' drying time.

A study was performed to better understand any potential effects of this choice on parameter estimation and/or modelling. This was achieved by comparison of model shape, accuracy and parameter estimation for one up to ten terms of the infinite series for with and without added air flow and for both species.

Table 3.9 shows that the model fit (represented by R^2) increases as the number of terms used increases, with the magnitude appearing to converge. However, the parameter estimated value for D_e does not significantly change as the terms used increases (the value for D_e was around 0.1% lower for one term compared with ten terms). An example of the effect of the number of terms used on model shape is shown in Figure 3.10.

Table 3.9; R^2 and D_e for increasing number of series terms.

U. ohnoi; Radiative drying	R^2										D_e
Terms	1	2	3	4	5	6	7	8	9	10	
40°C	.927	.946	.949	.950	.950	.950	.950	.950	.950	.950	3.18e-8
50°C	.957	.973	.976	.976	.977	.977	.977	.977	.977	.977	5.47e-8
60°C	.931	.949	.952	.953	.953	.953	.953	.953	.954	.954	8.75e-8
O. intermedium; Radiative drying	R^2										D_e
Terms	1	2	3	4	5	6	7	8	9	10	
40°C	.775	.801	.804	.805	.805	.806	.806	.806	.806	.806	2.32e-8
50°C	.922	.943	.943	.944	.944	.944	.945	.945	.945	.945	3.63e-8
60°C	.951	.969	.972	.973	.973	.973	.973	.973	.973	.973	4.82e-8
U. ohnoi; Convective drying	R^2										D_e
Terms	1	2	3	4	5	6	7	8	9	10	
40°C	.949	.983	.990	.993	.994	.994	.995	.995	.995	.995	1.17e-7
50°C	.950	.982	.989	.992	.993	.993	.994	.994	.994	.994	1.40e-7
60°C	.951	.984	.991	.994	.995	.996	.996	.996	.996	.996	1.48e-7
O. intermedium; Convective drying	R^2										D_e
Terms	1	2	3	4	5	6	7	8	9	10	
40°C	.927	.962	.969	.972	.973	.974	.974	.975	.975	.975	5.66e-8
50°C	.937	.971	.978	.981	.982	.983	.983	.983	.983	.983	6.66e-8
60°C	.939	.971	.978	.980	.981	.982	.982	.983	.983	.983	8.94e-8

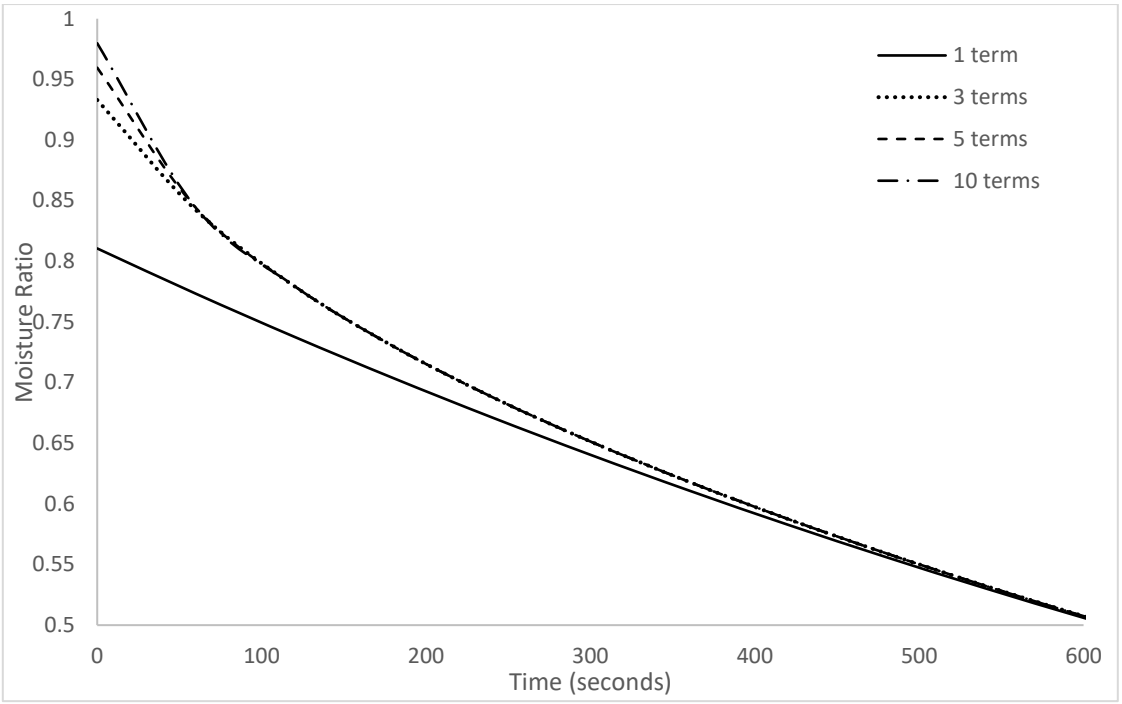

Figure 3.10; Example of model convergence as the number of series terms used increases for an arbitrary diffusivity, zoomed in on the area of relevance.

The increase in R^2 with the number of terms appears to be due to changes in model shape, shown in Figure 3.11a) for *U. ohnoi* radiation drying at 40°C, and zoomed on the initial period in Figure 3.11b). The initial period of the model increases with the number of terms used, while the later period (roughly below $MR = 0.5$) is the same for all. Most of the change is from the model value at $t = 0$. The true value should be $MR = 1$ at $t = 0$ (no drying yet occurred). For one term of the infinite series the value is $MR = 0.8106$. The value increases with the number of terms and converges toward $MR = 1$ at infinite terms. It can be concluded that a single series term is enough when only calculation of effective diffusivity is desired, or for predicting the time required for material to reach MR values below 0.5 for a given diffusivity. More series terms are required when model accuracy across all drying time (especially during the initial period) is desired. Ten series terms are used to sufficiently represent the infinite series across all times in this work for applications of the Fick's law analytical model unless otherwise stated.

3.4 - Conclusions

The equilibrium moisture content of both macroalgae species was evaluated over a wide range of temperature and humidity, representing typical conditions of drying equipment used to process macroalgae in the tropics. The GAB model was found to best represent the experimental data, with the highest R^2 value across the experimental data. It is noted that dissolution of proteins affected the expected response between the equilibrium moisture and temperature (at higher humidity, an increase in temperature resulted in a higher equilibrium moisture content rather than a decrease). This likely makes the GAB model empirical in this application, as it was not developed to represent this kind of interaction.

Thin layer drying kinetics for *U. ohnoi* and *O. intermedium* were evaluated under radiative heating as a function of temperature. The Fick's law analytical model was found to fit the experimental data well, while all tested empirical models collapsed to the Lewis model. Diffusivity was calculated to be from 3.18 to $8.75*10^{-8}$ m^2/s for *U. ohnoi* over the temperature range tested, while for *O. intermedium* diffusivity was from 2.32 to $4.82*10^{-8}$ m^2/s. Diffusivity results from the radiative heating experiments were found to fit an Arrenhius-type relationship with temperature, as was expected from the literature review. The activation energy E_a was calculated to be 41.3 kJ/mol for *U. ohnoi* and 34.1 kJ/mol for *O. intermedium*. These results are the same magnitude as those found for other macroalga and biomasses.

A comparison between drying with zero added air flow and drying with air velocity around 0.7m/s concluded that the addition of air flow increased the drying rate of the macroalgae. Analysis of the rate of change of drying showed that all tested cases with zero air flow were still solely limited by internal moisture diffusion, meeting model assumptions. This establishes the validity of the diffusion-based modelling approach for representing drying kinetics of macroalgae. The addition of flow must then have some effect on the effective diffusivity. The exact relationship between air flow and diffusivity should be determined for a wider range of flow rates in further experimentation.

Analysis of the application of the Fick's law model concluded that increase in the number of series terms increased the model accuracy (as shown by the R^2 value) but did not affect the parameter estimation for D_e. Ten terms of the infinite series were found to represent drying well for all times, with higher numbers of terms having little increase in accuracy. Another study of the effect of variance in the equilibrium moisture data found that the high relative variance in equilibrium had little effect on the parameter estimated diffusivity.

The experimental setups used in this chapter were acceptable for the comparison of drying with and without convective flows and were well suited to investigate the influence of temperature. However, they have limitations preventing their use in further study to determine the response between drying rates and variables other than temperature. The slab thickness L could not be controlled in either experimental setup. This is a potential source of error in the estimation for D_e, as any unknown variance in L will cause an apparent variance in D_e for a given condition set. Both algae species were noted to be highly compressible (bulk density is variable), which causes further uncertainty and inconsistency in the material mass for a given slab width unless it can be controlled. The convective drying equipment used only had one setting for air flow preventing any in depth study on gas velocities. The air flow rate, bulk density and slab thickness (determined by material load) were all identified as convective drying equipment design parameters in Chapter 2. A concise understanding of their effects on the macroalgae drying rate is therefore required to estimate drying times as a part of equipment design. In the following chapter a custom experimental setup that enables these variables to be defined and controlled is described.

Chapter 4

4. Equipment and Experimental Design

The previous chapter studied the thin layer drying kinetics of *U. ohnoi* and *O. intermedium* over a range of temperatures. A comparison of radiative and convective heating sources showed convection gave an increase in drying rate. Most industrial drying equipment utilizes convection drying, which has been illustrated to lead to higher rates. As such, an understanding of air flow effects on the effective diffusivity, as well as other variables identified to have possible effects on drying kinetics (bulk density, slab geometry) are required to develop models capable of facilitating robust equipment design. This chapter covers the design and commissioning of equipment used to investigate the effects of air velocity and material bulk density on the drying kinetics of algal biomass slabs. The equipment and measurement methods chosen provide in situ mass recording, avoiding potential issues associated with removing material from the drying chamber. Considerations are made to enable the investigation of phenomenon that are counter to F2L model assumptions, such as in situ measurement of material volume changes. Finally, the experimental design used to investigate the interaction of velocity and density is outlined, and an example of the data analysis methods used to process the raw data for use in modelling is presented.

4.1 Convective Drying Equipment

Chapter 3 evaluated the effect of temperature on drying rates of the two macroalgae over typical equipment ranges. The results also show air flow rate had effects on drying, leading to an increased rate compared to radiative heating without air flow. The equipment used in this chapter had several limitations preventing a better understanding of the effect of variables other than temperature on drying. Specifically, only one air velocity setting was available, limiting the comparison to with and without air flow. Other limitations of the equipment used were difficulty in controlling the slab geometry or width. Finally, the pack density of the macroalgae was identified as a potential variable effecting drying. The macroalgae used in this study are very compressible (from 30-50kg/m^3 loose, up to 500kg/m^3 or higher when compressed with significant force), and in the lab equipment used in Chapter 3 there was no mechanism to control density. To obtain a better understanding of variable effects on drying requires equipment that can control the velocity of drying gas, the pack density, and the shape of the material slab. Methods to achieve these aims are discussed in the following sections, using literature examples for methodology options whenever possible.

4.1.1 Air Velocity and drying gas source

Drying of biomaterials is most commonly studied using heated air as the drying medium (corresponding with the gas medium used in most drying equipment types). Air flow rates used in drying kinetics studies are typically between 0.5 to 3 m/s. This corresponds with the typical air velocity ranges used in industrial convective drying equipment, (listed as 0.5 to 2 m/s in Perry (1950), and as 0.5-1.5m/s in Richardson et al. (2002)). The heated air is usually provided either by a convective oven, or some type of fan or blower in combination with a separate heater. The effect of air velocity on the drying of biomaterials have been studied for several materials. Examples include brewers grain (using a blower and heater) (Chkir et al 2015), eggplant (Santacatalina et al 2016), red pepper (Scala et al 2007), *Durvillaea antarctica* (Uribe et al 2017) and *Himathalia elongata* (using a drying oven) (Gupta et al 2010). The advantage of the convective oven method is inbuilt controls for temperature. However, air flow rates may be unable to be varied, or dependent on position inside the oven. This type of equipment also limits the options available for measurement of sample mass (discussed in more detail in Section 4.1.3). An air fan in combination with a heater allows for control of air flow rates and temperature independently.

4.1.2 Material Bulk Density

Material bulk density is a variable that should affect the rate of drying for compressible materials like the macroalgae, but has not been well studied in biomass drying literature. The F2L model defines the material being dried as an infinite slab of a certain width. This makes the equation independent of the mass of material being dried, with the amount of material defined by the slab width (i.e. a greater mass is represented by increased slab width). However, materials that can be compressed (such as the macroalgae used in this study) can have differing total masses in a given slab width. A higher bulk density will result in more material and therefore more moisture in the slab volume, which in turn causes slower drying. Bulk density of a material is a potential equipment design variable for applications which utilize a fixed area for drying. In this work, material bulk density is controlled by using a fixed volume sample container, and varying the density by loading different amounts of sample mass into the container. A fixed volume container also provides better reliability in defining the slab width L.

4.1.3 Mass measurement

The mass of the sample is the measured variable in drying rate experiments. In examples from the literature material mass is most commonly measured by removing the material from the sample container, and using a separate analytical mass balance for measurement. Examples of studies using this method include drying of *Himathalia elongata* (Gupta et al 2010). An advantage of this method is the accuracy of measurement (analytical scales can be accurate to ±0.001g or less). However, this approach introduces error as the drying becomes intermittent and the material conditions vary when removed from the heat source (ie. cools down). Drying will be slowed for some period from this loss of temperature, as well as the time required for the material to heat back to the drying gas temperature. The errors will become larger as the frequency of measurement increases, or for materials or conditions with longer heating times.

In situ measurement of mass can reduce these source of errors. An example of the approach has been performed by Uribe for the macroalgae *Durvillaea antarctica* (Uribe et al 2017). In that study, a load cell was used to measure the mass of material while in situ. In situ measurement would prevent the heat loss errors discussed above but would be less accurate than measurement via analytical scale.

4.1.4 Volume Loss

In Chapter 3, the algal materials were noted to have significantly shrink in volume during drying. Shrinkage violates the F2L model assumption of constant slab geometry throughout the drying process. Measuring this volume loss in drying studies has been attempted for some materials, examples including potato slices (Hassini et al 2007), papaya (Kurozawa et al 2012), and calcium alginate (Vargas et al 2018). Sample volume changes were measured by Hassini through removal of the material from the sample container, and measured by using calipers. This has the same potential for errors as removal from heating for measurement of sample mass discussed above. This methodology also cannot be used alongside in situ measurement of sample mass, as it would negate its benefit of the material remaining in contact with the drying gas.

Kurozawa et al (2012) measured volume changes through taking images of material alongside a scale/ruler, and used image analysis software to measure changes. They also removed the material from the drying chamber to take images. Vargas also used image analysis (with images of material removed from the sample container) to record volume losses. The use of a transparent sample container to facilitate in situ image collection of the material as it is dries is preferable.

4.2 Equipment Design

Figure 4.1 shows the overall system diagram of the drying apparatus designed and utilized for this research. The major components are highlighted in the diagram (A to F) and each component is described in more detail in the following sections. Algae samples were placed in the sample container (F). A full to scale and dimensioned schematic is included in Appendix 2.

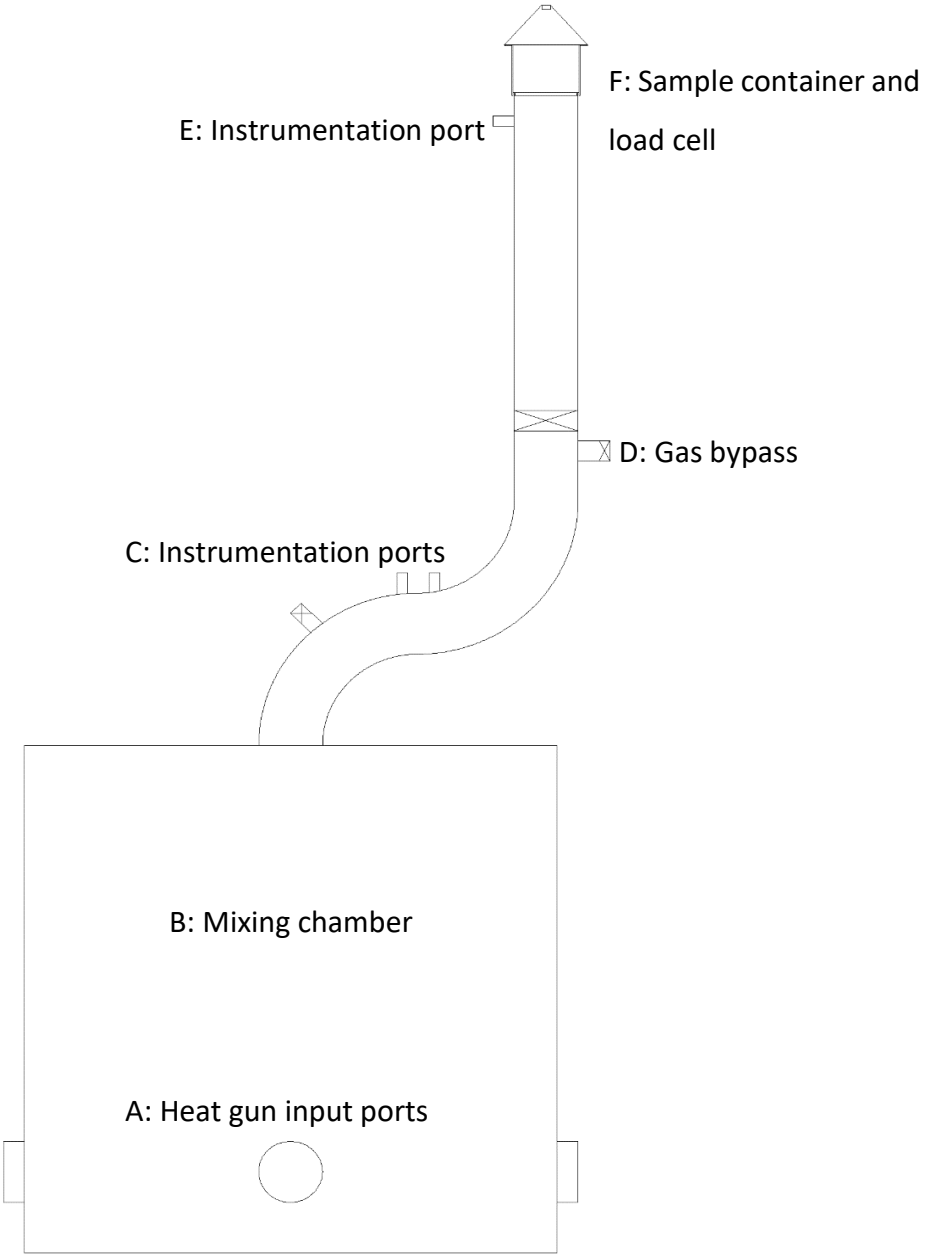

Figure 4.1; Simple diagram of experimental setup.

4.2.1 Load Cell

A load cell and data logger (shown in Figure 4.2) was used to measure sample mass in situ. The load cell used was an OMEGA LCAE-1kg cell (OMEGA Engineering, CT, USA). This load cell can measure up to 1kg of mass. The error in mass measurement from the load cell is listed as $\pm$ 0.03% of maximum load. The data logger records mass to two decimal places, and was set to record data every five seconds. Values are recorded as a .csv file, with the mass and the current time as two columns.

The load cell is sensitive to temperature, and is in line with the gas exhaust from the container. A deflection plate was mounted between the sample container and the load cell to prevent any effect from temperature on the recorded mass values.

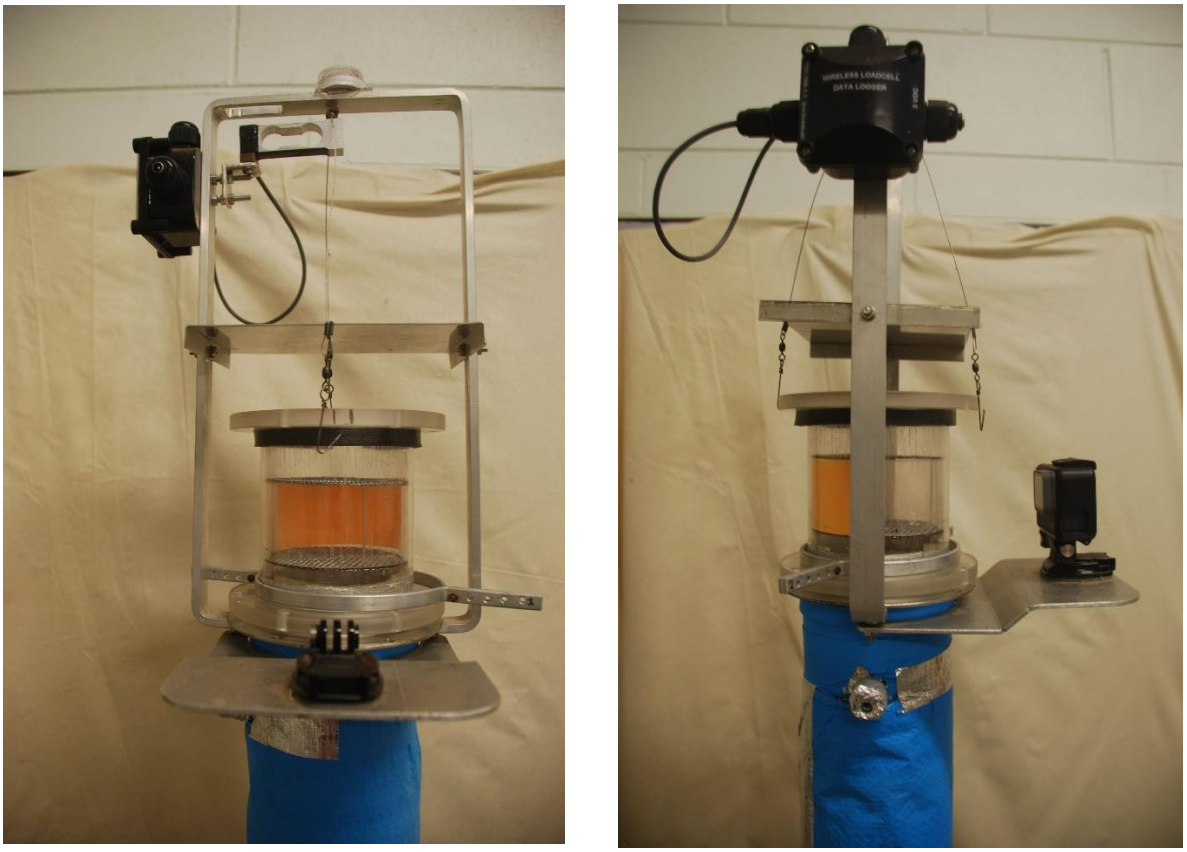

Figure 4.2; Sample container, load cell setup and camera mount; front and side images. Orange paper inserted behind spacer for contrast during image analysis.

4.2.2 Sample Container

The sample container (F in Figure 4.1, shown disassembled in Figure 4.3) was made of clear acrylic to allow for in situ visual analysis of material volume changes during drying. The sample chamber has a fixed volume, which allows for control of material bulk density by loading different initial masses of material into the chamber. The internal height of the sample chamber is set by a removable internal spacer. The centre of mass of the sample container is placed directly below the load cell. There are arms attached to the container to allow wires between the container and load cell to go around the gas deflection plate. The bottom of the sample container is designed to fit over a slightly narrower edge on the pipe end without touching the pipe. This is to minimize any gas flow loss without impacting the sample mass measurement.

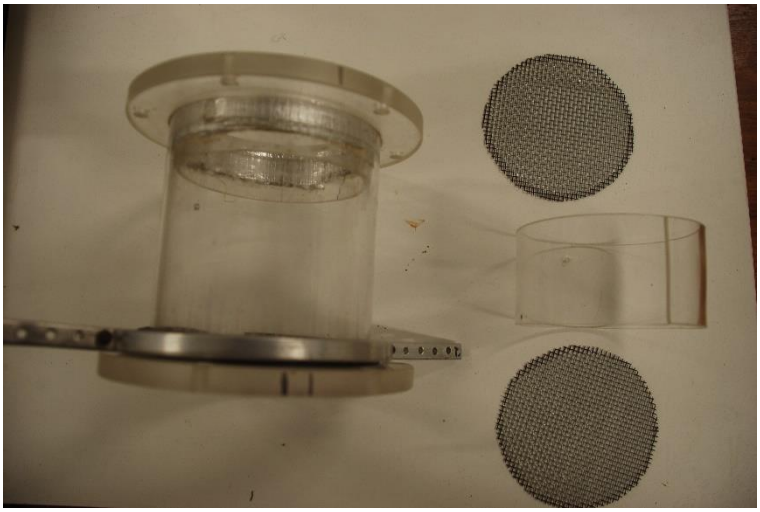

Figure 4.3; Sample container, including top and base mesh, and height spacer.

4.2.3 Heat and air source

The hot air source chosen for the equipment is four hot air guns (PHG 620 DCE, Bosch, Germany). These provide a controllable gas flow rate and temperature. Each heat gun has flow rate settings of 0 (off), 300 and 500L/min, and can set temperature independently of flow rates between 50 and 300°C in 10°C increments. The heat guns can be adjusted separately from each other to provide finer control of drying gas conditions. The air flow from the heat guns are directly input (A in Figure 4.1, shown in Figure 4.4) to a large mixing chamber (B in Figure 4.1; dimensions of 0.5x0.5x0.5m) to ensure the total flow to the sample container is homogenous before it reaches the sample container. All exterior

surfaces were covered in multiple layers of foil insulation, fixed in place with insulation tape, where possible to minimize heat losses to the surroundings.

Figure 4.4; Mixing chamber and heat gun input ports.

4.2.4 Valves, Piping and Instrumentation

The vertical length of pipe was chosen to ensure an even distribution of gas across the sample container (ref). A gas bypass (D in Figure 4.1) was included at the beginning of the vertical section, as it was anticipated that the gas flow may affect mass measurements through drag on the macroalgae. Enabling the bypass involves opening the exhaust valve (left most valve in Figure 4.5), then closing an internal butterfly valve in the vertical pipe (top lever in Figure 4.5). The bypass is disabled in reverse order. The length of the vertical pipe section is 0.55m, which was chosen be to at least 5 times as long as the pipe diameter to ensure an even distribution of air at the sample container. Several ports for independent measurement of air conditions are included in the piping between the mixing and sample chambers (C, E in Figure 4.1). Two are situated immediately after the mixing chamber (C in Figure 4.1, shown in Figure 4.5), while the third (E) is immediately before the sample container. One of the ports in the horizontal section is sized to fit a relative humidity probe (Center 313, Center Technology Corp., Taipei, Taiwan) while the second is sized to fit an air velocity probe (AM-4214SD, Lutron Electronics Enterprise, Taipei, Taiwan). The third port (E) is sized to fit the air velocity probe to enable measurement of air velocity directly before the sample container. A K type thermocouple was also used in the third port (with a plug to prevent air flow losses around the thermocouple) to measure drying gas temperature at the sample container.

Figure 4.5; Pipe before sample container, including instrumentation ports and bypass valve.

4.2.5 Image analysis

A camera mount was attached next to the sample container (shown in Figure 4.2), where a GoPro camera (Hero 5 Black, GoPro. Inc., USA) was attached to take images of the material as it is dried. A ruler was attached to the sample container when image capture was in use to provide a scale for the analysis.

4.3 Calibration and Experimental Error Analysis

4.3.1 Gas velocity

Each heat gun has flow rate settings of 0 (off), 300L/min and 500L/min, which are independent of temperature settings. The flow rate directly before the sample container according to each of these settings was measured using the hotwire anemometer. The errors in gas velocity measurements are the error of the anemometer used. This is stated as ±(0.1m/s + 5% of measurement). Table 4.1 lists the air flow measurements corresponding to differing heat gun settings (rounded to one decimal place), and the expected error. The flow range corresponds well to typical air velocities used in industrial drying equipment (0.5-2m/s as stated previously).

Table 4.4; heat gun settings and measured air velocity.

Flow Setting (1/2/3/4) (L/min)	Total flow (L/min)	Measured air velocity v_g (m/s)	Expected maximum error (± m/s)
300/0/0/0	300	0.4	0.12
500/0/0/0	500	0.7	0.135
300/300/0/0	600	0.8	0.14
500/300/0/0	800	1.1	0.155
300/300/300/0	900	1.2	0.16
500/500/0/0	1000	1.3	0.165
500/300/300/0	1100	1.5	0.175
300/300/300/300	1200	1.6	0.18
500/500/300/0	1300	1.7	0.185
500/300/300/300	1400	1.9	0.195
500/5000/500/0	1500	2.0	0.2
500/500/300/300	1600	2.1	0.205
500/500/500/300	1800	2.4	0.22
500/500/500/500	2000	2.7	0.235

4.3.2 Mass measurement

The flow of air upward through the sample container was noted in testing to have some effect on the mass measurement by the load cell. Testing was performed to determine whether this effect could be quantified by observing the measured mass from the load cell, and comparing the measurements with and without the drying gas bypass enabled. Direct observation of the recorded mass immediately showed the air flow had a non-constant effect on the sample mass measurement. An example of this effect is shown in Figure 4.6. Points represented with circles are measurements taken with air flow through the sample container; points represented with x's are taken when air flow is bypassed from the sample container. The point at t=0 seconds represents the sample mass immediately before drying starts.

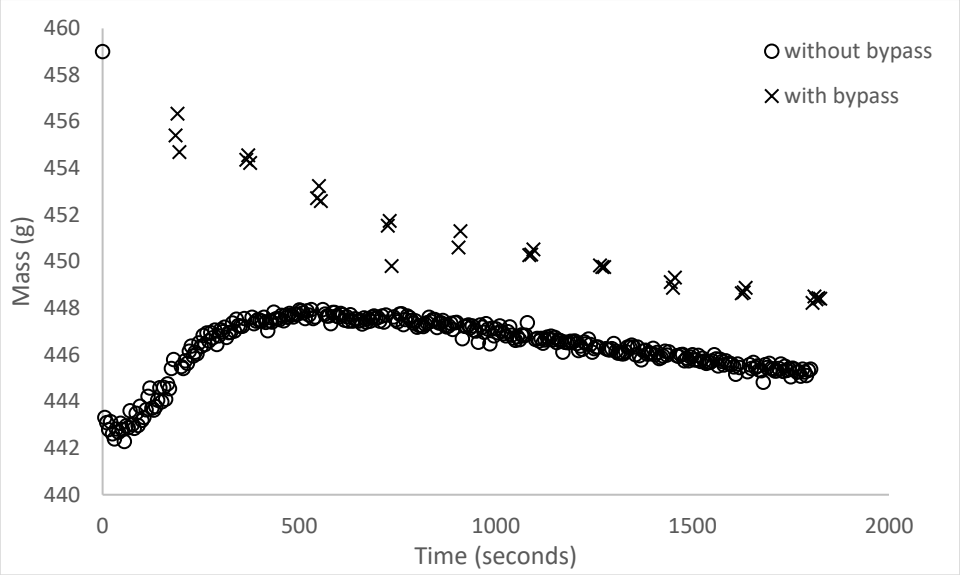

Figure 4.6; Mass vs time recording from load cell for drying of U. ohnoi, with and without gas flow bypass engaged.

From the shape of the lines in Figure 4.6, it is apparent that the air flow through the sample container has both a significant and non-constant effect on the in situ sample mass measurement via the load cell. The non-constancy of the interaction is likely due to the reduction in sample volume occurring as the material dries. As the volume decreases the surface area that can be 'pushed' on by the flow of air decreases, leading to an apparent increase in sample mass that is counter to the decrease actually occurring. The effect on sample mass is non-constant and therefore it is non-trivial to calculate the true mass from the values with interference. For simplicity of measurement, the gas bypass was engaged for ten seconds of every three minutes to get measurement without flow bypass while minimizing time without the heating gas in contact with the sample. Measurements over the bypass period were averaged to reduce noise in load cell recording.

Errors in mass measurement are those expected from variance in load cell measurement. This is listed as 0.03% of the maximum load of the cell, which is 1kg for the model used. This gives a maximum variance of $\pm$0.3 grams. This corresponds to a worst case percentage variance of around $\pm$10% for late stages of drying, where the sample mass is lowest.

4.3.3 Gas temperature

The expected variance in gas temperature measurements is the variance of the thermocouple used. K type thermocouples have an expected variance of ±2.2°C for the temperatures used in this experimentation.

Drying gas temperature variance will not affect the measurement of drying rates, or the parameter estimation for diffusivity for a given set of experimental data. However, it will affect the calculation of D_0 from the effective diffusivity (D_e) using the Arrenhius-type equations developed in Section 3.2.3. Carrying through the maximum variance in calculations for D_0 shows a maximum variance of around $\pm$10% (relative, rounded). The effect of temperature variance on D_0 is scalar and should not affect the overall response shape between drying rates and other variables.

4.3.4 Gas Humidity

The drying gas humidity is assumed to solely affect the equilibrium moisture value for the material, and not affect diffusivity for the conditions and experimental setup used. The listed error of the probe used for measurement of drying gas humidity is ±2.5%RH. This is equivalent to a variance of ±2%db for *U. ohnoi*, and ±1%db for *O. intermedium* at the intended drying temperature of 50°C and the average humidity of drying gas (calculated from equilibrium moisture models in Chapter 3). Varying M_e by 2%db for thin layer drying experimental data in Chapter 3 and performing parameter estimation caused $\pm$1.3% (relative) maximum change in D_e.

4.3.5 Bulk Density

Initial densities used are calculated by loading a known initial mass into the known fixed volume of the sample container, and varied by changing the initial mass. Measurement of the loading mass was performed using an independent analytical mass balance (ABJ 220-4M, KERN and Sohn GmbH, Germany), with a listed uncertainty of $\pm$0.001g. The recorded mass values were rounded to the nearest 0.01g, and the uncertainty in the measurement was considered to be insignificant compared to the variance between initial mass values.

The sample container volume was measured as 300 cm^3. The minimum mass that filled the sample container volume was found to be 10g of material for both algae species, corresponding to an initial density of 33kg/m^3. This was chosen as it should correspond to the fastest drying rate in relation to the material density. The maximum algae bulk density used was 100kg/m^3, as higher densities caused container instability (and therefore mass measurement instability) due to flow pressure drop. These densities represent the expected bulk density range in drying equipment – the material can be compressed further than this range, but requires force or a completely filled volume to achieve and is

atypical of applicable drying equipment types for these materials. The recorded initial mass values, the associated initial density (assuming an even distribution throughout the sample container volume) and the overall variance for that density (from the standard deviation of data points) are listed in Appendix 2. Densities used in modelling were rounded down to the nearest whole number. The final variance in each density conditions was calculated as 33kg/m^3±0.11%, 50kg/m^3±0.1%, 66kg/m^3±0.08% and 100kg/m^3±0.23%.

4.4 Experimental Design

The effects of air velocity and material bulk density on drying rates of the two macroalgae are to be studied with the equipment designed in Section 4.2. The possibility of interaction effects between these variables (for example, the drying rate response to increasing air velocity changes with bulk density increases) should also be considered. Experimental design principles were used to allow for the evaluation of these effects while minimizing the number of condition sets required.

Evaluation of the existence of interaction effects was performed using a two-level factorial design (Montgomery 2013). This design allows for the statistical evaluation of any interaction effect from four condition sets derived from 'low' and 'high' levels in the tested variables. Further condition sets were then tested to determine a clear understanding of the effects of each variable separately. A wider range of air velocities were tested to evaluate the potential existence of a 'critical' air velocity as discussed in Section 2.2.2. The condition sets used for both macroalgae are summarized in Table 4.2, with those used in the two-level factorial design listed in bold. All condition sets were repeated in triplicate.

Table 4.2; Experimental condition sets used for both macroalgae; sets used in two-level factorial analysis are listed in bold.

Gas velocity v_g (m/s)	Initial bulk density ρ (kg/m^3)	Replicates
0.4	**66**	**XXX**
0.7	66	XXX
1.1	66	XXX
1.3	66	XXX
1.7	66	XXX
2.0	**66**	**XXX**
2.0	**33**	**XXX**
2.0	50	XXX
2.0	100	XXX
0.4	**33**	**XXX**

4.5 Equipment Operating Procedure

Operation procedure for equipment is as follows;

1. Set heat gun flow rates to achieve the required flow rate at the sample container. Block any unused heat gun ports.
2. Adjust the gun temperature settings until the gas temperature at the sample container is at the required value. Let the system run for 20-30 minutes to ensure the system is at steady state temperature.
3. Record the relative humidity of the gas stream.
4. Turn on load cell data collection system, ensuring no weight is on the load cell during initialization. Set collection interval to 5 seconds.
5. Measure and record the sample container mass and the fresh algae mass with a separate mass balance.
6. Load fresh algae mass into the sample container corresponding with the desired initial bulk density (10g for 33kg/m^3, 15g for 50 kg/m^3, 20g for 66 kg/m^3, 30g for 100 kg/m^3).
7. Open the gas bypass valves (open the exhaust valve first, then close the butterfly valve).
8. Attach the sample container to the load cell wires, ensuring the container does not have weight on the piping.

9. Clear the data recording in the collection system and wait 20-30 seconds to obtain a stable initial mass point.
10. Close the gas bypass (open butterfly valve then close exhaust valve) and simultaneously start a separate timer.
11. At the desired data point interval (e.g. 3 minutes), open the gas bypass for 10 seconds before closing again. This obtains 3 points of mass measurement via the load cell and data logger (at 0, 5 and 10 seconds of bypass) without flow interference.
12. At end of drying time, shut off heat guns (or open gas bypass if repeat experiments at current settings are desired) and save the mass vs time data from the collection system.

4.6 Data Analysis Methods

4.6.1 Moisture ratio (MR) vs time profile

The following is an example of the method used to convert raw data from the load cell and logger (i.e. mass vs time) to the form used in drying modelling (i.e. moisture ratio vs time) for a single repeat of a given condition set. This methodology was performed for each repeat and for each condition set for both macroalgae. Experimental conditions used to illustrate the data analysis method are 50°C, 1.3m/s air velocity and 66 kg/m^3 bulk density of material. The macroalgae used was *U. ohnoi*. The algae was collected and centrifuged as outlined in Section 3.1. Drying time for the experiment was thirty minutes. It was chosen to perform all repeats for a given condition set with fresh material from a single day to minimize variance of the material, as growth conditions of the macroalgae were uncontrolled. This limited the time available for each repeat, and not all conditions were dried to equilibrium.

A fresh sample of macroalgae was collected immediately prior to use in experimentation. It was then centrifuged to remove all surface moisture. This provides a consistent initial amount of moisture in the sample, and helps meet model assumptions regarding limiting stages of drying. The samples were stored in an airtight container until loaded into the sample container to minimize any moisture losses. The material was evenly distributed as possible through the sample container volume. Images of the loaded algae material in the sample container are shown in Figure 4.7. A subsample of the collected algae material was removed and dried at 110°C using a moisture analyser to determine the dry mass of material and moisture percentage. The results of this analysis are detailed in Table 4.3. The dry mass of the macroalgae is assumed to be a constant and independent of the drying process or conditions used.

a) b)

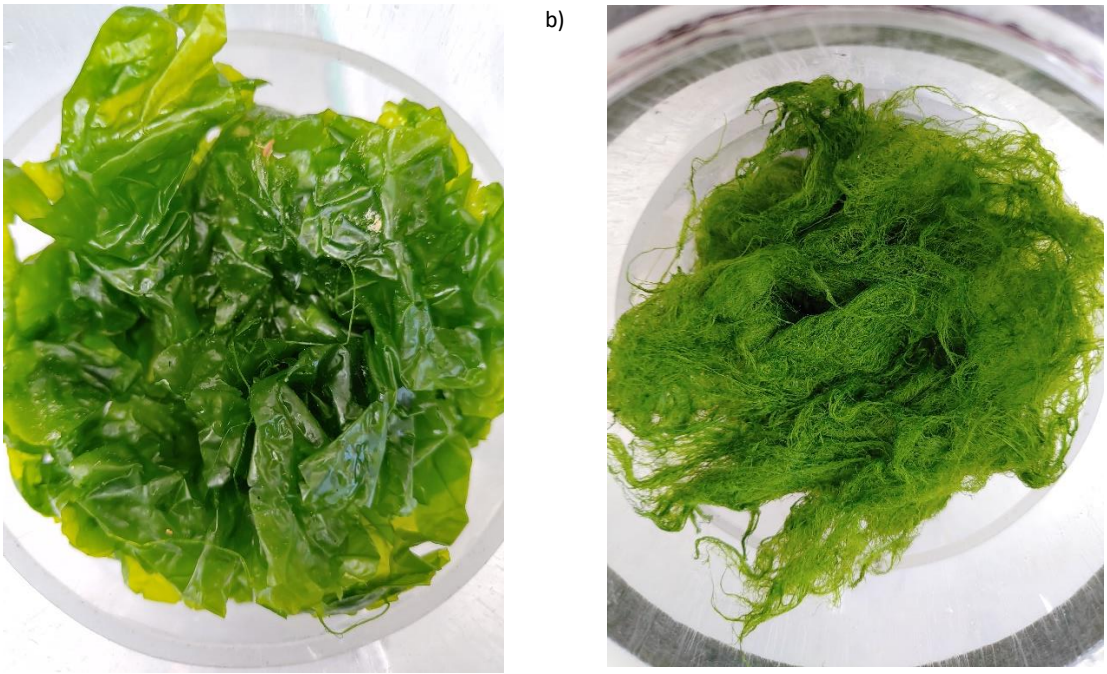

Figure 4.7; Loaded sample container a) *U. ohnoi* b) *O. intermedium*

Table 5.3; Initial properties of the fresh algae material.

Initial mass (g)	1.311
Dry mass (g)	0.287
Moisture fraction (%wet basis)	0.7811

The raw data was recorded as mass vs time values and imported to Excel. The recorded time was converted to seconds from drying start. The data points that did not correspond with the gas bypass cycle were then removed. The recording interval usually resulted in three time and mass values for a given bypass cycle. These points were averaged to a single value for each bypass cycle. The mass of the unloaded sample container was then subtracted from each recording. The final mass (g) vs time (s) data is shown in Table 4.4, and graphed in Figure 4.7 (the mass value at $t = 0$ was measured using a separate mass balance before loading the sample container as per experimental procedure in Section 4.5);

Table 4.4; Converted U. ohnoi mass vs time. Measurements at 1632.5 and 1822.5 seconds were averaged from four and ten data points respectively; the first three are shown.

Time (s)	Point 1	Point 2	Point 3	Averaged Mass (g)	Container Mass (g)	Algae Mass (g)
0	-	-	-	-	-	19.99
205	456.12	455.16	455.97	455.75	440.22	15.53
375	453.44	453.47	453.22	453.38	440.22	13.16
550	452.07	451.98	453.18	452.08	440.22	11.86
730	450.68	451.18	451.13	451.00	440.22	10.78
910	450.07	450.66	450.37	450.37	440.22	10.15
1090	449.71	449.3	449.46	449.49	440.22	9.27
1270	448.19	449.08	449.13	448.80	440.22	8.58
1450	448.03	448.59	448.27	448.30	440.22	8.08
1632.5	448.17	447.82	448.1	448.04	440.22	7.82
1822.5	447.97	448.6	447.85	447.94	440.22	7.72

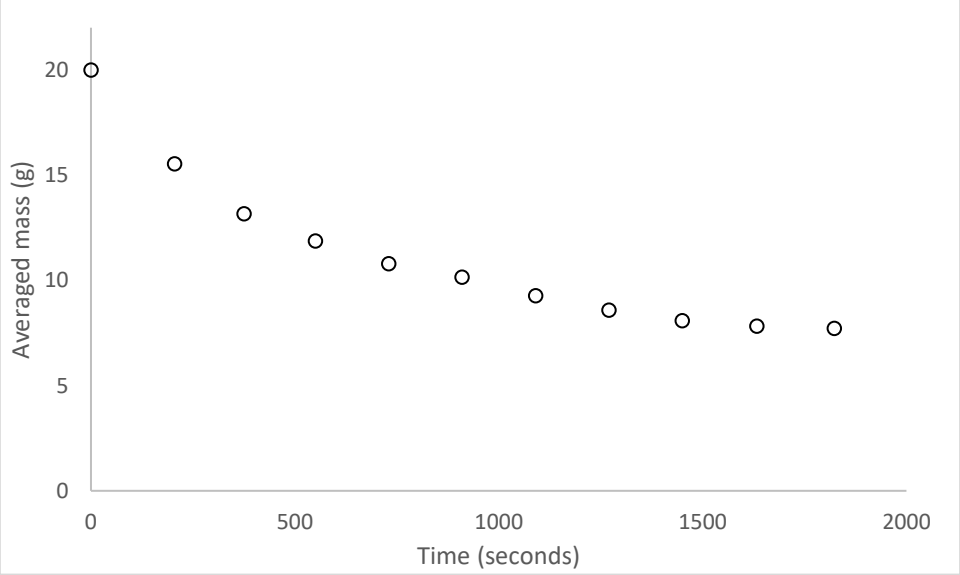

Figure 4.8; Averaged algae mass against time.

The initial recorded mass and the moisture percentage from the subsample were used to determine the dry mass of the sample (m_D);

$$m_D = 19.99 \times (1 - 0.7811) = 4.38g$$

The sample dry mass was then used to convert the mass vs time recording to moisture content in %dry basis via the following, where m_t is the mass in grams at time t;

$$M(\%dry\ basis, as\ decimal) = \frac{(m_t - m_D)}{m_D} \quad (4.1)$$

For example, at $t = 0$;

$$M = \frac{(19.99 - 4.38)}{4.38} = 3.564$$

The converted data is shown in Table 4.5 and graphed in Figure 4.8;

Table 4.6; U. ohnoi moisture in % dry basis vs time.

Time (s)	Averaged Mass (g)	Dry Mass (g)	M (%db)
0	19.99	4.38	3.564
205	15.53	4.38	2.546
375	13.16	4.38	2.005
550	11.86	4.38	1.708
730	10.78	4.38	1.461
910	10.15	4.38	1.317
1090	9.27	4.38	1.116
1270	8.58	4.38	0.959
1450	8.08	4.38	0.845
1632.5	7.82	4.38	0.785
1822.5	7.72	4.38	0.763

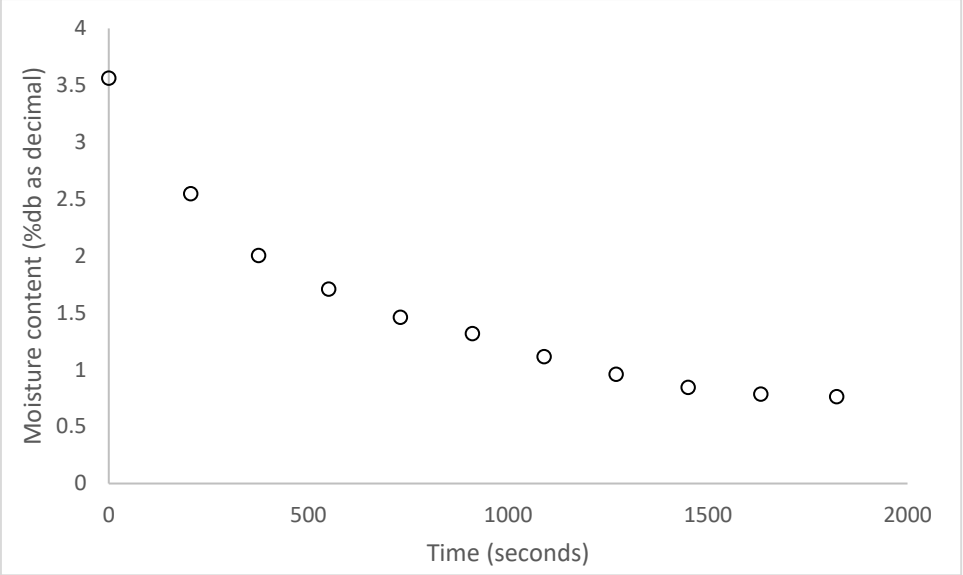

Figure 4.9; Moisture content in %db against time.

The equilibrium moisture content (M_e) was determined from the measured temperature and humidity data via the GAB model determined in Section 3.2.2. The M_e value at 50°C and 10%RH for *U. ohnoi* is 0.16. The dimensionless moisture ratio (MR) is then calculated via the following;

$$MR = \frac{(M - M_e)}{(M_0 - M_e)} \tag{4.2}$$

Where M is the moisture content in %db at time t, M_0 is the moisture content in %db at $t = 0$ and M_e is the equilibrium moisture content in %db. The final experimental data is shown in Table 4.6 and graphed in Figure 4.9.

Table 4.7; U. ohnoi moisture ratio vs time.

Time (s)	M_{db} (%db)	M_e (%db)	MR
0	3.564	0.16	1
205	2.546	0.16	0.701
375	2.005	0.16	0.542
550	1.708	0.16	0.455
730	1.461	0.16	0.382
910	1.317	0.16	0.340
1090	1.116	0.16	0.281
1270	0.959	0.16	0.235
1450	0.845	0.16	0.201
1632.5	0.785	0.16	0.184
1822.5	0.763	0.16	0.177

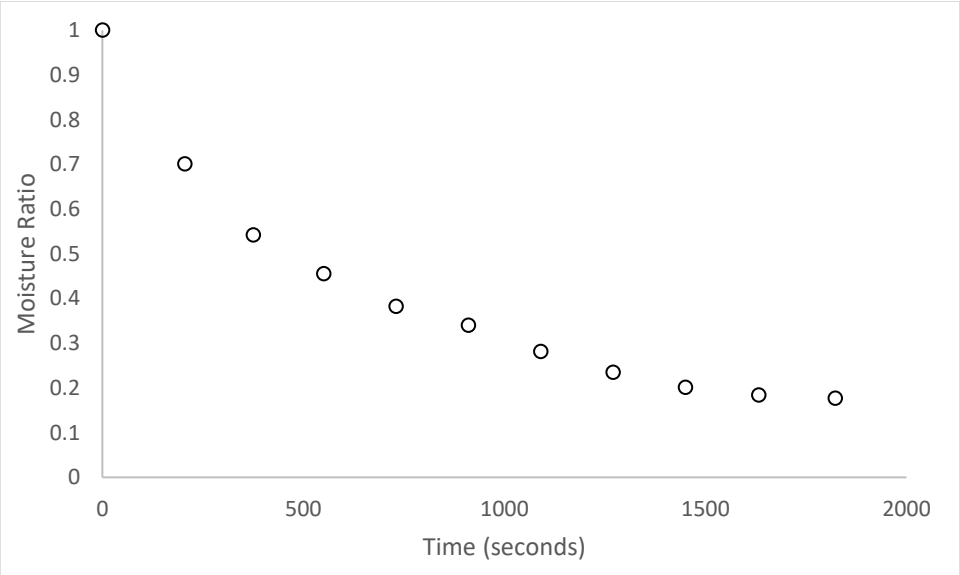

Figure 4.10; U. ohnoi moisture ratio vs time data for a single replicate; drying at 50°C, 1.3m/s air velocity and 66 kg/m³ bulk density.

4.6.2 Image analysis

The following is an example of the method used to convert images of algae material in the sample container during drying to a slab width (*L*) value at each time for a single repeat of a given condition

set. Experimental conditions used to illustrate the data analysis method are 50°C, 2m/s air velocity and 66 kg/m^3 bulk density of material. The macroalgae used was *O. intermedium*.

First, an understanding of the limits of volume losses in the experimental setup was obtained through direct measurement of the initial and final (i.e. material dried to completion at experimental temperature and humidity) widths. The results of this analysis are detailed further in Section 6.2. The general result is that both species of macroalgae lose 22% of slab width in any given dimension (volume loss is equal in all directions) as a result of being dried to equilibrium at the temperature and humidity used in experiments. This translates to an initial slab width of 4.5cm, and a final slab width (at $MR = 0$) of 3.5cm.

Images taken by the camera (described in Section 4.2.5) were used to provide in situ analysis of volume losses over time. The camera was set to take an image every minute (lowest available frequency) of the sample container and ruler scale. The images that correspond to the gas bypass cycle (eg at 3,6,9… minutes) were chosen for the analysis to prevent potential error from gas flow moving the material during the image capture. The software used for analysis was ImageJ (Schneider et al. 2012).

ImageJ can use a known scale in an image to measure the number of pixels for a known length, then measure length between any two points in the image from that scale. The known horizontal width of the sample container or an included ruler scale was used in this way to measure the width of the sample in each image. It was noted that parallax error caused apparent and significant differences between the known container width and the ruler scale included in the images. To bypass this error the measurements of slab width taken from image analysis were used to determine a percentage change between the measured initial width and the expected final dimension as per the known limits of volume loss. This percentage change was then used to estimate the true slab width between the known initial and final values. Horizontal measurements of the material slab were used to determine the percentage change to minimize effects of absolute measurement error, noting that volume losses were equal in all directions.

Each image was imported into ImageJ, and the line tool is used to mark out the known distance across the sample container or ruler. The line length in pixels is retained in the program as a length per pixel. A standardized grid (size of 1.2cm^2/square) was added to the image to ensure measurements are taken from the same position on each image. The line tool is then be used to measure the width of the sample along the three horizontal grid lines overlayed on the alga material using the retained pixel scale. An example of a sample image in ImageJ with the grid overlay is shown in Figure 4.10. The three measurements are averaged to account for irregularities in the sample. The initial measurement is

used to calculate the expected width at equilibrium. The measurements are then converted to a percentage change and used to estimate the true slab width as described above. The raw data and conversions for the example data set are shown in Table 4.7, and a graph of slab width against time is provided in Figure 4.11.

An example of the calculations for the t=910 seconds row in Table 4.7 is included below. It is known that the initial and final values (at t=0 and t=5422.5 respectively) correspond with the known slab widths of 4.5cm and 3.5cm. The initial and final averaged values from image analysis are 4.9 and 3.7.

At t=910 seconds, the measured average value is 4.4. The percentage of volume loss at this time is the percentage of the total loss (shown as a decimal);

$$\%\ of\ loss, t = \frac{Avg_{t=0} - Avg_t}{Avg_{t=0} - Avg_{t,final}} \tag{4.3}$$

$$\%\ of\ loss, t = \frac{4.9 - 4.4}{4.9 - 3.7} = 0.417$$

This percentage is then used to scale between the known measurements at t=0 and t=final to estimate the true slab width;

$$L_t = L_{t=0} - \%loss, t\left(L_{t=0} - L_{t,final}\right) \tag{4.4}$$

$$L_t = 4.5 - 0.417(4.5 - 3.5)$$

$$L_t = 4.1cm$$

This methodology is repeated for each time.

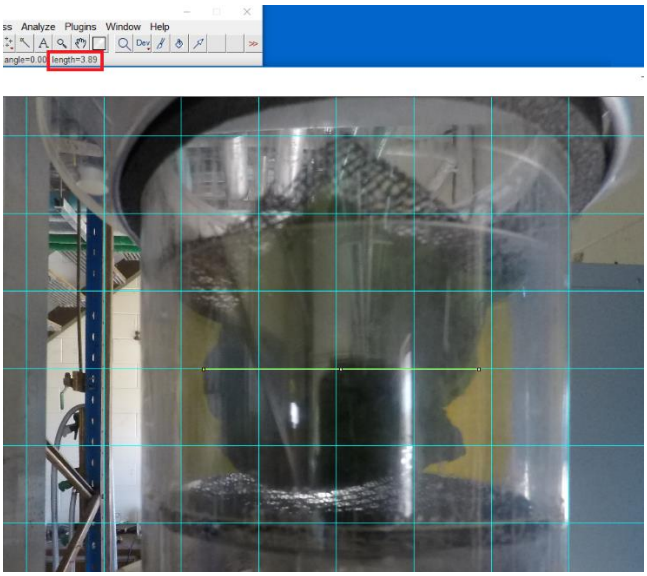

Figure 4.11; Standardized grid and measurement (yellow line across centre grid overlaid; measurement circled in red) across centre horizontal grid line overlaid on the material in ImageJ.

Table 4.8; raw data and conversion to estimated slab width for a single repeat; drying of O. intermedium at 50°C, 2m/s air velocity and 66 kg/m³ bulk density.

Time (s)	High	Mid	Low	Average (rounded)	Percentage change (%)	Slab width (*L*, m)
0	5.1	4.7	4.9	4.9	0	0.045
310	4.8	4.6	4.6	4.7	16.7	0.043
615	4.7	4.5	4.3	4.5	33.3	0.042
910	4.5	4.5	4.2	4.4	41.7	0.041
1210	4.4	4.4	4.2	4.3	50	0.040
1510	4.3	4.4	4.2	4.3	50	0.040
1815	4.2	4.3	4.2	4.2	58.3	0.039
2112.5	4.2	4.3	4.2	4.2	58.3	0.039
2410	4.2	4.2	4.1	4.2	58.3	0.039
2710	4.1	4.2	4.0	4.1	66.7	0.038
3010	4.1	4.2	4.0	4.1	66.7	0.038
3310	4.1	4.1	3.9	4.0	75	0.038
3612.5	3.8	4.0	3.9	3.9	83.3	0.037
3910	3.8	4.0	3.8	3.9	83.3	0.037
4210	3.7	3.9	3.7	3.8	91.7	0.036
4505	3.7	3.9	3.7	3.8	91.7	0.036
4805	3.7	3.8	3.7	3.7	100	0.035
5105	3.7	3.8	3.6	3.7	100	0.035
5422.5	3.7	3.8	3.6	3.7	100	0.035

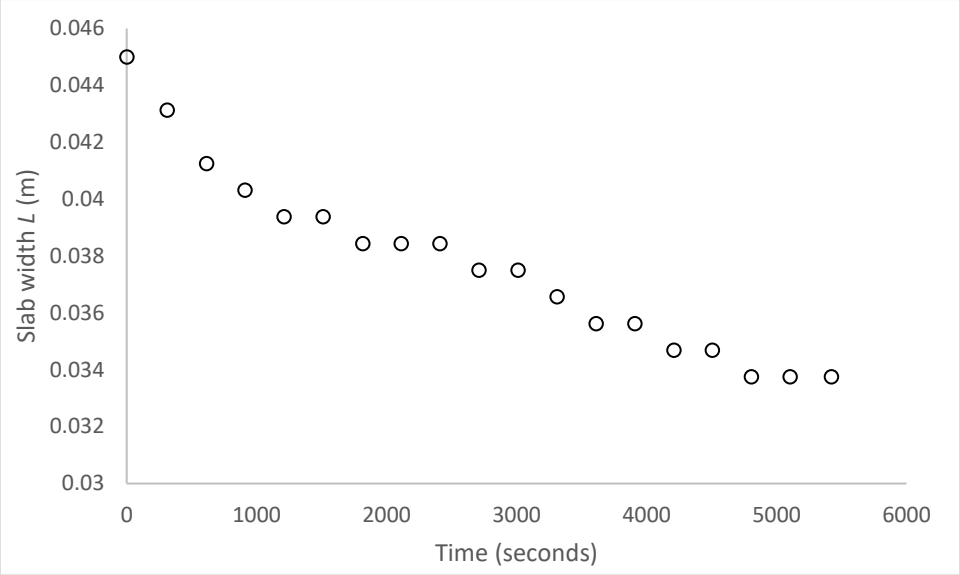

Figure 4.12; estimated slab width vs time for O. intermedium drying at 50°C, 2m/s air velocity and 66 kg/m³ bulk density.

4.7 Conclusion

This chapter covered the equipment and experimental design for the analysis of drying kinetics of compressible biomaterials. The apparatus was designed and custom built to be able to control drying air velocity (between 0.4 and 2.7m/s), temperature (from 40 to 60°C) and bulk density of material (between 33 and 100 kg/m^3 for both macroalgae) to represent conditions typically used in industrial biomass drying equipment. Measurement methods were chosen such that dependent variables (sample mass and slab dimensions) are able to be recorded in situ, minimizing potential sources of error. Experimental conditions were chosen to facilitate statistical analysis of the influence of material bulk density and drying air velocity on drying rates.

Chapter 5

5. Drying Kinetics Modelling

The experimental apparatus described in chapter 4 was utilized to generate moisture ratio against time data for both algal species over a range of operating conditions and geometric constraints. The effects of initial density and gas velocity on the drying kinetics for both species of macroalgae are investigated. The experimental data are analysed to verify that algae drying occurs as a single falling rate drying period, justifying the use of Fick's second law (F2L) as a theoretical model representing the data.

Moisture ratio versus time profiles are used to parameter estimate for the effective diffusivity (D_e) which best fits the F2L model under the assumption of constant slab thickness. The quality of model fit is discussed and reasons for discrepancies in the model are highlighted. Differences in the quality of raw data and model fit between the two species are discussed. The resulting D_e values are compared to D_e values for other types of biomass.

Statistical analysis (ANOVA) is presented to quantify the significance of density and gas velocity on the predicted D_e values. This analysis is utilized to derive a model for D_e as a function of gas velocity, initial density and temperature. This model is then assessed for fit against the experimental data.

5.1 Methodology Overview

A complete and detailed summary of approaches, methodology and conditions used in experimentation is presented in Chapter 4. The apparatus utilized in the drying trials is described in Section 4.2. The experimental design is described in Section 4.4 and outlines a series of experiments examining the effects of air flow velocity (v_g, 0-2 m/s) initial bulk density of sample (ρ, 33-100 kg/m^3) and their potential interaction.

The raw experimental data of mass against time from experiments were converted to moisture ratio versus time. An analytical solution to Fick's second Law model was fit to moisture ratio versus time data sets. Model fitting was performed by minimization of the total sum of square errors between the model and experimental data, with the model representing the best fit to all three sets of data at a given condition. Ten terms of the infinite series were used in modelling to ensure convergence in the

infinite series solution (as discussed in Section 3.3.2). These calculations were performed using Microsoft Excel using the solver function with GRG nonlinear solver method assuming constant relative variance in the experimental data. The objective function is summarised in Equation 5.1, where *m* corresponds to the number of data sets. The objective function (Obj) was minimized by varying the magnitude of the effective diffusivity parameter (D_e).

$$Obj = \sum_{m=1}^{3} \left(\sum (MR_m - MR_{exp})^2 \right) \tag{5.1}$$

5.2 Results

Graphs of triplicate moisture ratio against time data for each condition set and species are shown in Figures 5.1 to 5.4. As can be seen in Figures 5.1 and 5.2, the data repeatability is high for *U. ohnoi*. However, Figures 5.3 and 5.4 show that repeatability is lower for some *O. intermedium* data sets. This trend in repeatability is consistent with the observations from thin layer and equilibrium moisture experiments in Chapter 3, where *O. intermedium* data had more variance. *O. intermedium*'s single-cell wide strands tend to become entangled and form clumps during harvesting and dewatering. This leads to a less consistent or controllable distribution of material across the sample container volume. The clumping could also potentially shield some portion of the material to heat exposure, causing less consistent drying across the material slab.

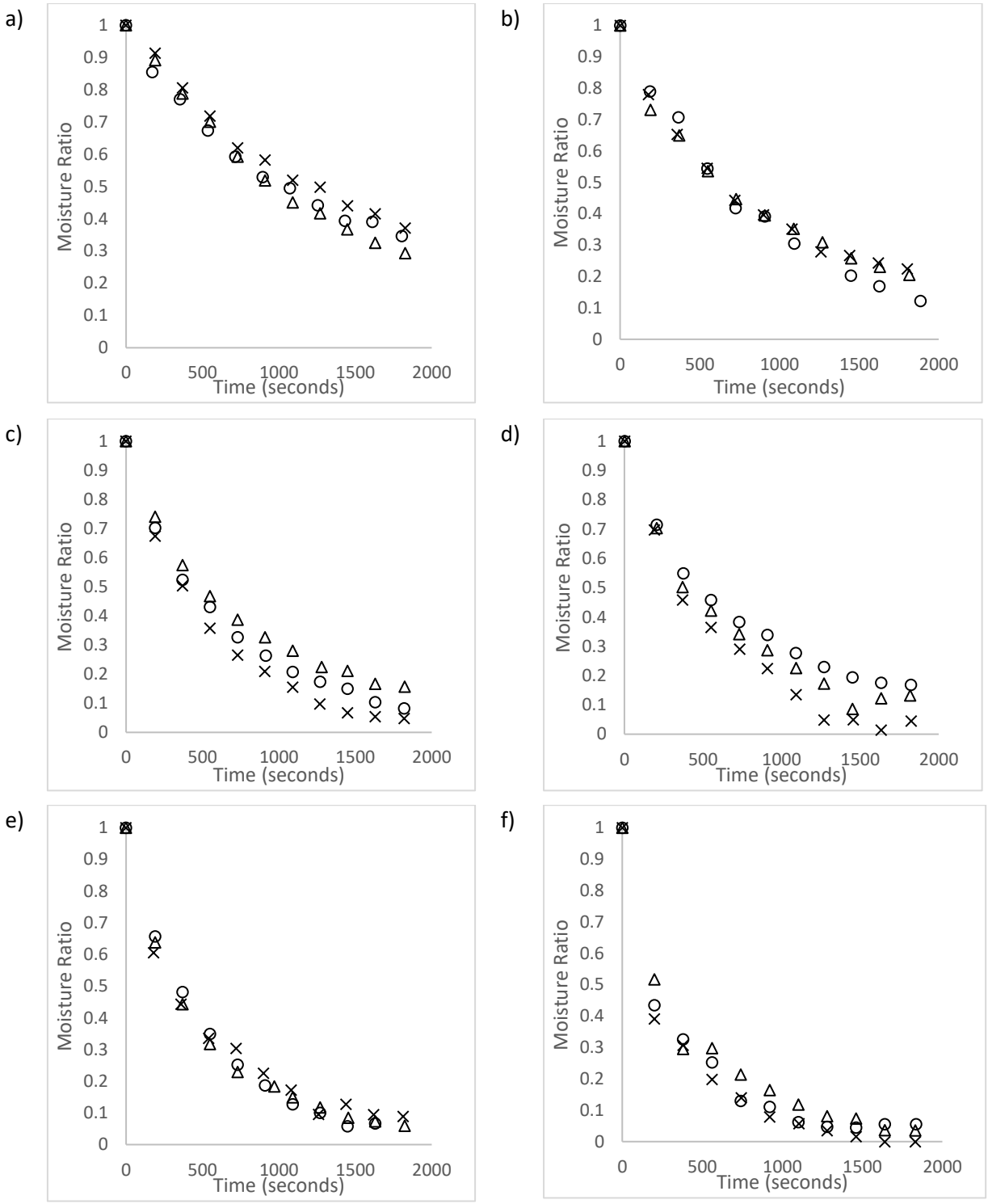

Figure 5.1; *U. ohnoi* drying at 50°C, 66kg/m³; raw data triplicates; a) 0.3m/s b) 0.7m/s c) 1.1m/s d) 1.3m/s e) 1.7m/s f) 2.0m/s.

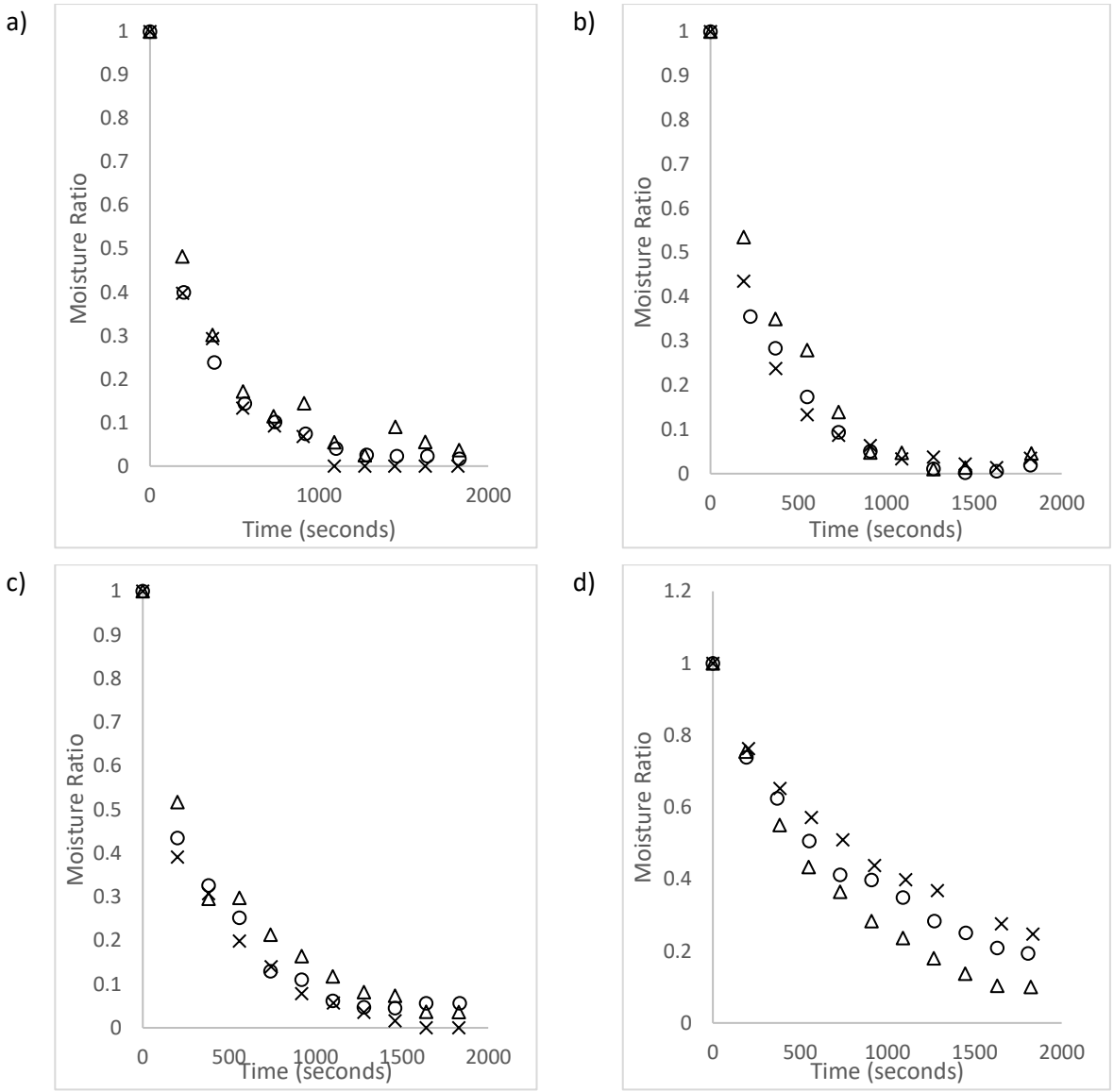

Figure 5.2; *U. ohnoi* drying at 50°C; raw data triplicates; a) 2m/s, 33 kg/m³ b) 2m/s 50kg/m³ c) 2m/s 100kg/m³ d) 0.4m/s 33kg/m³.

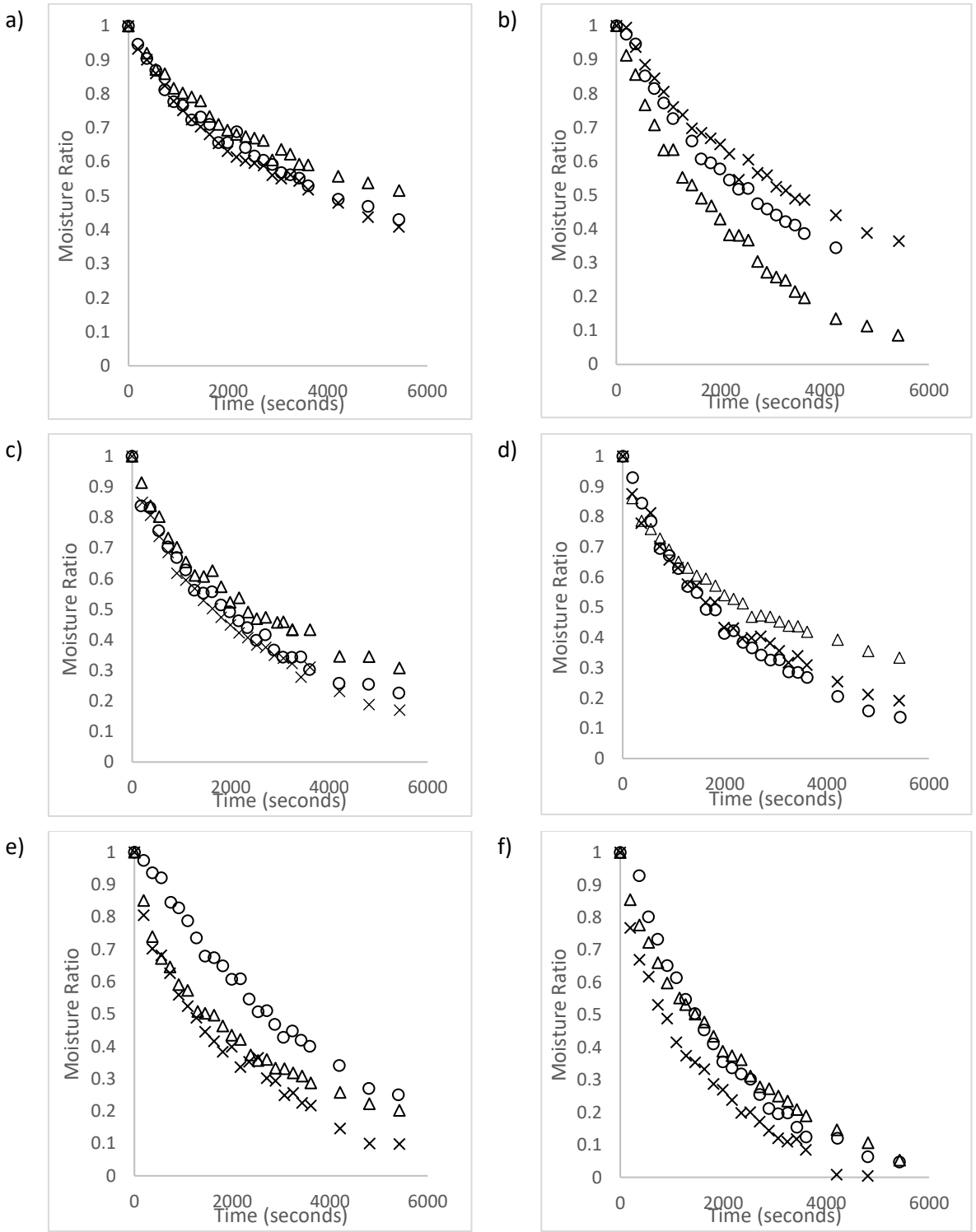

Figure 5.3; *O. intermedium* drying at 50°C, 66kg/m³; raw data triplicates; a) 0.3m/s b) 0.7m/s c) 1.1m/s d) 1.3m/s e) 1.7m/s f) 2.0m/s.

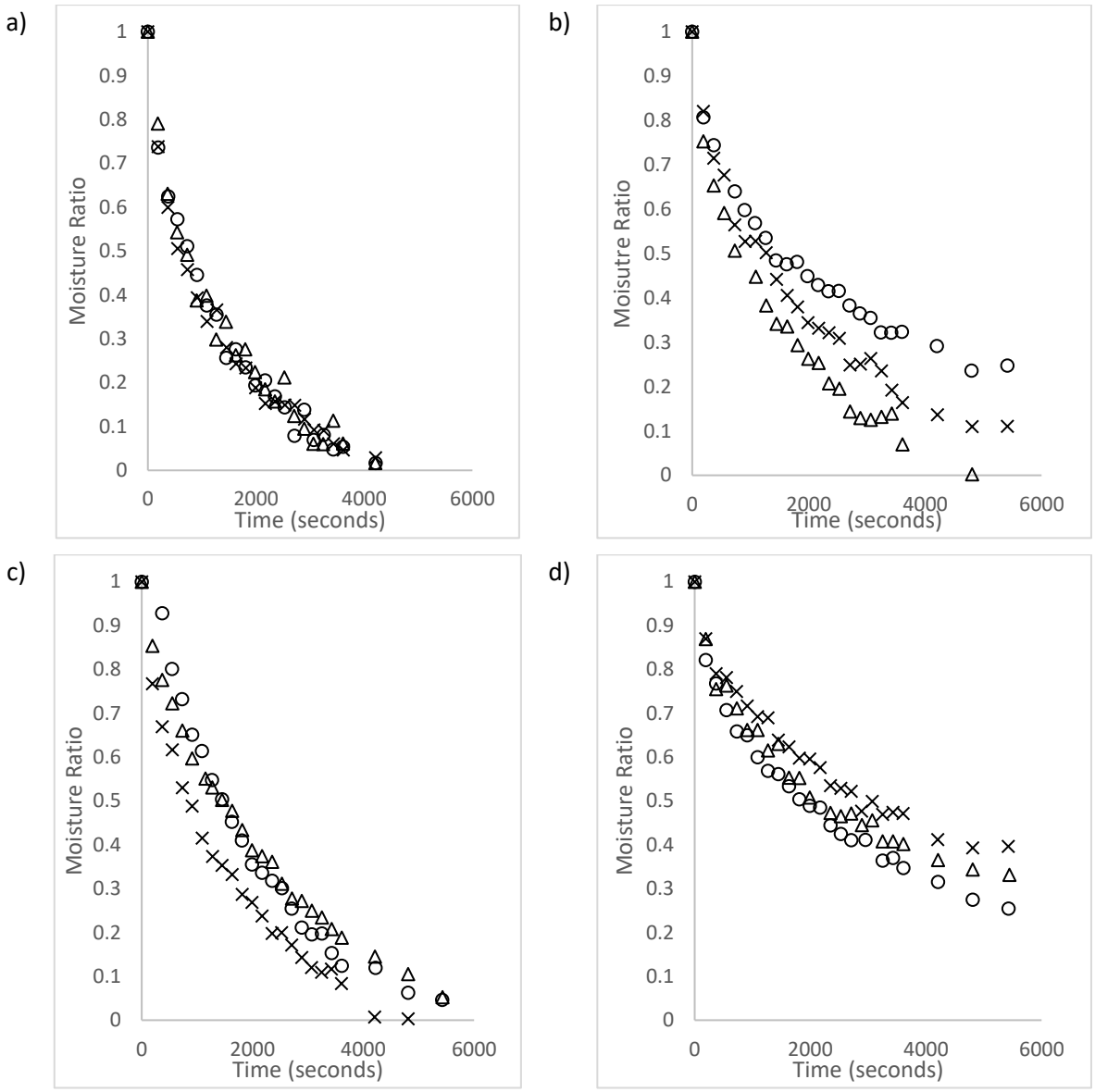

Figure 5.4; *O. intermedium* drying at 50°C; raw data triplicates; a) 2m/s, 33 kg/m³ b) 2m/s 50kg/m³ c) 2m/s 100kg/m³ d) 0.4m/s 33kg/m³.

5.2.1 Falling rate assumption validity

Analysis of the rate of change of moisture ratio against time can be used to determine the validity of the assumption of a single falling rate period during drying. Meeting this assumption is essential to the use of the F2L model for representation of drying, as a single falling rate period implies drying is purely limited by diffusive moisture transfer for those conditions. This analysis was performed by calculating the rate of change of moisture ratio from averaged experimental data via second order forward Taylor series method, shown in Equation 5.2;

$$\frac{dMR_t}{dt} = \frac{(4MR_{t+1} - 3MR_t - MR_{t+2})}{2t_{step}} \quad (5.2)$$

Graphs of the rate of change of MR against time are shown in Figures 5.5 to 5.8. These figures also include solid lines which represent the rate of change of MR calculated by deriving the fitted F2L model. This provides examples of the expected shape of a single falling rate drying period. A constant rate period during drying would show as a horizontal line on those graphs.

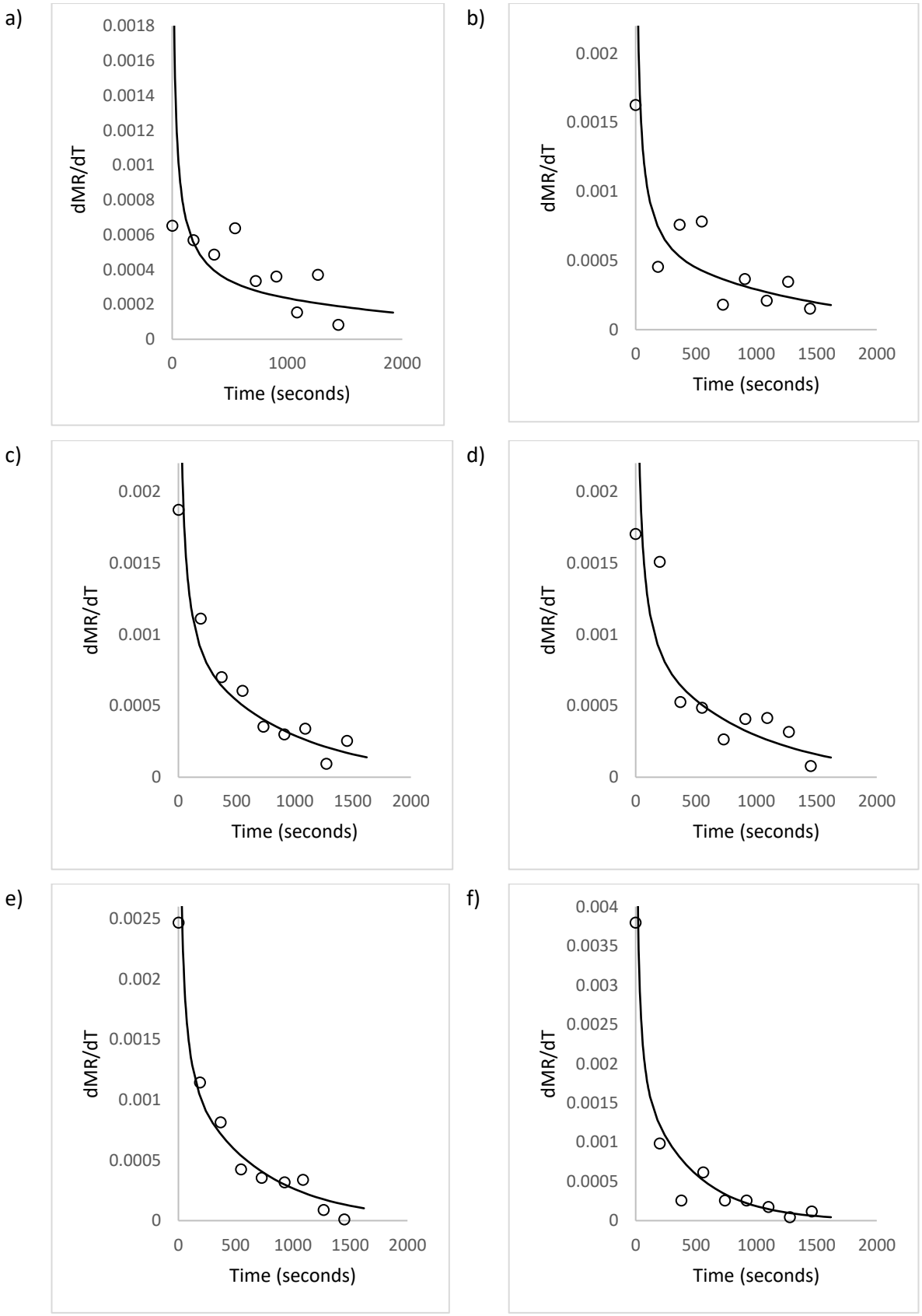

Figure 5.5; *U. ohnoi* MR rate of change; 50°C, 66kg/m³ ; a) 0.3m/s b) 0.7m/s c) 1.1m/s d) 1.3m/s e) 1.7m/s f) 2.0m/s. Points are numerically determined from experimental data; lines represent the best fit single falling rate period.

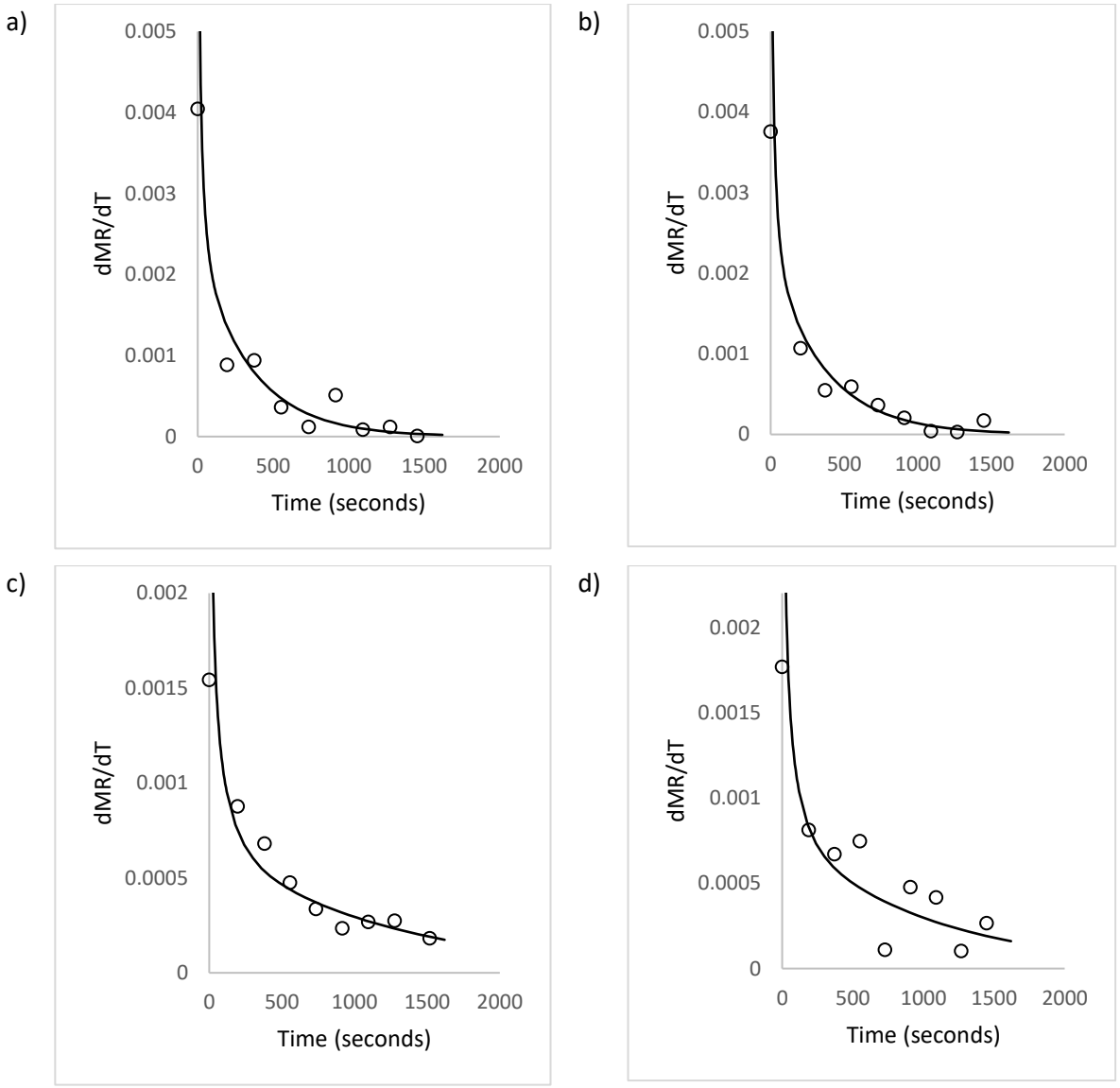

Figure 5.6; *U. ohnoi* MR rate of change; 50°C; a) 2m/s, 33 kg/m³ b) 2m/s 50kg/m³ c) 2m/s 100kg/m³ d) 0.4m/s 33kg/m³. Points are numerically determined from experimental data; lines represent the best fit single falling rate period.

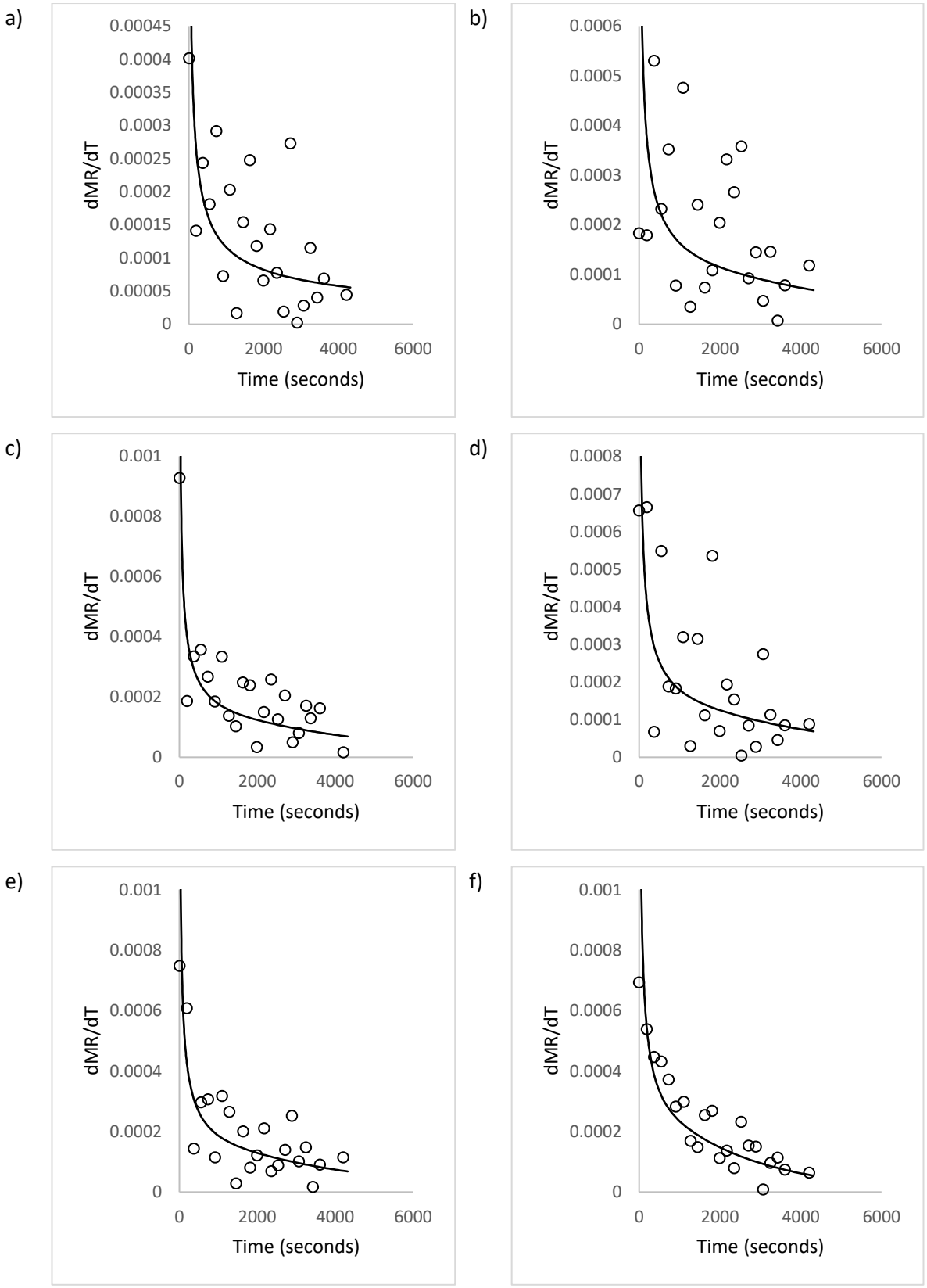

Figure 5.7; *O. intermedium* MR rate of change; 50°C, 66kg/m³ ; a) 0.3m/s b) 0.7m/s c) 1.1m/s d) 1.3m/s e) 1.7m/s f) 2.0m/s. Points are numerically determined from experimental data; lines represent the best fit single falling rate period.

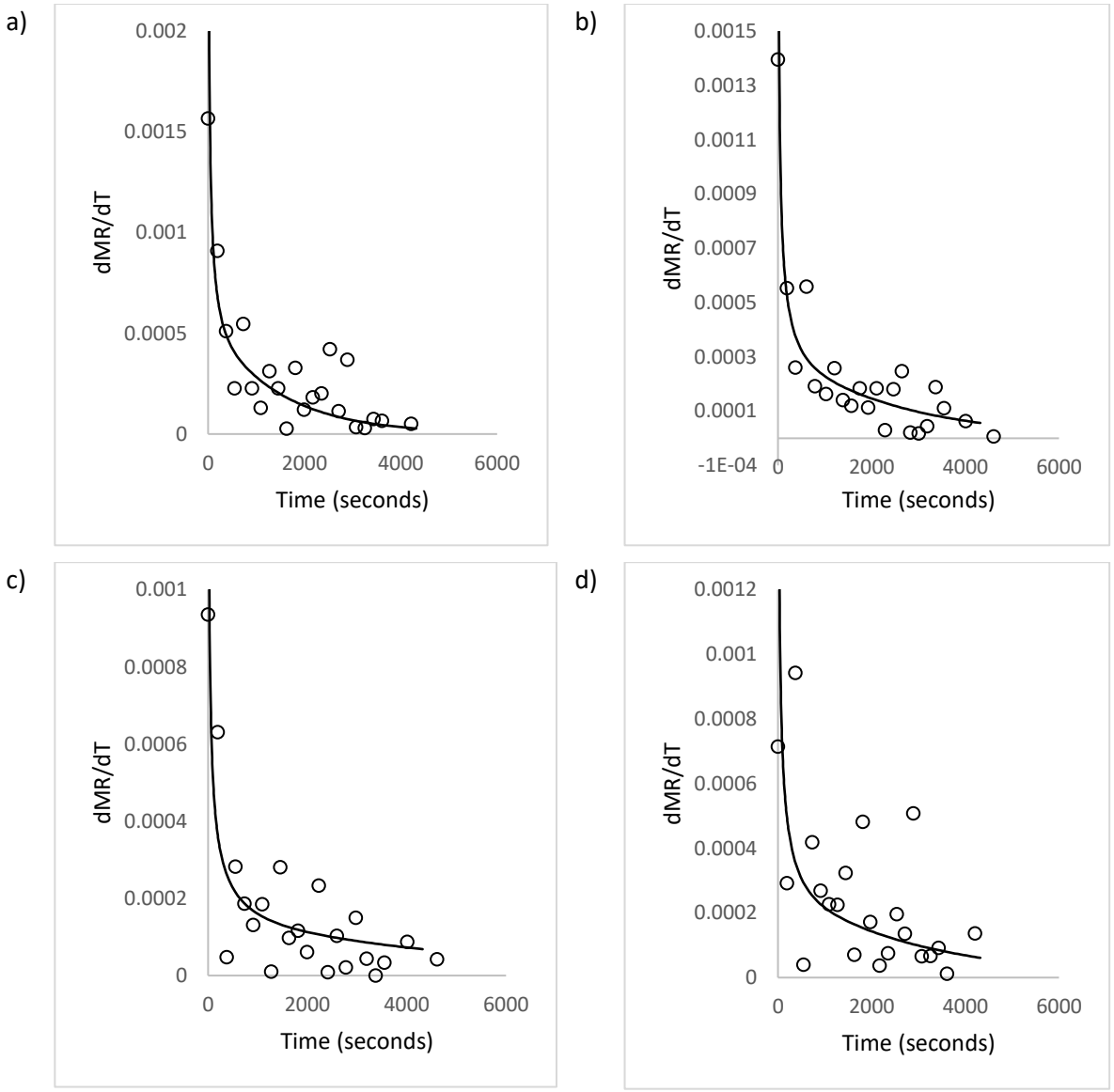

Figure 5.8; *O. intermedium* MR rate of change; 50°C; a) 2m/s, 33 kg/m³ b) 2m/s 50kg/m³ c) 2m/s 100kg/m³ d) 0.4m/s 33kg/m³. Points are numerically determined from experimental data; lines represent the best fit single falling rate period.

The experimental $\frac{dMR}{dt}$ are generally the same shape as those from a single falling rate period, with no indication of a constant rate drying period. Statistical analysis comparing the experimental data and the model derivative was performed by correlation in SPSS software. A summary of the analysis is shown in Tables 5.1 and 5.2. Significance below 0.05 indicates that the experimental data is significantly correlated with the model derivation at the 95% confidence level. The Pearson's correlation value indicates the accuracy of the correlation, with a value of 1 indicating a perfect accuracy between the expected shape for a single falling rate period and the experimental data for that condition set.

Table 5.9; *U. ohnoi*; correlation analysis between data and model rate of change.

U. ohnoi		Rate of change correlation	
Density(kg/m^3)	Velocity (m/s)	Pearson's Correlation	Sig. (two-tailed)
66	0.4	.576	.105
66	0.7	.906	.001
66	1.1	.933	.000
66	1.3	.823	.006
66	1.7	.966	.000
66	2	.992	.000
33	2	.990	.000
50	2	.996	.000
100	2	.938	.000
33	0.4	.923	.000

Table 5.10; *O. intermedium*; correlation analysis between data and model rate of change.

O. intermedium		Rate of change correlation	
Density(kg/m^3)	Velocity (m/s)	Pearsons Correlation	Sig. (two-tailed)
66	0.4	.645	.001
66	0.7	.095	.674
66	1.1	.895	.000
66	1.3	.610	.003
66	1.7	.811	.000
66	2	.785	.000
33	2	.904	.000
50	2	.948	.000
100	2	.880	.000
33	0.4	.539	.010

In Tables 5.1 and 5.2, most data sets show a high correlation to the F2L model shape, indicating the experimental and F2L model data are statistically likely to have the same shape at the 95% confidence

level. Anomalies were in the 0.7m/s, 66kg/m^3 set for *O. intermedium* and the 0.4m/s, 66kg/m^3 set for *U. ohnoi*. These data sets had a higher level of variance compared to others and is probably the cause of the lack of significance. Overall, the shape of the experimental $\frac{dMR_t}{dt}$ curves are statistically likely to be directly correlated to the theoretical $\frac{dMR_t}{dt}$ curve. This can be interpreted as showing that drying of the macroalgae under the experimental conditions tested is overall well represented by diffusion, and shows a single, completely falling rate drying period. The deviations from this correlation are likely caused by the experimental data variance; *O. intermedium* had a large variance due to material property factors, and it is the data set showing most deviation between direct experimental data and the theoretical curves.

5.2.2 Diffusion-based Drying Modelling

The parameter estimation method detailed in Section 5.1 was used to fit the model to the average of triplicate convective drying data. Graphs comparing the model and experimental data are shown in Figures 5.9 to 5.12, with experimental data represented by the average of triplicates. A summary of estimated effective diffusivities at all conditions is provided in Table 5.3 and 5.4 for *U. ohnoi* and *O. intermedium* respectively.

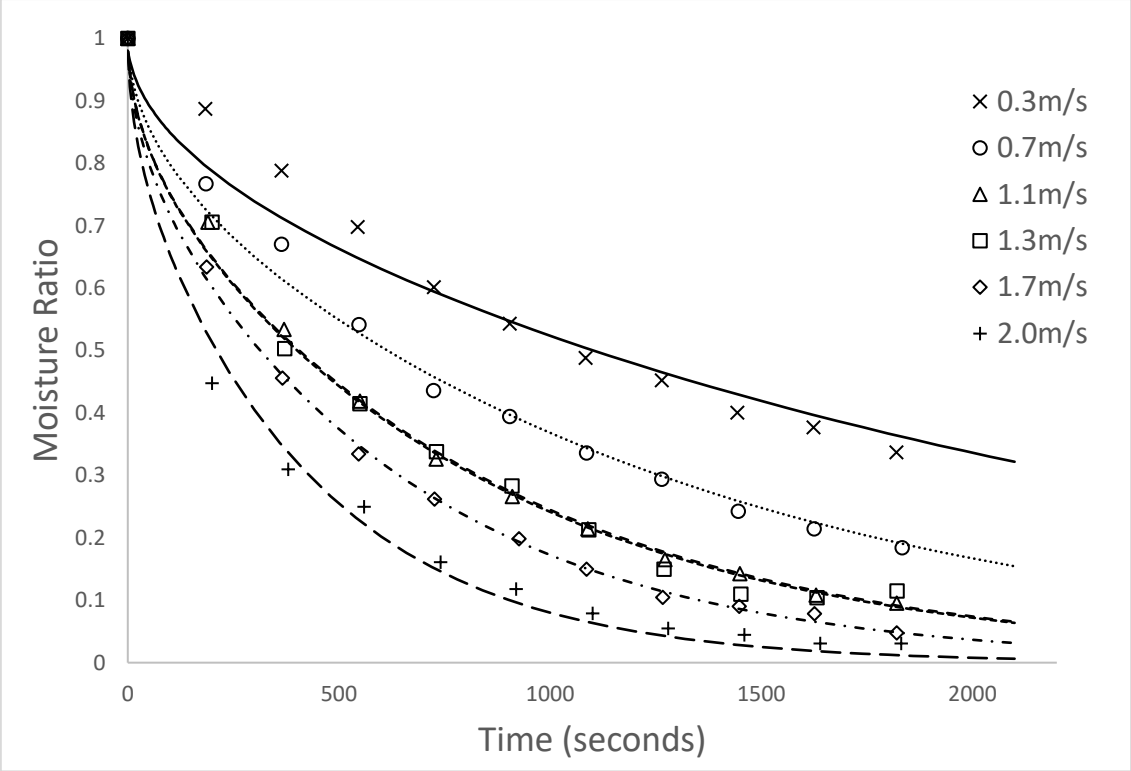

Figure 5.9; U. ohnoi drying model fit at varying air velocity. Temperature is 50°C, bulk density is 66kg/m3.

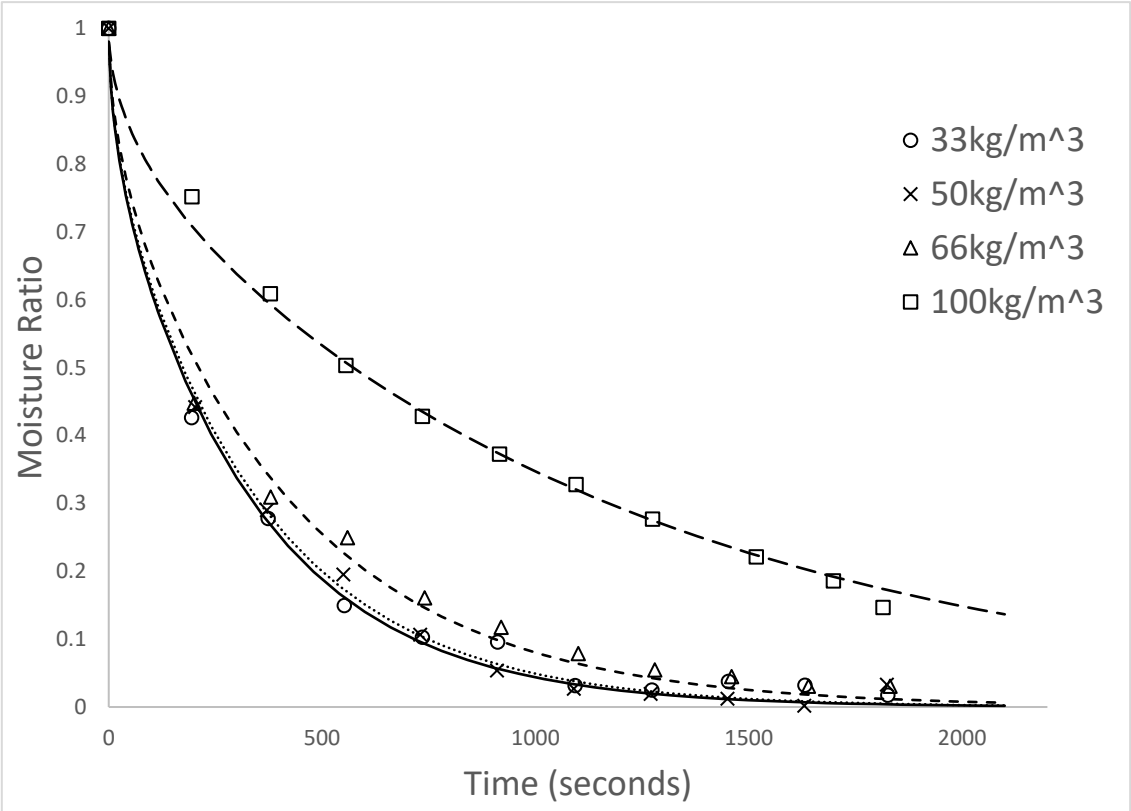

Figure 5.10; *U. ohnoi* drying model fit at varying initial bulk density. Temperature is 50°C, air velocity is 2m/s.

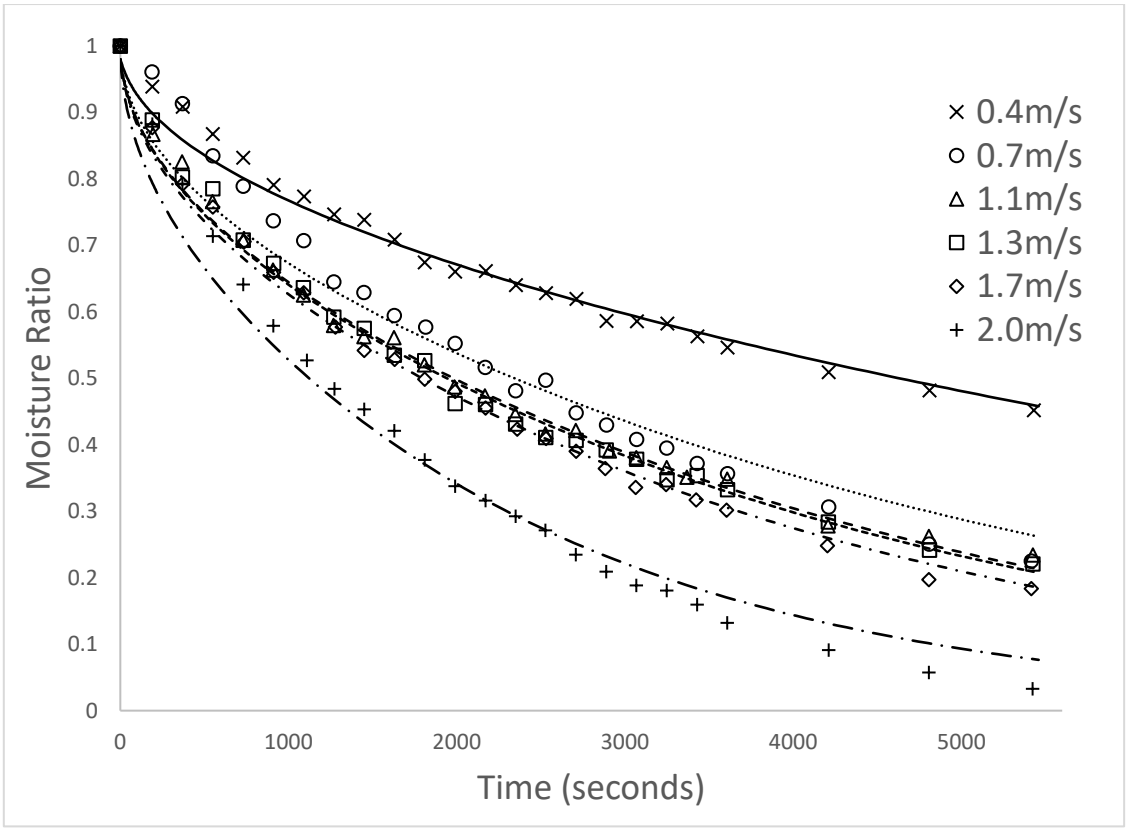

Figure 5.11; O. intermedium drying model fit at varying air velocity. Temperature is 50°C, bulk density is 66kg/m3.

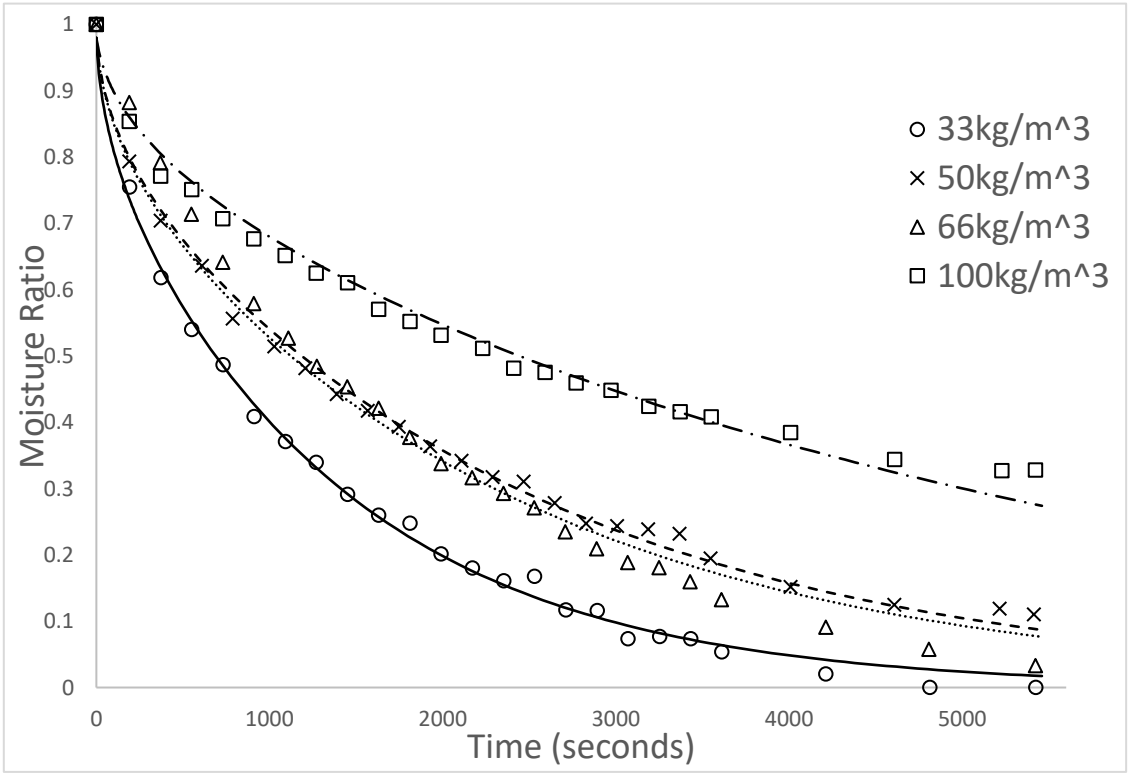

Figure 5.12; *O. intermedium* drying model fit at varying initial bulk density. Temperature is 50°C, air velocity is 2m/s.

The general fit of the Fick's second law model to the experimental data is excellent (R^2 values for all experimental conditions were above 0.95). However, the model has a tendency to under predict the experimental data for moisture ratios between one and 0.3, then over predict as the moisture ratio approaches zero. The results show that air velocity and initial density of the material have a significant effect on the drying rate for both materials. Diffusivity increases as air velocity increases, while it decreases as the bulk density increases, making drying fastest at high air velocity and low bulk density.

The effect of material bulk density on the drying rate was as expected, with increased bulk density causing a lower drying rate for both algae species. There are two mechanisms by which the bulk density is affecting the drying rate. The first is that increased bulk density increases the absolute amount of moisture in the material slab. More moisture to be removed should increase the time required to fully dry the slab of material. The F2L model cannot directly account for this change – moisture is measured as the ratio of liquid to dry solids, which does not change with bulk density. As such, this effect appears as reduced effective diffusivity. The second mechanism is that the increased amount of material in the slab is causing an increase in the physical resistance to moisture transfer. It makes logical sense to consider both of these effects as a part of the internal material properties that are covered by the effective diffusivity.

As discussed in Section 2.2.2, the rate of convective transfer of moisture is expected to be far greater than the rate of diffusive transfer, such that there is no significant period where surface moisture exists. The relationship for Bi_m covered in Section 2.2.2 gives an expected value of around 150 for the system for the lowest rate of convection and highest diffusivity (at least three orders of magnitude higher than the value of 0.1, where the system is expected to become limited by convective transfer). The study of drying rate of change in Section 5.2.1 corroborates these expectations; the data shows there is no period of constant rate drying (characterised by a significant surface moisture film) where drying was limited by convective transfer. Further increases to convective transfer rate (in a system where surface moisture is immediately removed) should not be affecting the overall drying rate.

Some studies assert the existence of a 'critical' velocity point, where further increases in gas velocity do not correspond with an increase in drying rate (Friere et al 2001). The results of this study did not find a critical velocity point for the range tested (0.4-2 m/s), but it may exist at a higher velocity. The range of velocity tested covers those typically used in drying equipment. Although drying should be fastest at the critical point, an understanding of drying rates at typical equipment conditions is of significant practical value for equipment design. Gas flow rates above the range tested are unlikely to

be viable for use in practice due to entrainment of the macroalgae particles and excessive running costs.

The most likely mechanism by which gas velocity is appearing to affect the internal drying rates is through gas penetration into the slab, with higher velocity causing more penetration. This would reduce the effective slab width, leading to faster overall drying. This effect is likely to occur for loose particulate materials (eg. the macroalgae used in this study, and also biomaterials like sugar cane bagasse and tobacco (Bezzina et al 2018)) but should not occur for materials composed of solid slabs such as wood or fruit slices.

In this study the air velocity effect was represented by taking a constant L and instead changing D_e, i.e. using D_e as a lumped parameter. A more accurate method better aligned with the physical situation would be to determine a relationship between the effective slab width and air velocity. However, observing and quantifying this relationship is not feasible with the current experimental setup, making it impossible to validate slab width predictions. Macroalgae have a complex and irregular geometry so air flows and channels through the particulate material cannot be easily simulated or identified, and such simulations cannot be scaled up to industrial levels. The method chosen in this research results in D_e being a lumped parameter, incorporating diffusion resistance, material properties that effect drying rates, and effects from external conditions such as temperature and gas velocity.

Table 5.11; *U. ohnoi* diffusivity at each condition set.

Density(kg/m^3)	Velocity (m/s)	D_e(x10^{-8}, m^2/s)	R^2	RMSE	X^2
66	0.4	36.1	0.944	0.145	0.0082
66	0.7	64.8	0.981	0.093	0.0039
66	1.1	98.3	0.969	0.131	0.0075
66	1.3	99.4	0.959	0.157	0.0100
66	1.7	127	0.992	0.072	0.0019
66	2	190	0.979	0.119	0.0053
33	2	240	0.986	0.099	0.0038
50	2	230	0.938	0.167	0.0126
100	2	69.6	0.980	0.111	0.0047
33	0.4	82.1	0.986	0.091	0.0033

Table 5.12; *O. intermedium* drying at each condition set.

Density(kg/m^3)	Velocity (m/s)	D_e (x10^{-8}, m^2/s)	R^2	RMSE	X^2
66	0.4	8.60	0.944	0.100	0.0036
66	0.7	17.0	0.784	0.287	0.0315
66	1.1	20.1	0.949	0.127	0.0063
66	1.3	20.5	0.933	0.154	0.0089
66	1.7	22.2	0.812	0.252	0.0267
66	2	35.5	0.920	0.218	0.0174
33	2	57.8	0.87	0.216	0.0207
50	2	33.6	0.934	0.128	0.0061
100	2	16.3	0.932	0.176	0.0128
33	0.4	29.9	0.989	0.078	0.0022

5.2.3 Diffusivity model

The diffusivity of both species was modelled as an Arrenhius-type relationship with temperature in Chapter 3. The relationship is shown in Equation 5.3 below, and model parameters for both species at zero gas velocity are reproduced in Table 5.5.

$$D_e = D_0 \exp\left(-\frac{E_a}{RT}\right) \tag{5.3}$$

Table 5.13; Activation energy and D_0 (from radiation drying data shown in Section 3.2.4.).

Algae	E_a (kJ/mol)	D_0 (m^2/s)	R^2
U. ohnoi	41.3	0.24	0.968
O. intermedium	34.1	0.012	0.948

As discussed in Chapter 2, E_a is related to internal moisture binding strength, while D_0 is the expected diffusivity at arbitrarily high temperature. The simplest approach is to assume that E_a is a constant for a given material, and D_0 varies to account for differences in drying rate as a result of variables other than temperature. By starting with the parameter estimated D_e values (Tables 5.3 and 5.4), the value for E_a for each species in Table 5.5 can then be used to calculate D_0 at each condition set. These D_0 values are shown in Tables 5.6 and 5.7. D_0 values from the thin layer radiative experiments in Section

3.2.4 are included in these tables as a zero air velocity point. The differences in scale between the two species is due to their material properties and drying rate. Graphs of the trends of D_0 with air velocity (a)) and initial density (b)) are shown in Figures 5.13 and 5.14 for both species. The graphs show a generally linear relationship between diffusivity and each variable, with the thin layer D_0 values (as a zero gas velocity point) matching exceptionally well with the convective drying results. This reinforces the validity of the use of thin layer experimentation to determine activation energy and diffusion coefficients for biomaterials.

Table 5.14; *U. ohnoi* D_0 at each condition set.

Density(kg/m^3)	Velocity (m/s)	D_0 (average)(m^2/s)
66	0	0.24
66	0.4	1.71
66	0.7	3.07
66	1.1	4.66
66	1.3	4.71
66	1.7	6.02
66	2	9.01
33	2	11.38
50	2	10.91
100	2	3.30
33	0.4	3.89

Table 5.15; *O. intermedium* D_0 at each condition set.

Density(kg/m^3)	Velocity (m/s)	D_0 (average)(m^2/s)
66	0	0.0118
66	0.4	0.028
66	0.7	0.0553
66	1.1	0.0654
66	1.3	0.0667
66	1.7	0.0722
66	2	0.116
33	2	0.188
50	2	0.109
100	2	0.0530
33	0.4	0.0972

a)

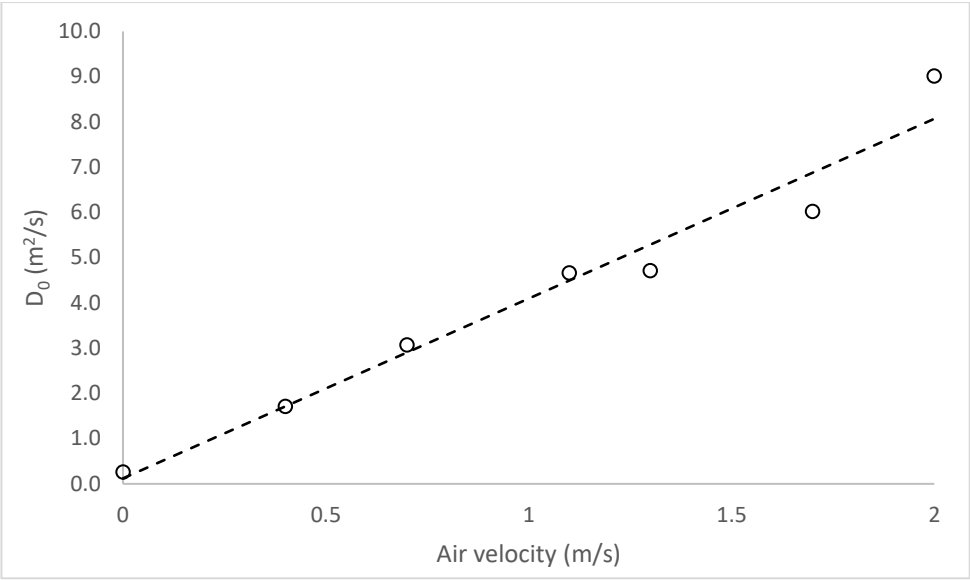

b)

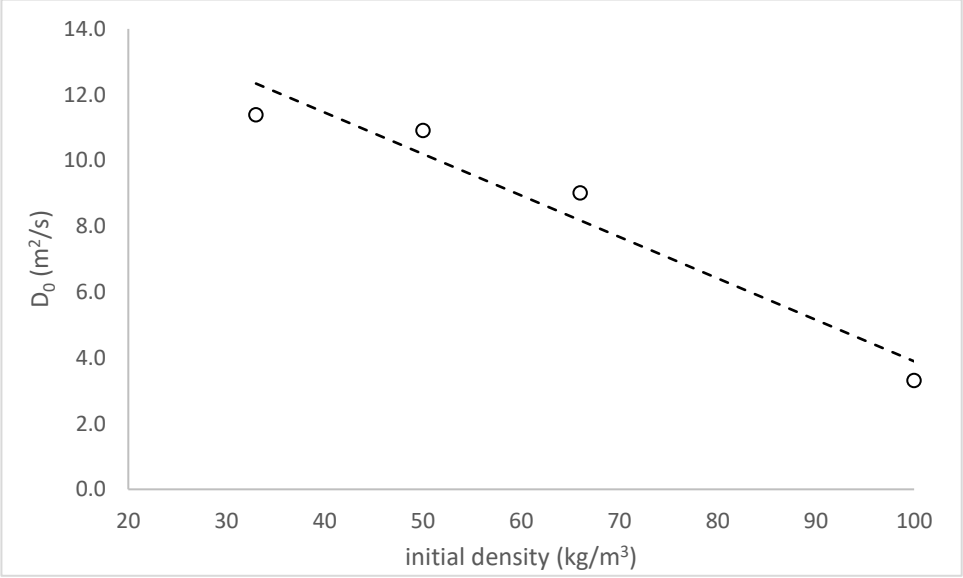

Figure 5.13; *U. ohnoi* D_0 as a function of a) air velocity, with density constant at 66 kg/m^3 b) initial bulk density, with air velocity constant at 2m/s.

a)

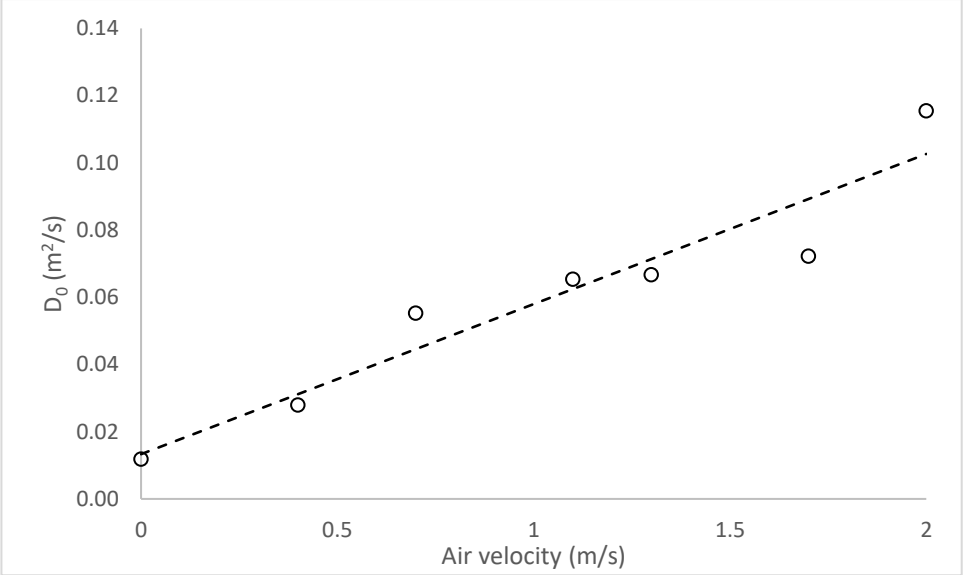

b)

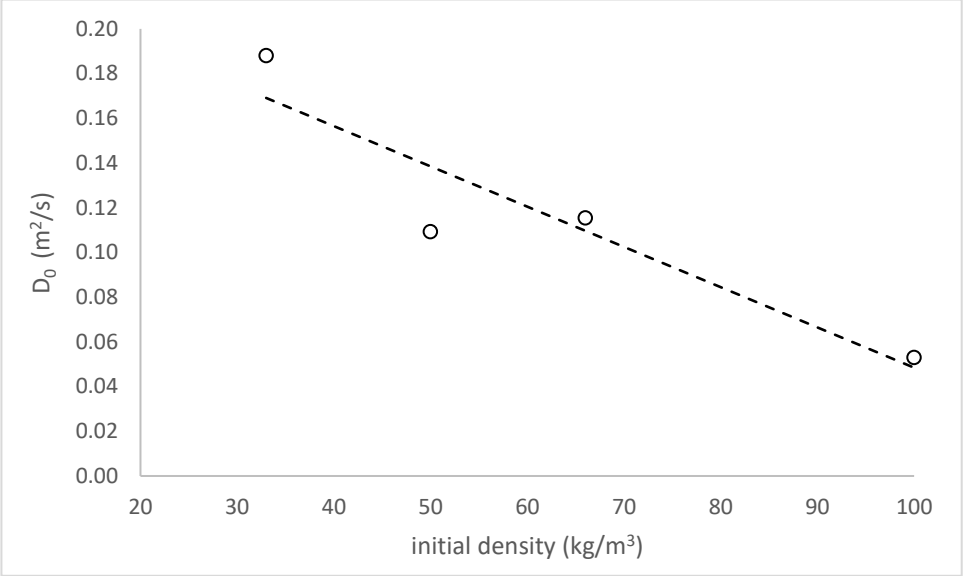

Figure 5.14; *O. intermedium* D_0 as a function of a) air velocity, with density constant at 66 kg/m³ b) initial bulk density, with air velocity constant at 2m/s..

The data in Tables 5.6 and 5.7 was used for statistical analysis to determine a relationship between D_0, gas velocity and initial bulk density, and to determine the significance of any interaction effects between the gas velocity and material density in their effect on D_0. This analysis performed in SPSS software via general linear univariate method, as the response of D_0 was shown to be linear in Figures 5.13 and 5.14. The results of the statistical analysis are summarized in Table 5.8. The F value is a qualitative measure of the magnitude of associated variable effects, and the significance indicates the

statistical likelihood of that variables relationship to diffusivity, with values below 0.05 indicating statistical significance at a 95% confidence level.

Table 5.16; Statistical analysis of variable relationship for D_0.

	F-value	Significance
Ulva ohnoi		
Velocity	38.63	.000
Initial density	42.93	.000
Interaction	0.06	.809
Oedogonium intermedium		
Velocity	6.03	.001
Initial density	9.35	.000
Interaction	1.18	.290

The statistical analysis shows that the effect of velocity and initial bulk density are linear and significant at 95% confidence (with significance below 0.05). The interaction between velocity and initial density is both much lower in magnitude and is not significant at the 95% confidence level.

The overall relationship between D_0, the drying gas velocity and the initial bulk density can be represented as a sum of their linear effects as their interaction was found to be insignificant. This relationship was calculated in SPSS as a part of the univariate analysis for *U. ohnoi* as;

$$D_0 = 6.904 + 4.34v_g - 0.113\rho \quad (5.4)$$

Where v_g is the air velocity in m/s and ρ is the material bulk density in kg/m^3. The fit between this model and the experimental D_0 results across all data sets (shown in Table 5.6) is R^2 =0.947.

For *O. intermedium*;

$$D_0 = 0.138 + 0.0454v_g - 0.00187\rho \quad (5.5)$$

Where the model fit to experimental D_0 values across all data sets (shown in Table 5.7) is R^2=0.897.

Inputting these relationships for D_0 into the Arrenhius-type relationship gives the following models for effective diffusivity as a function of temperature, air velocity and initial bulk density.

For *U. ohnoi*;

$$D_e = \left(6.904 + 4.34v_g - 0.113\rho\right)\exp\left(-\frac{41300}{RT}\right) \quad (5.6)$$

And for *O. intermedium*;

$$D_e = \left(0.138 + 0.0454v_g - 0.00187\rho\right)\exp\left(-\frac{34100}{RT}\right) \quad (5.7)$$

The predicted diffusivity from these models and their ability to represent the experimental data at each condition set is summarized in Tables 5.9 and 5.10.

Table 5.17; *U. ohnoi* modelled diffusivity fit to experimental results.

Density(kg/m^3)	Velocity (m/s)	D_e (f(ρ, v_g, T_g))(x10^{-8}, m^2/s)	R^2	RMSE	X^2
66	0.4	24.9	0.815	0.264	0.0270
66	0.7	52.3	0.935	0.182	0.0131
66	1.1	89.0	0.961	0.145	0.0095
66	1.3	107	0.955	0.168	0.0111
66	1.7	144	0.983	0.109	0.0045
66	2	171	0.974	0.132	0.0066
33	2	250	0.987	0.089	0.0034
50	2	209	0.983	0.114	0.0048
100	2	90.3	0.862	0.242	0.0276
33	0.4	104	0.930	0.197	0.0161

Table 5.18; *O. intermedium* modelled diffusivity fit to experimental results.

Density(kg/m^3)	Velocity (m/s)	D_e (f(ρ, v_g, T_g))(x10^{-8}, m^2/s)	R^2	RMSE	X^2
66	0.4	10.1	0.906	0.118	0.0061
66	0.7	14.3	0.755	0.286	0.0359
66	1.1	19.8	0.949	0.129	0.0063
66	1.3	22.6	0.920	0.156	0.0106
66	1.7	28.2	0.734	0.255	0.0377
66	2	32.4	0.913	0.216	0.0188
33	2	51.4	0.978	0.110	0.0042
50	2	41.6	0.825	0.244	0.0269
100	2	12.9	0.831	0.181	0.0149
33	0.4	29.0	0.931	0.176	0.0130

5.3 Discussion and Analysis

The following is a summary of the relevant drying theory and new considerations needed to describe the mechanisms by which gas velocity and material bulk density are affecting drying rates in the above work. Important considerations include the geometry of the material setup, and its relationship to the underlying assumptions of the F2L model, which are outlined in Section 2.1.2. To facilitate discussion the material geometry used in the development of the Fick's Law analytical equation is shown below in Figure 5.15 (reproduced from Chapter 2). See Figure 2.3 for examples of the expected moisture profiles across the slab width.

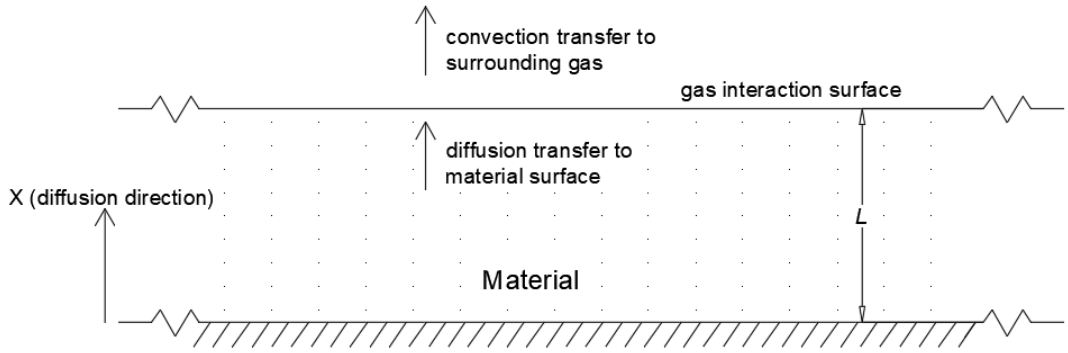

Figure 5.15; Diagram of material geometry assumed in the development of the Fick's law analytical drying model. Moisture is assumed to diffuse in the x direction toward the material surface, where it undergoes convection into the surroundings.

Drying is considered as two separate stages: diffusion transfer of moisture through the material to the gas interaction surface (defined as the boundary between the material and the drying gas bulk); and convection transfer of moisture from the interaction surface to the surrounding gas. The second stage is rate limiting only when excess free moisture is on the material surface. The Fick's law model assumes that the convective moisture transfer is sufficiently fast such that all surface moisture is immediately removed, and therefore diffusion transfer through the material to the surface is the rate limiting stage. At low gas velocity convection can be limiting and increases in gas velocity can lead to an increased drying rate. However, as increased gas velocity leads to increased rates of convective mass transfer, there will be a point where drying rates become limited by diffusion. This point has previously been defined as a 'critical' gas velocity, because further increases to the drying gas velocity above this point should not affect the drying rate. Some studies have shown results that fit this critical velocity assumption, including Friere et al. (2001) using olive bagasse, and Mulet et al (1987) using small cubes of carrot. In this hypothesis, the external gas flow rate should not be able to affect the internal diffusive transfer for a material best represented by the geometry in Figure 5.15. The mechanisms described is most suitable for solid blocks of material (e.g. wood) or single layers of material particles (such as the geometry chosen by Friere et al. (2001)), but may not be appropriate for porous biomaterials such as the macroalgae species used in this thesis.

The experimental results in this work show trends that go against this mechanism with respect to air velocity and material density and their observed effect on drying rates. Considering the impact of bulk material density first, an alternate mechanism involving gas penetration is proposed. Increases in material bulk density decrease the void fraction in the slab. A decrease in void fraction results in an increase in material physically blocking the diffusion pathways to the material surface (i.e. presenting

a physical resistance to diffusion) and therefore a decrease in the effective diffusivity is observed with increased density. The upper limit of this effect would be at zero void fraction, where the material can effectively be considered as a solid block, as represented by Figure 5.15, with L as the full slab width. Zero void fraction implies that there should be no opportunity for gas to penetrate into the slab.

Considering the impact of gas velocity on the drying rate, experimental results in this work show that drying rates for both macroalgae increased as the drying gas velocity increased. In a porous biomaterial, it is expected that increases or decreases in air velocity cause more or less gas penetration into the particle bed, respectively. Figure 4.7 shows images of the material loaded into the sample container, with visible gaps between separate pieces of the macroalgae. The hypothesis posed in this work is that increased penetration via higher gas velocity works to reduce the average distance between the particle surface and the surrounding gas interaction surface (the distance denoted as L in Figure 5.15). However, in this case the drying gas interaction surface is not the external edge of the material slab as defined in Figure 5.15 but is internal to the material slab due to the effect of drying gas penetration. The upper limit of this effect is then where the drying gas fully penetrates the slab such that the gas boundary layer surrounds the minimum material dimension (i.e. the smallest individual particle within the bulk material). This reduces the geometry to that described in Figure 5.15, with L being equal to a single particle width. The point where this occurs could also be referred to as a 'critical' velocity in that further increases in gas flow should not affect drying rates.

Under this new mechanistic description the algae material is better represented as a slab comprised of many individual particles, where the smallest particle dimension would be a single particle or cell. This geometry is shown in Figure 5.16. The mechanisms described above by which air velocity and initial density are affecting drying can be represented using this geometry, and are outlined below.

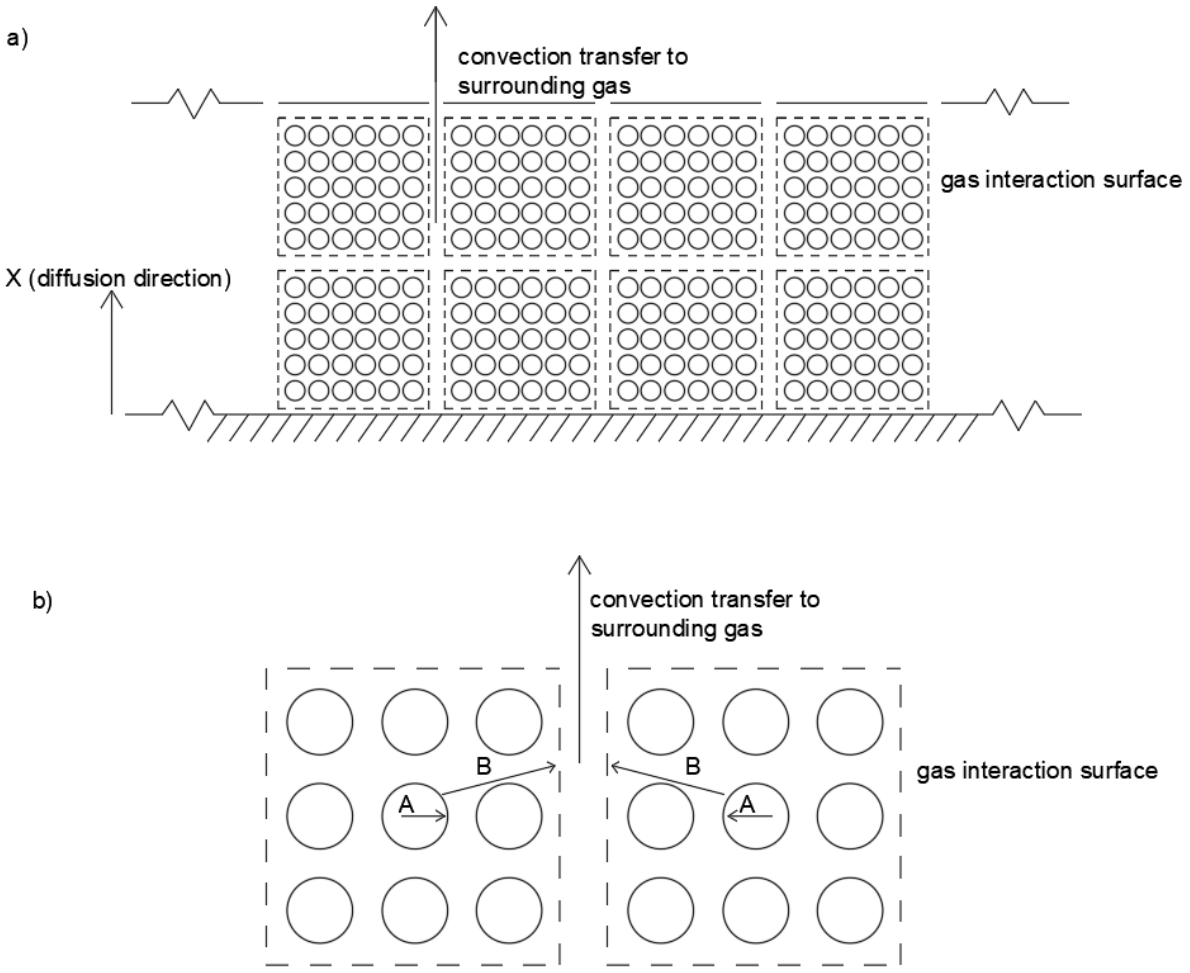

Figure 5.16; Proposed new material geometry that includes the expected mechanisms of air velocity and material density effects on drying rate. a) shows the overall effect of air velocity dividing the material into smaller 'blocks' due to gas flow penetration. b) shows drying mechanism and diffusive transfers within a given 'block'.

In Figure 5.16, internal moisture diffusion is shown as two separate stages (mechanisms A and B). Dotted lines represent the acting surfaces where convection transfer occurs. Mechanism A represents internal moisture diffusion through a particle to the particle surface, while mechanism B represents moisture transfer through a given 'block' to the gas interaction surface. This second stage is what is believed to be affected by changes in bulk density and air velocity via the mechanisms described above. It is then expected that this stage is the rate limiting step for conditions where a relationship between air velocity and/or material bulk density and drying rates exist. Experimental results in this thesis suggest that drying is in a single falling rate period under all experimental conditions investigated; as such, mechanism B (as the rate limiting step) is likely a diffusive transfer. Thus, the application of the F2L model in the above work is noted to have lumped the moisture transfer represented as A (not rate limiting) and B (rate limiting) together.

The impact of air flow can be understood by considering flow penetration which acts to separate the bulk material into 'blocks' of particles. As discussed above, increases in air flow rate cause increased slab penetration which breaks up the bulk material into even smaller blocks. The lower and upper limits of the air flow effect are as described above, where no flow results in no penetration and L is best represented as the full slab width. The upper limit occurs at some maximum gas velocity where the blocks are reduced to the dimensions of an individual particle width. The impact of density is represented by less or more particles per 'block'. Thus, an increase in the number of particles per unit volume in the slab both acts as an increased physical barrier to internal diffusion and increases the absolute amount of moisture required to be removed for that volume. The lack of interaction between gas velocity and bulk density is expected to occur because the gas velocity is separating the material into the same sized blocks within the fixed container volume, but with more particles per block as the bulk density increases.

5.4 Conclusions

The Fick's law analytical drying model well represents drying of both algae species across the conditions tested, covering conditions expected in typical drying equipment. The model has a high level of correlation, with R^2 values at 0.9 or higher. Testing showed that drying was in a falling rate period for all times and all conditions, meeting model assumptions and justifying drying being represented by diffusion modelling.

The experimental results show that the velocity of the drying gas and initial bulk density of material have a significant effect on the drying rate. An increase in air velocity correlated with an increase in drying rate, while an increase in initial bulk density caused a decrease in drying rate. The two variables had no statistically significant interaction effect on drying over the conditions tested. Both density and air velocity have a linear relationship to diffusivity in the experimental results. The results from thin layer radiative drying tests in Chapter 3 also align with results from this chapter as a zero gas velocity point, confirming the temperature relationship determined in Chapter 3 (i.e. the activation energy E_a) can also be used in the model formulation derived from these experiments.

The drying and modelling results suggest that initial bulk density be included in model formulations for D_0 to best represent drying of compressible materials, such as fibrous biomass and macroalgae. It is important that bulk density be defined clearly in reported diffusion studies for similar material. The experimental results show that small absolute changes to bulk density can have significant effects on

drying rates, which may be a cause of variance in calculated diffusivity values between studies of the same material. Bulk density is a controllable design variable for certain types of drying equipment (e.g. solar or assisted solar). Increasing bulk density allows for more material to be processed for a given area, but the trade off with respect to drying times must be considered. This work enables that trade-off to be quantified. It is expected that the magnitude and specific relationship between bulk density and drying rates will be dependent on material properties and particle geometry, and should be evaluated experimentally for a given material.

Insight into mechanisms of porous biomaterial drying have been provided by this experimental work. It is expected that air flow is affecting drying rates through gas penetration into the material slab, which is in turn affecting the average distance to the gas interaction surface (L). This leads to an upper limit where gas flow is sufficient to reduce L to a single particle width, and this point is expected to match the 'critical' velocity point described in literature for drying of very thin layer material. Direct modelling of air flow through large and irregular particles to relate gas velocity with an 'effective' slab width is computationally complex; the pragmatic option of modelling the effect as changes to the effective diffusivity with a constant slab width was taken in this work, and is sufficiently accurate in representing the experimental data. A discussion of methods to prove or disprove the presented drying theory are outlined in Chapter 7.

The models presented were noted to deviate from experimental data at the initial and final periods of drying. Both macroalga have significant volume losses occurring during drying, whereas the model used assumes no volume changes occur. This could be a cause of the noted deviations between model and experimental data. Analysis of these and other phenomena as to whether their inclusion in drying kinetics modelling can improve fit is performed in the following chapter.

Chapter 6

6. Model Extension and Scale-up

Chapter 5 presented experimental data showing the drying kinetics of *U. ohnoi* and *O. intermedium* are affected by the velocity of drying air and the material bulk density. This was consolidated with results presented in Chapter 3 to form a function for the effective diffusivity dependent on the drying gas temperature, drying gas velocity and the material bulk density. The model has an overall high fit to the experimental data, but the base F2L model has a tendency to deviate from the experimental results at both the early and late stages of drying. Good fit at the late stage of drying is especially important for prediction of drying times in the design of industrial equipment. This deviation was hypothesised to be due to assumptions made in the F2L model not being true. In particular, the assumptions of constant slab geometry and the material immediately reaching drying temperature through all of the slab were thought to be unrepresentative of real conditions. Adjustment of the model to account for these phenomena are hypothesised to lead to an improved model fit.

In this chapter, adjustments are made to the F2L model to account for observed differences between the model assumptions and reality. In this chapter measured slab dimensions during drying experiments are presented. The correlation between slab dimensions and moisture ratio are investigated. In addition, a method to account for time required for the material heating to the drying gas temperature is investigated. This heating period becomes increasingly relevant as the scale of drying increases.

There are two priorities in the modelling of material drying kinetics. The first is to provide a greater understanding of the theory and mechanics of drying. The second is to provide a good representation of real industrial drying equipment, so that the model can be used for optimization and equipment design. As such, the final test for the model is to test its ability to use the model in an industrial setting for predicting total drying times - it is important that the model is able to be utilised and scaled up for application in an industrial setting. The model's ability to represent drying on a larger scale was tested with drying data obtained using a pilot scale flighted rotary dryer for both species of algae. In an industry setting slab length is more difficult to estimate; effects of slab width and the heating period are accentuated, providing a good platform for testing model validity.

6.1 Model Assumptions

To recap, the development of the analytical solution of Fick's law as applied to drying of an infinite slab includes the following major assumptions;

- Drying is always limited by moisture diffusion in the material to the surface inferring that convection transfer of surface moisture to the gas bulk is always faster than internal diffusion.
- Drying gas volume is sufficiently large that moisture transfer from the solids to the gas does not change the gas properties (temperature and humidity).
- The geometry of the material sheet is constant throughout all drying time. The loss of moisture from the material does not cause any corresponding loss of volume for the slab.
- Temperature is isothermal, and the material immediately reaches the drying gas temperature.

The first two assumptions are relatively well representative of conditions in the experiments presented in Chapter 5. For example, the analysis in Section 5.2.1 proved that drying was always in a falling rate period in all convective drying conditions, indicating that drying was limited by diffusion of moisture through the material slab. Furthermore the small scale of the laboratory testing makes meeting the second assumption trivial – there was a maximum total of 25g of water removed by 1500L/min of air, over 30 minutes for *U. ohnoi* and 90 minutes for *O. intermedium*.

In practice, the latter two assumptions are clearly not met in the drying of macroalgae. The macroalgae used in this study have significant volume losses during drying. Individual particles of the macroalgae lose up to 50% of their volume when fully dried. This results in the slab width L no longer being constant, which could in turn result in significant differences in drying rate compared to what is expected by the model. This could be an explanation of the under-prediction of drying at late stages, where the experimental data shows faster drying than the best fit from model prediction (see Figures 5.9 to 5.12).

Referring to the final assumption outlined above, the assumption of isothermal temperature is not correct in reality. The material being dried starts at room temperature, and is heated up to the drying gas temperature over some initial heating period. This inconsistency in the early stages of drying aligns with the deviations shown in the experimental data, where the worst fit between the F2L model and experimental data was at the initial stage of drying and particularly evident at the slowest air velocity tested.

Adjustments to the F2L model to account for these two phenomena (volume losses during drying, true material temperature) could potentially improve model fit, especially in the initial and late stages of

drying. The following sections include work testing whether these adjustments can improve model fitting.

6.2 Volume Losses during Drying

Qualitative analysis of both species of macroalgae before and after drying found that the material exhibited significant shrinkage during drying, as opposed to model assumptions of no volume changes. The following section describes the results of experimentation and the corresponding modelling methodology used to quantify the volume losses and outlines model adjustments for their inclusion. An evaluation of whether this adjustment improves the model's ability to accurately predict drying end point times is provided.

6.2.1 Review of kinetics studies including volume loss

A general review of drying models that include adjustments for the effects of volume loss was performed by Katekawa and Silva (2006). The review covers methods used in literature to incorporate material volume losses into drying kinetics models. The majority of the work focuses on modelling of drying through numerical approaches, predominately aimed at representing drying and shrinkage for the study of internal phenomena (e.g. pore size changes and/or formation) rather than drying itself. The inclusion of volume loss in an analytical approach to drying models (the approach used in this thesis) is noted as sufficient for engineering purposes of representing drying for equipment design. The addition of volume losses in an analytical modelling approach is therefore a focus in further literature reviews. Some relevant examples of drying studies with this approach include Musielak (2008), Vargas et al (2018), Kurozawa et al (2012), Hassini et al (2007) and Hernandez et al(2000).

Vargas et al (2018) experimentally determined drying rates for calcium alginate droplets in a packed bed dryer. The material was found to lose up to 60% of its volume during drying. Rather than propose a shrinkage model, shrinkage of the material was measured directly via image analysis (with the material removed from the dryer for image capture), and an empirical equation for the diameter versus time was developed. Modelling of drying with the inclusion of this volume loss was performed using a version of the F2L analytical drying model for spherical geometry, modified to the new time dependent diameter;

$$MR = \frac{6}{\pi^2}\sum_{n=1}^{\infty}\left(\frac{1}{n}\right)^2 \exp\left(-\left(\frac{2n\pi}{d_t}\right)^2 D_e t\right) \quad (6.1)$$

Where d_t is the measured sphere diameter at time t. Modelling without inclusion of volume losses deviated from experimental data at the initial and late periods of drying, while the inclusion of volume losses improved model fit for both periods. The experimental results in Section 5.4 for the macroalgae showed similar deviations between the model and experimental data. See Figures 5.9 to 5.12 for examples of this deviation.

Kurozawa et al (2012) determined drying rates for cubes of papaya in a convective tray dryer with the inclusion of volume loss. Volume losses during drying were measured through image analysis, with material removed from the dryer for image capture as per Vargas et al (2018). Visual analysis of their data indicates that there is a strong linear relationship between the slab surface area and the moisture content, similar to observations made by others, including Musielak (2008). They used an adjusted F2L model for slab geometry to include volume losses via the introduction of an equation for Length as a function of time (L_t). The equation is shown below;

$$MR = \frac{8}{\pi^2}\sum_{n=0}^{\infty}\frac{1}{(2n+1)^2}\exp\left(\frac{(2n+1)^2\pi^2 D_e t}{4(L_t)^2}\right) \quad (6.2)$$

Where L_t is the slab width at time t. They used a previously determined model for fruit and vegetables to relate volume losses to moisture content and initial density (with the slab width L calculated from changes in surface area through the assumption of isotropic volume loss);

$$\frac{A_t}{A_0} = (aM_t + b)^n \quad (6.3)$$

$$a = \frac{\rho_0}{(M_0 + 1)} \quad (6.4)$$

$$b = 1 + a - \rho_0 \quad (6.5)$$

Where A_0 is the initial surface area, A_t is the surface area at time t, and n is a model fit parameter. They graphed $\frac{A_t}{A_0}$ against moisture content to determine n and validate the model.

Musielak (2018) utilised a diffusion based partial differential equation (PDE) model to represent drying in a packed bed of shrinking particles. The full set of equations and associated boundary conditions were solved through a numerical approach, which they noted took considerable time per solution (up

to 30 minutes). Key assumptions in their approach were that the porosity (or bulk density) of the bed was assumed constant, as the shrunken particles fall into the freed space. The shrinkage model employed assumed that the volume loss is linear and solely caused by moisture losses during drying, such that;

$$V_t = V_0\big(1 - \alpha(X_0 - X_t)\big) \tag{6.6}$$

Where V_t is the bed volume at time t, V_0 is the initial bed volume, X_t is the moisture content at time t, X_0 is the initial moisture content, and α is the loss coefficient.

Hassini et al (2007) experimentally measured drying of potato slices in a convective tray dryer. The experimental data was used to compare numerical and analytical approaches to modelling drying kinetics with the inclusion of volume losses. The potato slices had very high volume loss during drying (up to 77%). Drying was represented by three different drying periods each being characterised by their own diffusivity. The analytical model was the same as used by Kurozawa (2012), and their data both showed a linear relationship between slab width and moisture content and that all volume losses were caused by moisture loss during drying. Their results show that the inclusion of volume losses led to a substantially different value for the diffusivity and better model fit compared to those obtained by assuming a constant slab width. The values differed by up to 90% at the slowest tested drying conditions. This is higher than the differences found by Vargas (2018), and is likely due to the high percentage volume loss for the potato slices. The comparison between numerical and analytical modelling approaches with inclusion of volume losses showed a smaller difference in D_e of around 20-30%. This difference was noted to be exacerbated by the multiple drying periods used in modelling. There was large uncertainty in their approximation of the transition point between drying periods, and were only certain about the diffusivity in the last stage. Their conclusion was that the analytical modelling approach was sufficient as an approximation of drying. This quality of fit for the F2L analytical approximation is likely to be better for materials with single drying periods (i.e. *U. ohnoi* and *O. intermedium*, as demonstrated in Section 5.3).

Hernandez et al (2000) studied drying kinetics of mango and cassava using an analytical drying model with modelling to represent slab width changes. They used the F2L model, with the slab width L replaced with L_t, the slab width at time t. They related the moisture content to the slab width using the following;

$$\frac{L_t}{L_0} = \Delta L_f + (1 - \Delta L_f)\frac{M_t}{M_0} \tag{6.7}$$

Where ΔL_f is the fractional difference between the initial and final slab width. This type of model has been shown to work for other food materials (Lang et al 1994, Mulet 1994). The paper provides a mathematical analysis of the use of a changing value for L in the F2L analytical model. A variable L was shown to still provide a true solution to Fick's law diffusion equation if several inequalities are met. These inequalities were shown to be true only at the end of drying, and for the defined centre line of the slab. This implies there will always be some deviation in result between the use of numerical and analytical approaches with the inclusion of variable L. They conclude that the analytical solution approach still provides a good fit to their experimental data, and that the approach is appropriate for engineering purposes.

The conclusions to be made from this review are that the approach of modifying the F2L analytical solution to represent slab geometry changes (using L_t instead of L) is sufficiently valid and well-suited for equipment design. A linear relation between L and moisture content has been shown to work for food materials, although it is unknown if this is the case for porous biomaterials such as algae. The benefits of modelling by a first principles approach, with a mathematically complex representation of volume losses, are minimal when the objective is to use models to undertake equipment design. First principles approaches typically involve parameters with a great deal of uncertainty and have prohibitive solution times for industrial applications. Acceptable simplifying assumptions for representation of drying are that volume losses are isotropic (equal in all directions) and that volume loss is solely due to moisture loss from the material.

6.2.2 Experimental Length Data

Analysis of volume losses during drying were performed using the equipment outlined in Chapter 4. Images of the material drying were captured with a GoPro camera attached next to the sample container (see Figure 4.2 in Section 4.2.1). Image capture and analysis was performed in triplicate for each condition and for both algae species. These images were used to determine the changes in the slab width during drying via the analysis method outlined in Section 4.6.2.

The averaged experimental length vs time data is shown in Figures 6.1 and 6.2 below. In this figures, for *U. ohnoi*, drying conditions were 50°C, 0.7m/s air velocity and 66 kg/m^3 bulk density, while for *O. intermedium* the conditions were 50°C, 2.0 m/s air velocity and 66 kg/m^3 bulk density.

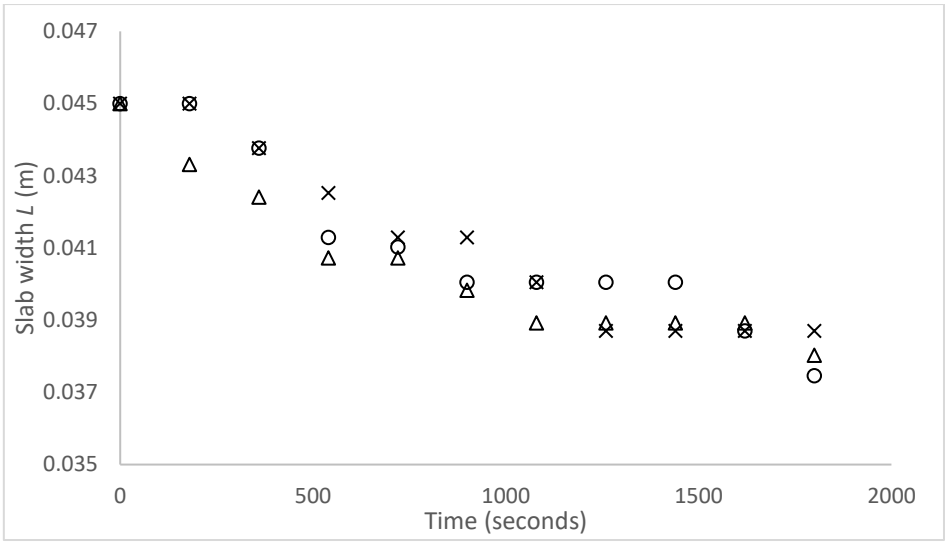

Figure 6.1; Triplicate measured length vs time for U. ohnoi at 50°C, 0.7m/s air velocity and 66 kg/m³ bulk density.

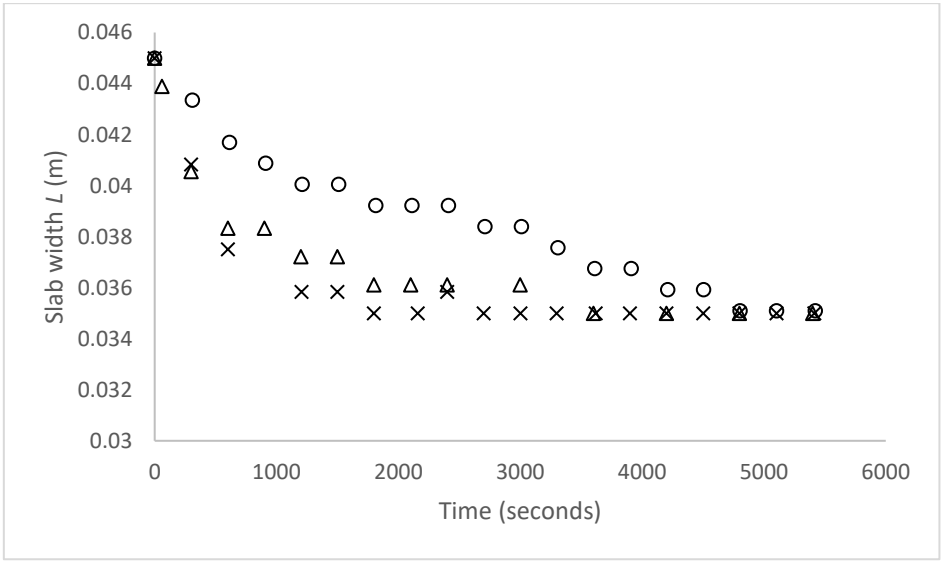

Figure 6.2; Triplicate measured length vs time for O. intermedium at 50°C, 2m/s air velocity and 66kg/m³ bulk density.

The repeatability of the length vs time data is similar to the repeatability of moisture ratio data for both species. The data has an overall shape that is similar to moisture ratio against time, where the fastest rate of change in length is in the initial period. The slab width appears to decrease from 0.045m to 0.035 during drying at these conditions for both macroalga species.

Testing was performed to ascertain whether the bulk density of the material influenced the overall volume loss for the slab. This was performed by loading the sample container with different density samples for both materials and drying for 72 hours at lab bench conditions. The models developed in Chapter 3 show the equilibrium moisture content for drying experiments was 9%db for *U. ohnoi* and

4%db for *O. intermedium* for drying conditions (50°C and 10%RH) compared with 15%db for *U. ohnoi* and 5%db for *O. intermedium* at lab bench conditions (25°C and 40%RH). As such, endpoints of drying should well represent those in experimental testing and therefore should not affect results. The percentage volume loss was 25% (rounded) in all directions for all densities tested, with no significant change in volume loss for different densities.

6.2.3 Analysis

The literature review in Section 6.2.1 indicated that volume losses during drying are likely related to moisture losses. The studies identified have also shown a linear relationship between volume losses and moisture content for food materials (Hernandez et al 2000, Musielak 2018, Kurozawa et al 2012). The general shape of the experimental data in Figures 6.2 and 6.1 show a similar exponential decay (i.e. compared to moisture content against time profiles), which indicates that this type of relationship may also exist for the macroalgae.

The experimental data for moisture content is recorded as a non-dimensional value MR. It represents the extent of drying that has yet to occur as a decimal value between 1 and 0. Slab widths were recorded as a dimensioned value, which makes comparison or relation to the non-dimensional moisture content more difficult. As such, slab widths were instead converted to a non-dimensional ratio to facilitate analysis. The non-dimensional slab width (represented as L_D) at a given time was determined by the following equation;

$$L_D = \frac{L_t - L_\infty}{L_0 - L_\infty} \tag{6.8}$$

Where L_t is the slab width at time t, L_0 is the initial slab width and L_∞ is the final slab width (at $t = \infty$). The value L_D represents the percentage of volume losses that are yet to occur during drying. At $t = 0$, L_D is equal to 1 and indicates no volume loss has occurred; at $t = \infty$, L_D is equal to 0 and indicates all volume losses from drying has occurred. This makes both the moisture ratio and slab width non-dimensional values with the same range (1 to 0). This facilitates the comparison of moisture and volume losses over time.

Examples of L_D vs MR are shown in Figure 6.3 for the raw data sets shown in Section 6.2.2. The non-dimensional slab width visually appears to be highly correlated to the MR value for each data set. Correlation of L_D and MR obtained from the experimental data was performed in SPSS to statistically determine whether a relationship exists between the two values and the significance of that correlation. Results are shown in Table 6.1. The results can be interpreted with the Pearson correlation

representing the level of correlation between L_D and MR, with values closer to 1 indicating a higher correlation. Significance values of 0.05 or lower indicate the correlation is statistically significant at the 95% confidence level.

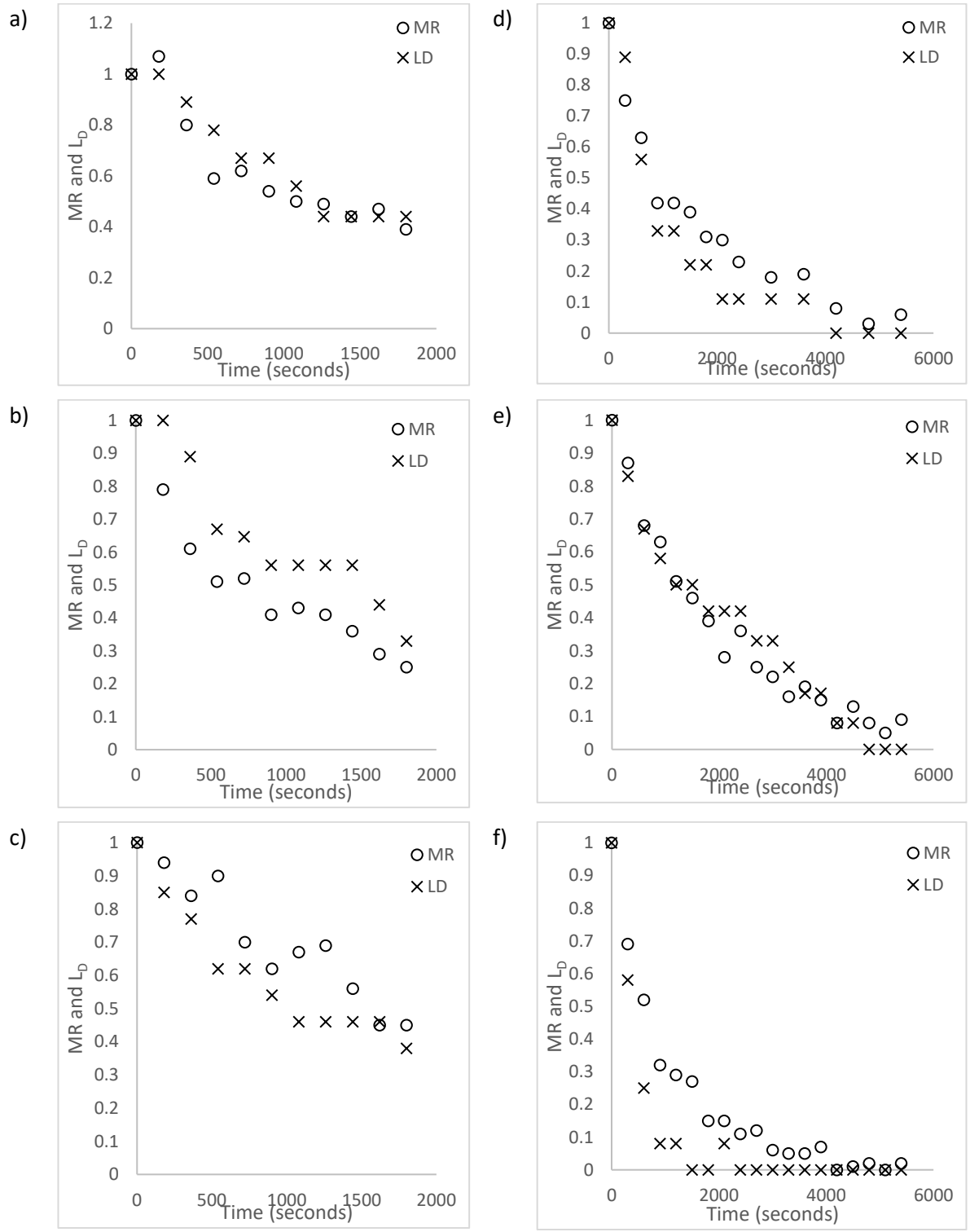

Figure 6.3; Average of triplicates comparison between MR and L_D; a-c) U. ohnoi, at 50°C, 0.7m/s air velocity and 66 kg/m³; d-f) O.intermedium, at 50°C, 2m/s air velocity and 66kg/m³.

Table 6.19; Pearsons correlation and between L_D and MR for data sets in Figure 6.3.

U. ohnoi	Pearsons correlation
Repeat 1	0.938
Repeat 2	0.926
Repeat 3	0.885
O. intermedium	
Repeat 1	0.960
Repeat 2	0.975
Repeat 3	0.940

This statistical analysis validates the assumption of linearity between moisture and volume losses. Statistical significance was below 0.05 for all sets and indicates the correlation is significant at the 95% confidence level. Coefficients of the linear relation between the two variables can be determined from graphing L_D against MR and fitting a straight-line model (presented as $L_D = aMR + b$, where a and b are model constants). Results of the linear modelling are shown in Table 6.2.

Table 6.20; Linear relationship coefficients for L_D as a function of MR.

Macroalga	Repeat	a	b
U. ohnoi	1	0.96	-0.01
	2	0.94	-0.13
	3	0.86	0.19
O. intermedium	1	1.01	-0.12
	2	0.99	0.01
	3	0.91	-0.07

Considering the variance in the experimental data, and assuming that the volume losses are solely caused by moisture loss, it is reasonable to assume L_D (the non-dimensional ratio of volume loss) is equal to MR (the non-dimensional ratio of moisture loss) and therefore $a = 1$ and $b = 0$, such that;

$$L_D = MR \tag{6.9}$$

This relation enables the slab width at any time t (L_t) to be calculated from the MR value at time t (MR_t) rather than from direct measurement of length versus time. This modelling approach simplifies the analysis of volume changes during drying of macroalgae in that the only extra measurement, required compared to typical modelling that assumes a constant L, is the final sheet width L_∞. From Equation 6.9, the model for L_t is;

$$MR_t = L_D = \frac{L_t - L_\infty}{L_0 - L_\infty} \tag{6.10}$$

$$L_t - L_\infty = MR_t(L_0 - L_\infty) \tag{6.11}$$

$$L_t = L_\infty + MR_t(L_0 - L_\infty) \tag{6.12}$$

The model equations and implementation process involved in including the impact of length within the F2L model are summarized;

$$L_t = L_0 \; ; \; t = 0 \tag{6.13}$$

$$L_t = L_\infty \; ; t = \infty \tag{6.14}$$

$$L_t = L_\infty + MR_t L_\Delta \; ; \; t > 0 \tag{6.15}$$

$$L_\Delta = L_0 - L_\infty \tag{6.16}$$

Where L_t is the slab width at time t, L_0 is the initial slab width, L_∞ is the slab width at equilibrium (or the final slab width) and L_Δ is the difference between initial and final slab widths. Replacing L in the F2L equation with Equation 6.15 changes the analytical model to;

$$MR = \frac{8}{\pi^2} \sum_{n=0}^{\infty} \frac{1}{(2n+1)^2} \exp\left(- \frac{(2n+1)^2 \pi^2 D_e t}{4\left(L_\infty + MR_{exp,t} L_\Delta\right)^2} \right) \tag{6.17}$$

6.2.4 L_t model without experimental MR data

It is noted that the L_t model presented (Equation 6.14) cannot be directly used without experimental data for the moisture ratio against time (i.e. $MR_{exp,t}$). L cannot be calculated at a given point in time without the corresponding experimental value for MR at the same time. While this may be utilized to parameter estimate for diffusivity, this requirement prevents the model from being used to predict

drying at conditions outside those already tested in Chapter 5, for which experimental MR data is available.

To get past this restriction, the model can instead be solved in a stepwise method, using the boundary conditions at $t = 0$ to define the initial step. At $t = 0$, the slab width (L) is equal to the initial width L_0. The value for MR can then be predicted at $t = 0$ and $L = L_0$ using the model irrespective of the magnitude of D_e. For example, the value for MR at $t = 0$ is equal to 0.979 when ten infinite series terms are used .

At the next time step (for example, at $t = 60$ seconds) the value for L_t can be calculated using the value of MR at the previous time step ($t = 0$). For the experimental setup used, where the initial slab width is known ($L_0 = 0.045$m), and the material shrinks by a total of 25% ($L_\Delta = 0.25 * 0.045 = 0.01125$) the value for L is then calculated via;

$$L_t = L_\infty + MR_{t-\Delta t} L_\Delta \tag{6.18}$$

$$L_{t=60} = 0.03375 + (0.979)(0.01125) = 0.0448 \tag{6.19}$$

This updated value for L_t can then be used to calculate MR at $t = 60$. The method is then repeated over the desired time frame. This method should have no significant difference when compared to the use of experimental data to predict L when a sufficiently small time step is used. An example using a time step of one minute is compared to modelling using experimental data (i.e. Equation 6.14) in Figure 6.4 for the drying of *U. ohnoi* at 50°C, 0.4m/s air velocity and 66 kg/m^3 material bulk density. Correlation between the two curves in SPSS gives a Pearson's value of 1.000 and significance of 0.000, indicating that there is no statistical difference and the two methods are functionally identical. Similar results were obtained for other drying conditions and for *O. intermedium* with the one minute time step. A one minute time step is small enough to have no signficant difference between modelling using experimental data and modelling using the time step method and thus one minute time steps were deemed sufficient for this study.

$$MR_t = \frac{8}{\pi^2} \sum_{n=0}^{\infty} \frac{1}{(2n+1)^2} \exp\left(-\frac{(2n+1)^2 \pi^2 D_e t}{4(L_\infty + MR_{t-\Delta t} L_\Delta)^2} \right) \tag{6.20}$$

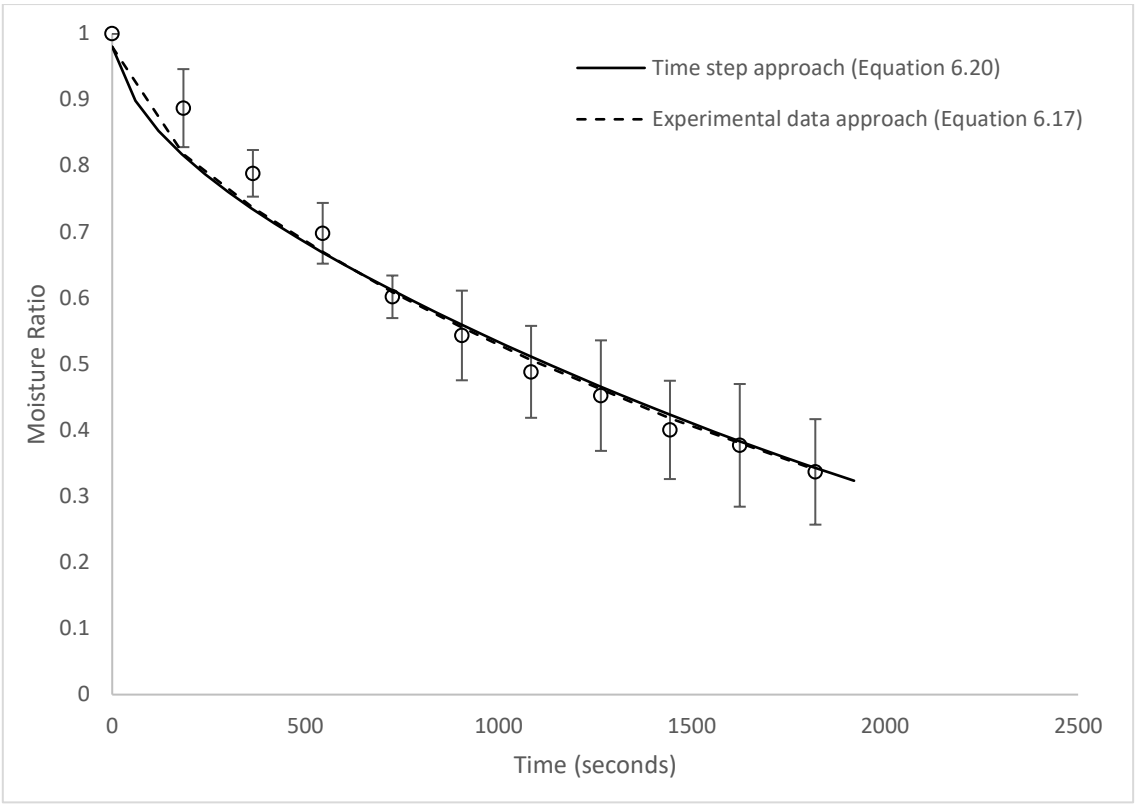

Figure 6.4; Comparison of modelling via experimental data and time step methodology; U. ohnoi at 50°C, 0.4m/s air velocity and 66kg/m³ bulk density.

6.2.5 Diffusivity model including slab volume loss

L_t calculated from the experimental MR data was used in parameter estimation with Equation 6.17 to calculate D_e as a function of gas velocity and bulk density with the inclusion of volume loss. Graphs comparing model fit between the constant L (see Chapter 5) and shrinkage models are shown in Figures 6.5 to 6.8. The constant L model is represented by the solid line, while the shrinkage model with varying L is represented by the dashed lines. D_e as a function of gas velocity and bulk density can then be used with the stepwise approach (Equation 6.20) to predict drying times without experimental data or at new conditions.

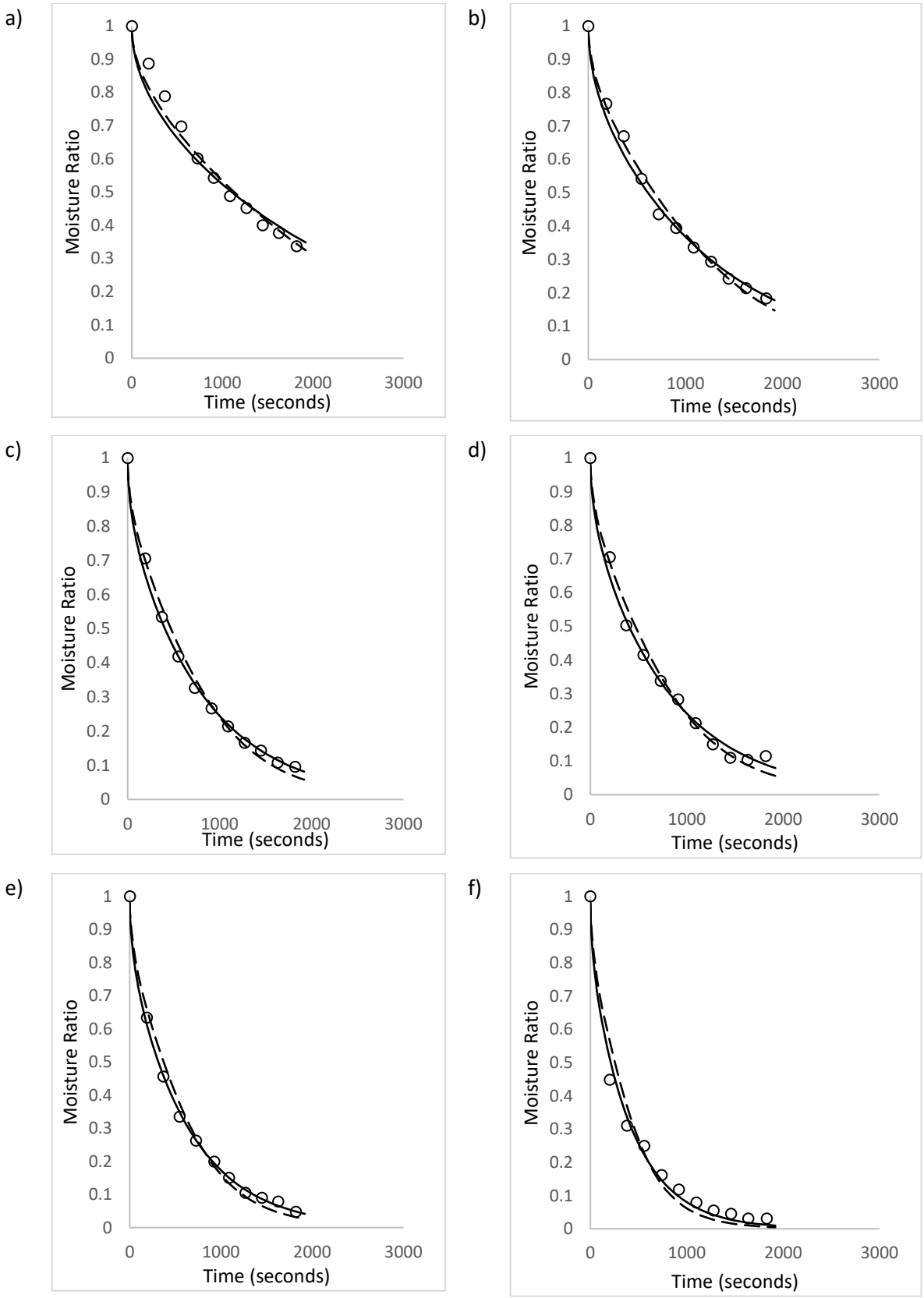

Figure 6.5; Fit comparison between constant L and L_t models; U. ohnoi at 50°C, 66kg/m³, a) 0.4m/s b) 0.7m/s c) 1.1m/s d) 1.3m/s e) 1.7m/s f) 2m/s.

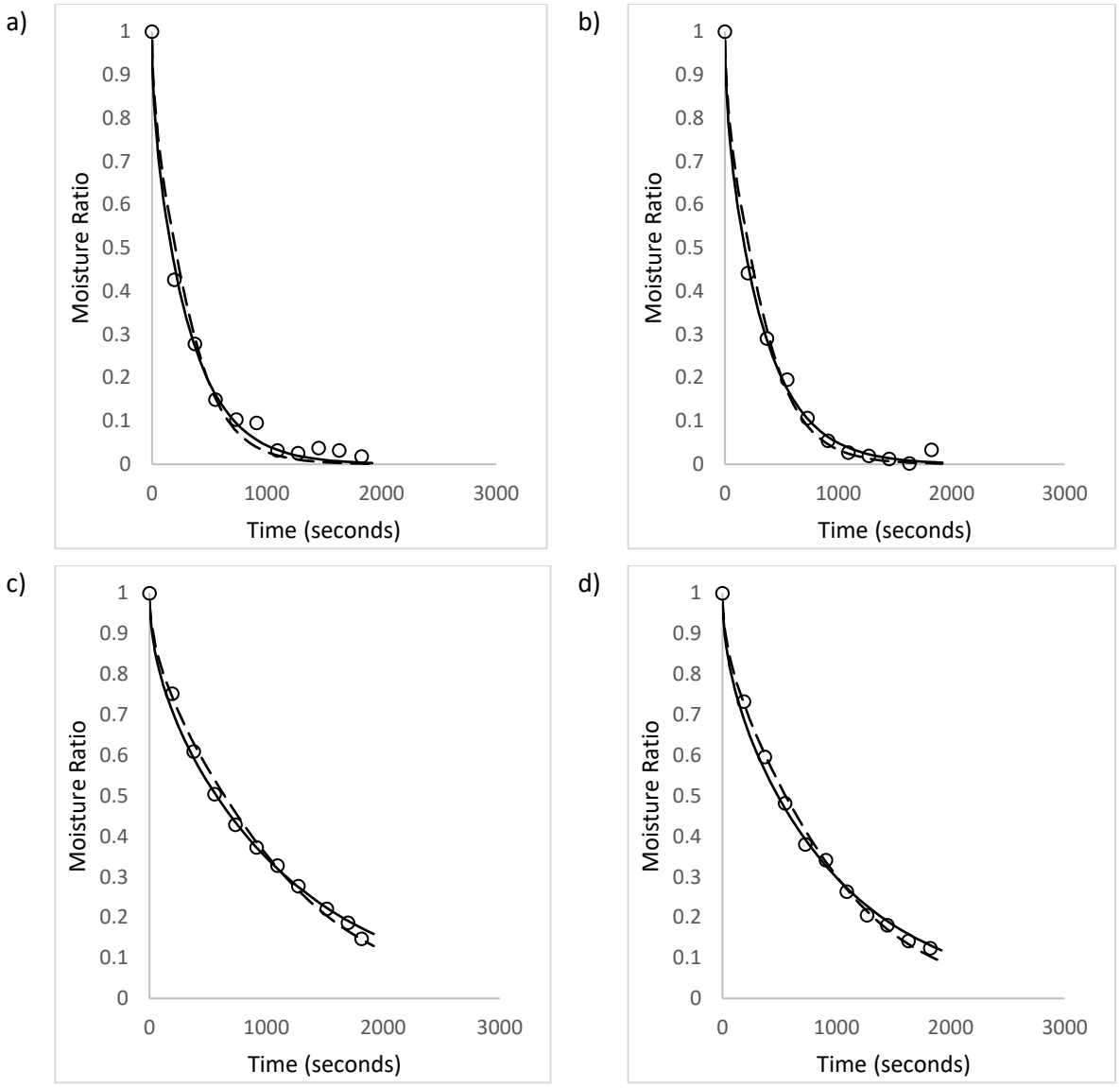

Figure 6.6; Fit comparison between constant L and L_t models; U. ohnoi at 50°C, 2m/s, a) 33kg/m³ b) 50kg/m³ c) 100kg/m³; d) 50°C, 0.4m/s, 33kg/m³.

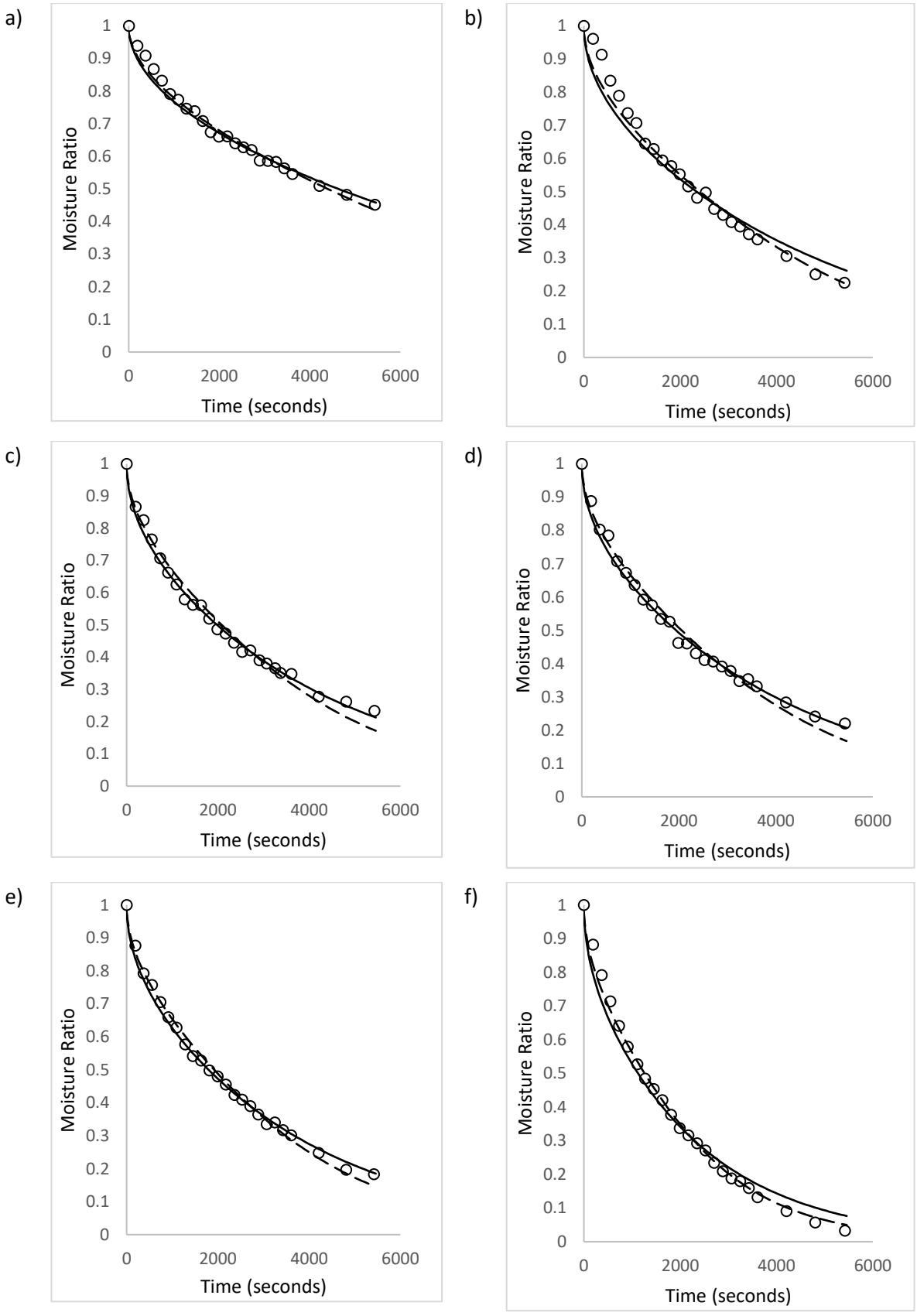

Figure 6.7; Fit comparison between constant L and L_t models; O. intermedium at 50°C, 66kg/m³, a) 0.4m/s b) 0.7m/s c) 1.1m/s d) 1.3m/s e) 1.7m/s f) 2m/s.

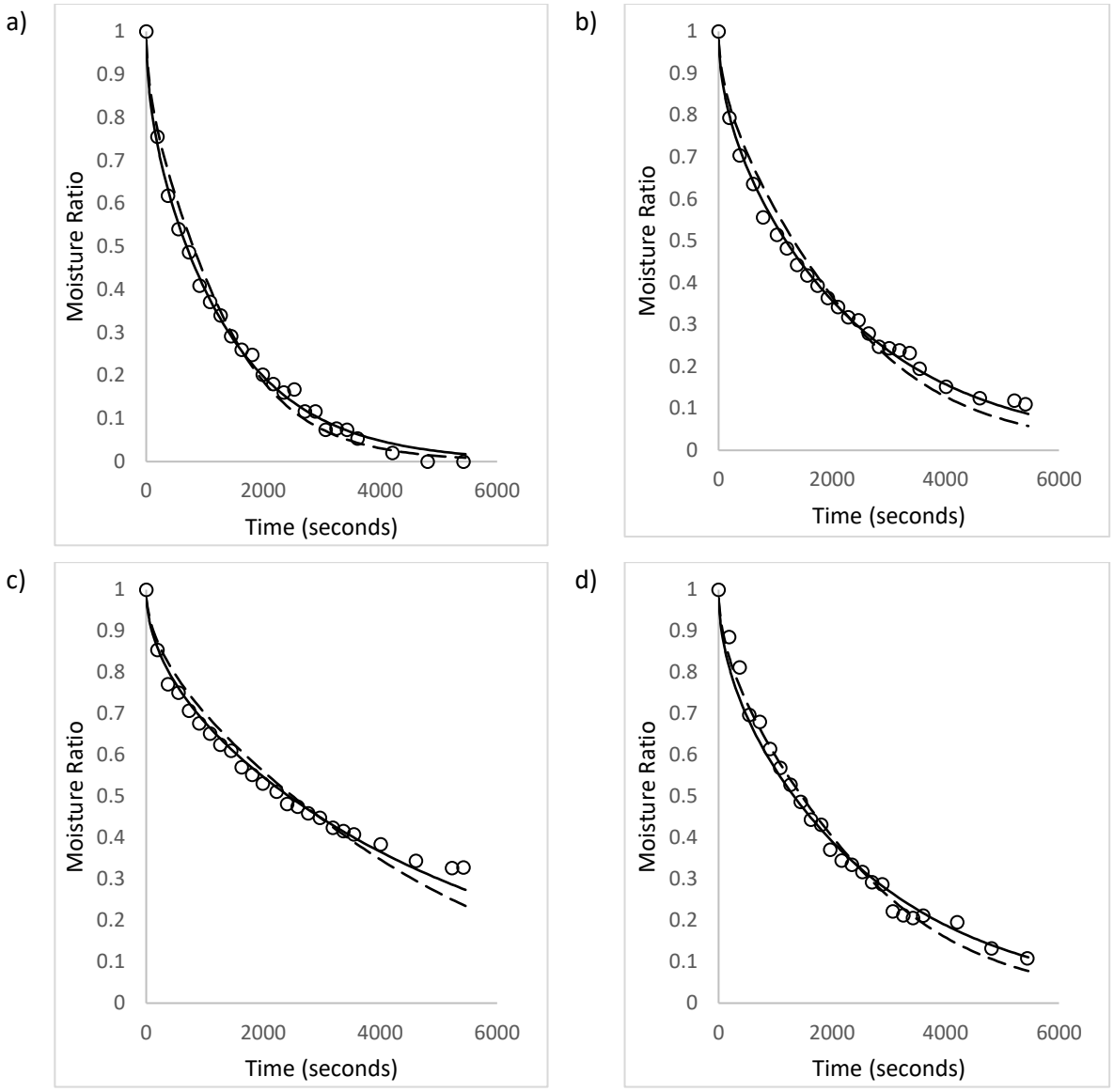

Figure 6.8; Fit comparison between constant L and L_t models; O. intermedium at 50°C, 2m/s, a) 33kg/m³ b) 50kg/m³ c) 100kg/m³; d) 50°C, 0.4m/s, 33kg/m³.

In general, the L_t model shows some improvement of fit at both the early and late stages of drying (e.g. in Figure 6.7 f)). The model predicts a lower D_e in all conditions tested when volume losses are included. This makes logical sense – drying is slower initially (where the slab geometry has little change from its width) because of a lower predicted diffusivity, while it is faster at late stages because the slab width is decreased. Tables 6.3 and 6.4 show the predicted diffusivity and model fit parameters for the L_t model for both algae species. In general, model fitting is still generally high. All data sets show R^2 values above 0.95 for *U. ohnoi*, and most above 0.9 for *O. intermedium*.

Table 6.3; D_e model parameter estimation results and model fit with the inclusion of volume losses for U. ohnoi.

Density (kg/m^3)	Velocity (m/s)	D_e(*10^{-8} m^2/s)	R^2	RMSE	X^2
66	0.4	27.3	0.968	0.109	0.0047
66	0.7	45.5	0.989	0.076	0.0022
66	1.1	66.1	0.977	0.116	0.0057
66	1.3	66.7	0.969	0.139	0.0076
66	1.7	84.4	0.989	0.081	0.0027
66	2	125	0.971	0.141	0.0073
33	2	158	0.983	0.108	0.0045
50	2	151	0.986	0.101	0.0038
100	2	48.3	0.953	0.151	0.0095
33	0.4	56.1	0.988	0.085	0.0028

Table 6.4; D_e model parameter estimation results and model fit with the inclusion of volume losses for O. intermedium.

Density (kg/m^3)	Velocity (m/s)	D_e(*10^{-8} m^2/s)	R^2	RMSE	X^2
66	0.4	6.95	0.957	0.087	0.0028
66	0.7	12.7	0.852	0.236	0.0215
66	1.1	14.7	0.956	0.119	0.0053
66	1.3	14.9	0.949	0.134	0.0068
66	1.7	16.1	0.856	0.229	0.0204
66	2	24.4	0.949	0.173	0.011
33	2	38.6	0.985	0.091	0.003
50	2	23.2	0.890	0.207	0.0175
100	2	12.2	0.926	0.139	0.0068
33	0.4	20.9	0.953	0.159	0.009

As performed previously for constant L, D_0 can be evaluated as a function of air velocity and density using the new D_e values. The diffusivity values in Tables 6.3 and 6.4 were used in SPSS to calculate a regression model for D_0 as a function of air velocity and material bulk density (as outlined in Section 5.5). The results of the regression are as follows; for *U. ohnoi* (R^2 of the regression model is 0.950);

$$D_0 = 4.597 + 2.79v_g - 0.0726\rho \quad (6.18)$$

And for *O. intermedium* (R^2 is 0.898);

$$D_0 = 0.0933 + 0.029v_g - 0.00119\rho \quad (6.21)$$

The final time step model for drying kinetics of *U. ohnoi* including D_0 as function of density and air velocity, and changes in slab width L as a function of moisture loss is;

$$MR_t = \frac{8}{\pi^2}\sum_{n=0}^{\infty}\frac{1}{(2n+1)^2}\exp\left(-\frac{(2n+1)^2\pi^2 D_e t}{4(L_\infty + MR_{t-\Delta t}L_\Delta)^2}\right) \quad (6.22)$$

$$D_e = \left(4.597 + 2.79v_g - 0.0726\rho\right)\exp\left(\frac{-41300}{RT}\right) \quad (6.23)$$

And *O. intermedium* is;

$$MR_t = \frac{8}{\pi^2}\sum_{n=0}^{\infty}\frac{1}{(2n+1)^2}\exp\left(-\frac{(2n+1)^2\pi^2 D_e t}{4(L_\infty + MR_{t-\Delta t}L_\Delta)^2}\right) \quad (6.24)$$

$$D_e = \left(0.0933 + 0.029v_g - 0.00119\rho\right)\exp\left(\frac{-34100}{RT}\right) \quad (6.25)$$

Where v_g is air velocity in m/s, ρ is bulk density in kg/m^3, R is the ideal gas constant in J/mol.K, T is drying temperature in K, L_0 is the initial slab width, L_Δ is the difference between initial and final slab width, and t is the drying time in seconds. The model fit for diffusivity as calculated by the regression equations (6.21 and 6.23) at the drying conditions (as opposed to diffusivity values obtained directly from parameter estimation) is shown in Table 6.5 for *U. ohnoi* and Table 6.6 for *O. intermedium*.

Table 6.5; Diffusivity as calculated from drying condition model for U. ohnoi; D_e and model fit.

Density(kg/m^3)	Velocity (m/s)	D_e (f(ρ, v_g, T))(*10^{-8} m^2/s)	R^2	RMSE	X^2
66	0.4	19.4	0.859	0.230	0.0205
66	0.7	37.1	0.951	0.164	0.0102
66	1.1	60.6	0.971	0.129	0.0070
66	1.3	72.3	0.965	0.147	0.0087
66	1.7	95.9	0.981	0.111	0.0049
66	2	114	0.968	0.148	0.0081
33	2	164	0.983	0.107	0.0045
50	2	138	0.984	0.110	0.0045
100	2	61.5	0.894	0.208	0.0215
33	0.4	69.9	0.950	0.167	0.0116

Table 6.6; Diffusivity as calculated from drying condition model for O.intermedium; D_e and model fit.

Density(kg/m^3)	Velocity (m/s)	D_e (f(ρ, v_g, T))(*10^{-8} m^2/s)	R^2	RMSE	X^2
66	0.4	8.11	0.917	0.108	0.0054
66	0.7	10.8	0.827	0.236	0.0253
66	1.1	14.4	0.956	0.121	0.0054
66	1.3	16.1	0.941	0.132	0.0077
66	1.7	19.7	0.804	0.235	0.0278
66	2	22.4	0.943	0.167	0.0123
33	2	34.5	0.976	0.116	0.0047
50	2	28.2	0.847	0.233	0.0242
100	2	9.94	0.861	0.175	0.0128
33	0.4	20.2	0.951	0.159	0.0092

Prediction of D_e using the D_0 models derived above give an overall high fit to the experimental data. Most conditions show a model fit (R^2, fit to experimental triplicates) above 0.9. Worst fit is *O. intermedium,* with three data sets having fit below 0.85. These sets correspond to those with high variance in experimental data (shown in the triplicate data graphs in Chapter 5). Overall accuracy is higher than those achieved using the D_e model from drying conditions presented in Chapter 5. Modelling with inclusion of volume losses reduces the predicted time to low moisture ratio for a given condition set, for example time to MR=0.1 for *O. intermedium* at 2m/s gas velocity and 66kg/m^3 bulk density is about 600 seconds faster (around 10% decrease in predicted time). Removal of this under-prediction of drying rates should result in significantly less capital and energy use when designing drying equipment.

6.2.6 Conclusions

Adjustment of the Fick's law drying model to account for volume losses, noted to occur during drying of both macroalgae species tested, was found to improve model fit to experimental data. Volume losses were found to be directly correlated to moisture losses occurring during drying. This allowed for the prediction of volume loss through correlation to the moisture ratio. Drying model fit to the experimental data improved best at the initial and final stages of drying. Accuracy at the final period

is of particular significance for the use of drying models to predict drying times for the design of industrial drying equipment. The volume loss model shown provides less underprediction of drying at late stages, which reduces the predicted drying time to low moisture content (i.e. residence time) which is an important parameter used in equipment design. The inclusion of volume losses in the drying kinetics model is therefore recommended for materials that undergo significant shrinkage during drying, and modelling of slab width as a function of moisture content is recommended.

6.3 Heating Period

The Fick's Law theoretical model assumes that the material being dried is always at the same temperature as the drying gas. In reality, initial solids temperatures are typically at ambient conditions which are lower than drying gas temperatures. As such, there would be expected to be some initial period where the material is being heated and its temperature would rise over time to the drying gas temperature (i.e. there is a dynamic slab temperature). Examples of conditions where this phenomenon are more likely to have a significant impact on drying include high densities of material, thicker slabs (larger L) and lower gas velocities, all leading to reduced rates of convective and conductive heat transfer. This could be an explanation for the tendency of the Ficks law model to overpredict the extent of drying during the initial period. Obvious examples of such profiles for both macroalgae can be seen in Figures 6.4a), 6.6a), 6.6b), and 6.7d). Furthermore, these impacts would be expected to be even more significant and occur over a longer time period in industrial-scale drying where much larger material masses and thus rates of heat transfer occur. Determining the extent of this heating period and applying a non-constant temperature (and therefore a non-constant diffusivity) may be able to provide a better fit to experimental data for these conditions.

First principles modelling of the temperature distribution throughout the material slab against time is a complex undertaking that requires solving Fourier's Law of heat conduction. The base equation representing this process for an infinite slab for one direction is

$$\frac{\partial T}{\partial t} = \alpha \frac{\delta T^2}{\delta^2 x} \tag{6.26}$$

Where α is the thermal diffusivity and is equal to $\frac{k}{\rho C_p}$, k is thermal conductivity (w/m^2.s), C_P is the heat capacity at constant pressure (J/kg.K), and ρ is the material density (kg/m^3), and T is the temperature at position x and time t. The geometry of the material used (an infinite slab of width L) and the initial conditions is shown in Figure 6.9;

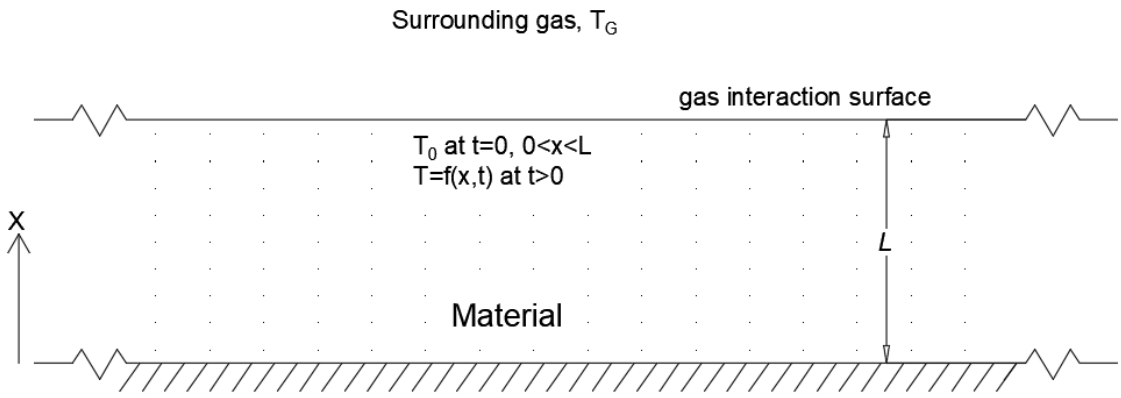

Figure 6.9; geometry of material slab and initial conditions for unsteady state thermal conduction through an infinite slab.

There are two resistances to heat transfer in this geometry; surface resistance related to convective heat transfer ($Q = h_c \Delta T$); and internal resistance related to heat conduction ($Q = k\Delta T$). The ratio between k and h_c is called the Biot number (Bi) where

$$Bi = \frac{h_c}{k} \tag{6.27}$$

This number is used to evaluate which of the two resistances is rate limiting. For $Bi < 0.1$, surface resistance (i.e. convection) is considered rate limiting. In this case it can be assumed that $T = T_s$ for all x, as internal heat conduction is much higher than external convection transfer.

For $Bi > 0.1$, internal heat diffusion is the rate limiting step. This indicates that T has to be considered as a function of position (x) across the material slab, and it can be assumed that $T_s = T_g$ at the material surface for t>0 as there is relatively little resistance to convection heat transfer.

Boundary conditions for the geometry under diffusion limitations are;

- $T = T_g$ at $x = L, t > 0$ (surface convective heat transfer is much faster than internal heat diffusion)
- $T = T_0$ at $t = 0$ for all x (even initial distribution of heat)
- $\frac{\partial T}{\partial x} = 0$ at impermeable surfaces ($x = 0$)

It is important to note that Replacing T with C in Equation 6.26 gives a mathematically identical equation to those used to describe mass diffusion (Equation 2.23). Furthermore, the above assumptions are the same as those used in the development of the F2L analytical model (with T

replacing C, as shown in Section 2.1.2). Both assume an even initial distribution throughout the slab, and that the surrounding bulk gas conditions do not change as a result of the heating (or drying) process. The assumption of heat diffusion through the slab being the rate limiting step is analogous to the assumption of the drying rate limited by internal mass diffusion. Thus, with the same base differential equation and boundary conditions, a similar analytical solution to represent the average temperature in the material slab as a dimensionless value can be developed. This derivation follows the same approach outlined in Appendix 1, with minor differences due to the direction of diffusive transfer (heat diffuses into the slab rather than mass diffusing out of the slab in the case of drying). This form of equation and diffusion direction was solved by Crank (1975) for mass diffusion into an infinite slab. The analytical solution, adapted for temperature T as a function of slab position x and time t is

$$T = T_0 + (T_g - T_0)\left(1 - \frac{8}{\pi^2}\left(\sum_{n=0}^{\infty}\frac{(-1)^2}{2n+1}exp\left(-\frac{\alpha(2n+1)^2\pi^2 t}{4L^2}\right)cos\left(\frac{(2n+1)\pi x}{2L}\right)\right)\right) \quad (6.28)$$

Or rearranged as;

$$\frac{T - T_0}{T_g - T_0} = 1 - \frac{8}{\pi^2}\left(\sum_{n=0}^{\infty}\frac{(-1)^2}{2n+1}exp\left(-\frac{\alpha(2n+1)^2\pi^2 t}{4L^2}\right)cos\left(\frac{(2n+1)\pi x}{2L}\right)\right) \quad (6.29)$$

Integrating across the slab width L to get a function for the average slab temperature as a function of time;

$$\frac{T - T_0}{T_g - T_0} = 1 - \frac{8}{\pi^2}\left(\sum_{n=0}^{\infty}\frac{1}{(2n+1)^2}exp\left(-\frac{\alpha(2n+1)^2\pi^2 t}{4L^2}\right)\right) \quad (6.30)$$

Or

$$TR = \frac{T_g - T}{T_g - T_0} = \frac{8}{\pi^2}\left(\sum_{n=0}^{\infty}\frac{1}{(2n+1)^2}exp\left(-\frac{\alpha(2n+1)^2\pi^2 t}{4L^2}\right)\right) \quad (6.31)$$

Where TR is the dimensionless ratio between the difference in temperature at time t ($T_g - T$) to the initial difference in temperature ($T_g - T_0$). It describes the percentage of heating that has not yet been achieved. For example, $TR = 0.1$ indicates that the average temperature of the slab has increased to within 10% of the (final) gas temperature.

Using Equation 6.27 and taking the approximation that K and C_P are equal to that of water ($K = 0.6\frac{W}{m.K}$ and $C_P = 4184\frac{J}{kg.K}$, as water ccomprises at least 80% of the initial algae mass);

$$\alpha = \frac{0.6}{66 \times 4184} = 2.17e^{-6}\frac{m^2}{s}$$

The convective heat transfer coefficient h_c for air is listed as 10-500 $\frac{W}{m^2 s}$ for forced air by Kosky et al. (2013). Taking the minimum of 10$\frac{W}{m^2 s}$ as a worst case scenario, the value of Bi is much greater than 0.1 and validates the assumption of heating limited by internal conduction. Some examples of the predicted average slab temperatures as a function of time for differing slab widths, assuming T_0 is 25°C and T_g is 50°C. The figure shows that the heating time is expected to be very sensitive to the value of L and therefore the scale of drying.

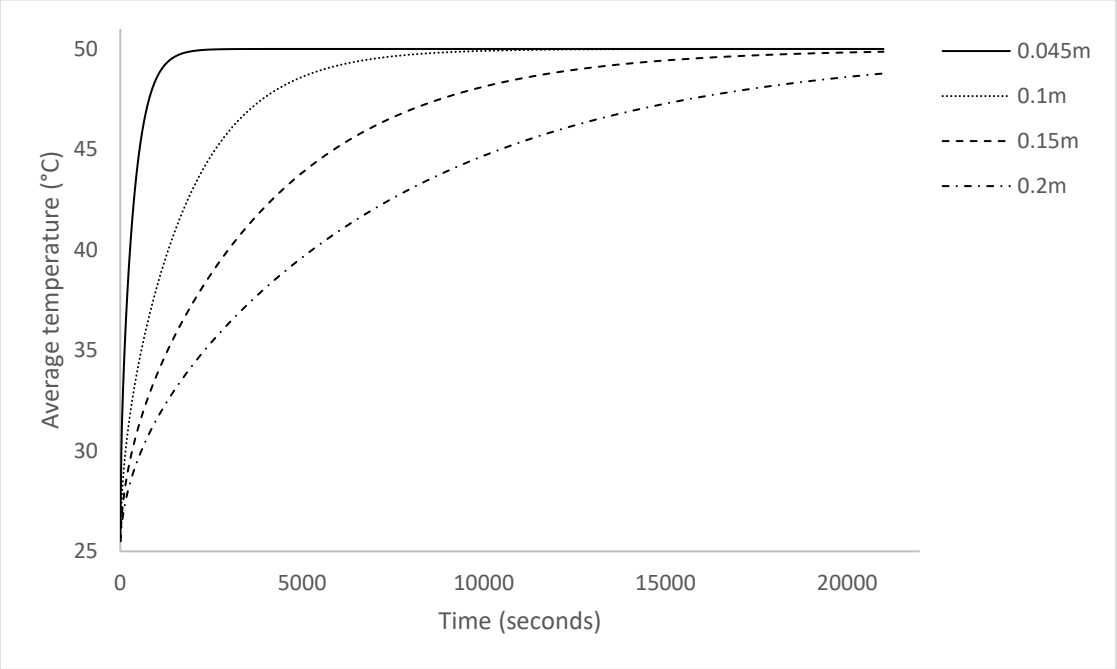

Figure 6.10; Example of the increase in heating time required as the macroalgae slab width increases. Initial temperature is 25°C, and surrounding gas temperature is 50°C.

6.3.1 Methodology

A simple and pragmatic approximation of slab temperature over time was used to test whether the inclusion of a non-constant material temperature could result in improved model fit. The aim of this modelling was to inform whether the heating time of the algae material has a noticeable effect on drying rates, and to test whether the predictions of a distinct heating time from Equation 6.31 are evident and confirmed by the experimental MR vs t data. This analysis was performed with experimental data obtained from the equipment outlined in Chapter 4.

In this model, the slab is assumed to require some finite time (t_H) to reach thermal equilibrium with the drying gas. The slab temperature is then represented as a linear increase in temperature between ambient and drying gas temperature across this time period.

The temperature model applied to the experimental data is summarized below;

$$T_t = \frac{T_g - T_0}{t_H} t + T_0; 0 \leq t \leq t_H \tag{6.32}$$

$$T_t = T_g; t > t_H \tag{6.33}$$

Where T_t is the material temperature at time t, T_g is the drying gas temperature, T_0 is the initial material temperature, and t_H is the length of time of the initial deviation in seconds.

The condition sets chosen to evaluate the effectiveness of this model adjustment are slowest drying conditions for both macroalgae species (50°C, 0.4m/s, 66kg/m^3) as these sets have the largest decrease in model accuracy over the initial time period. The modelled temperature (T_t) was used to calculate diffusivity (D_e) and MR at each time using the following;

$$MR_t = \frac{8}{\pi^2} \sum_{n=0}^{\infty} \frac{1}{(2n+1)^2} \exp\left(-\frac{(2n+1)^2 \pi^2 D_e t}{4(L_\infty + MR_{t-\Delta t} L_\Delta)^2}\right) \tag{6.34}$$

Where $D_e = D_0 exp\left(\frac{-43914}{RT_t}\right)$ for *U. ohnoi* and $D_e = D_0 exp\left(\frac{-31176}{RT_t}\right)$ for *O. intermedium*. Model fitting was performed by parameter estimation of D_0, minimizing the sum of square errors between the experimental data and model via;

$$Obj = \sum_{m=1}^{3} \left(\sum (MR_m - MR_e)^2\right) \tag{6.35}$$

6.3.2 Results

In the results that follow, the heating time period was varied from 0 to 24 minutes in 3 minute increments. D_0 was parameter estimated and the quality of fit (R^2) was quantified for each heating time. The 0 minute heating time is included to represent the assumption of no heating period i.e. that the material immediately reaches drying gas temperature ($T_t = T_g$). The quality of fit for each heating period time examined and the corresponding parameter estimated D_0 value are shown in Table 6.7 for *U. ohnoi* and Table 6.8 for *O. intermedium*. The MR versus time profiles for the heating period and

D_0 which provided the best R^2 are graphed alongside experimental data as well as the constant temperature model (Figure 6.9 for *U. ohnoi* and Figure 6.10 for *O. intermedium*).

Table 6.7; heating period length and D_0 parameter estimation results; *U. ohnoi* drying at 50°C, 0.4 m/s gas velocity, 66kg/m³ bulk density. Best fit is shown in bold.

t_H (minutes)	D_0 (m^2/s)	R^2
0	3.45	0.968
6	3.48	0.976
9	3.52	0.983
12	**3.58**	**0.986**
15	3.67	0.982
18	3.77	0.973
21	3.91	0.962

Table 6.8; heating period length and D_0 parameter estimation results; *O. intermedium* drying at 50°C, 0.4 m/s gas velocity, 66kg/m³ bulk density. Best fit is shown in bold.

t_H (minutes)	D_0 (m^2/s)	R^2
0	0.00760	0.957
6	0.00761	0.958
9	0.00762	0.960
12	0.00764	0.962
15	**0.00766**	**0.963**
18	0.00769	0.963
21	0.00772	0.963
24	0.00776	0.961

In general, the model fit improves as the heating period increases up to 12 minutes for *U. ohnoi* and 15 minutes for *O. intermedium*. These time periods correspond with the point where the constant temperature models demonstrate the highest correlation coefficient (R^2). The value for D_0 increases as the assumed heating period increases. This occurs because diffusivity must be higher to still fit experimental data when the material temperature is below gas temperature for an increasing period. Some examples of the best fit heating time for other condition sets are shown in Table 6.9.

The heating time to reach 90% of the temperature difference can be calculated by solving for the time to reach TR of 0.1 in Equation 6.31 for comparison with the results in Table 6.9. One series term is used in the following calculation as all other series terms converge to zero at low TR (this is shown for MR in Section 3.3.2);

$$TR = 0.1 = \frac{8}{\pi^2} exp\left(-\frac{2.17e^{-6}\pi^2 t_H}{4 \times 0.045^2}\right)$$

$$0.1234 = exp\left(-\frac{2.17e^{-6}\pi^2 t_H}{0.0081}\right)$$

$$ln(0.1234) = -\frac{2.17e^{-6}\pi^2 t_H}{0.0081}$$

$$2.0923 = 0.00264 t_H$$

$$t_H = 792\ seconds$$

Or slightly over 13 minutes. This is a significant fraction of the total drying time – it represents 44% of the total time for U. ohnoi and 15% of the total for O. intermedium. This time also visually lines up with the initial deviations from F2L prediction in experimental data (e.g. Figures 6.5a), b), 6.7a), b)), which further indicates that the slab temperatures may be a cause of this deviation.

Table 6.9; best fit heating periods for condition sets noted to have similar initial deviations from model prediction.

Macroalgae	Air velocity (m/s)	Initial Density (kg/m^3)	t_H (s)
U. ohnoi	0.4	66	720
	0.7	66	540
	0.4	33	540
O. intermedium	0.4	66	900
	0.7	66	720
	0.4	33	540

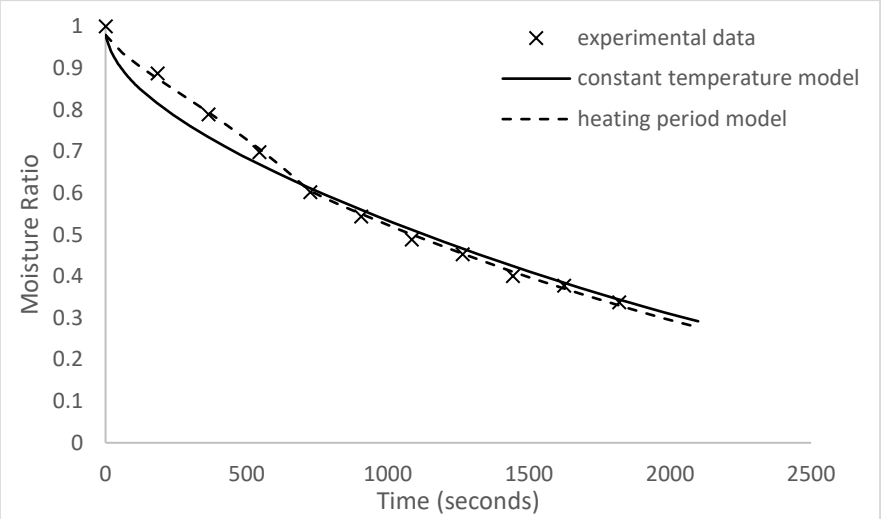

Figure 6.11; U. ohnoi drying at 50°C, 0.4m/s, 66kg/m³. Comparison of experimental data average, constant temperature model, and heating period model.

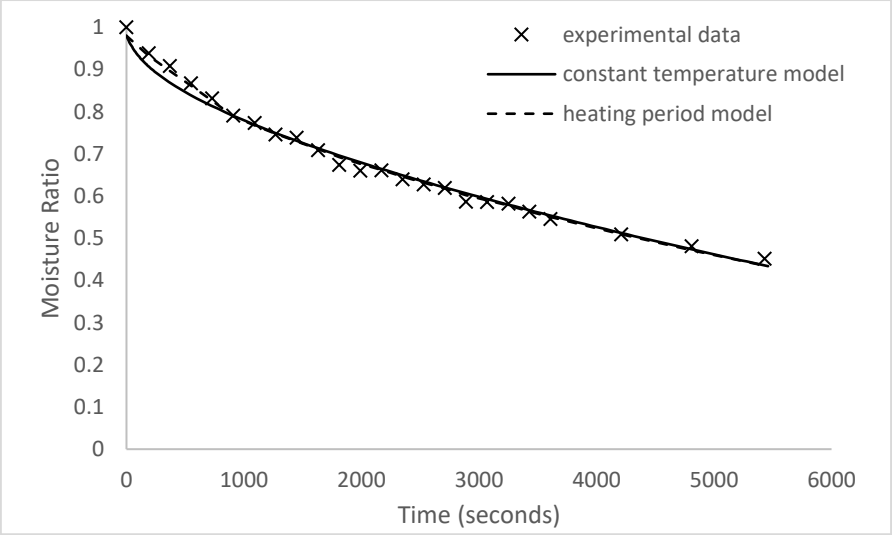

Figure 6.12; O. intermedium drying at 50°C, 0.4m/s, 66kg/m³. Comparison of experimental data average, constant temperature model, and heating period model.

The inclusion of a non-constant temperature over the initial deviation period was shown to further improve model fit in the tested condition sets for that stage. This indicates that the diffusivity of the material should be calculated from the material temperature rather than the assumption of material as isothermal at the surrounding gas temperature.

The significance of material temperature and heating time should increase as the amount of material is scaled up (i.e. large L), or for low convective heat transfer conditions such as low gas velocity. The theoretical model for average slab temperature (Equation 6.31) correlates well with the best fit heating period in Tables 6.7 and 6.8. The limitations of the current model are that the true value of α for the macroalgae are not known, and that the model currently has no ability to account for the apparent decrease in heating rate for higher air velocities. However, this aligns well with the earlier penetration mechanism described in Section 5.3. The values in Table 6.9 support that the gas velocity effect on conduction of heat may be acting similarly to moisture diffusion, in that as gas velocity increases there is a reduction in the effective slab width L, leading to a shorter heating period. Further analysis of the validity of the TR model (Equation 6.31) is recommended. This would include determining the real value of α for the macroalgae and comparison of model prediction with experimental data for slab temperature as a function of internal position and time. This is much more achievable experimentally because T is more easily measured at precise locations than moisture. A detailed model for slab temperature changes would be of use for modelling when high accuracy at the initial time period is required, or when the heating period is expected to be significantly large compared to the full drying time due to material properties or drying conditions.

6.4 Pilot Scale Modelling

The final validation for a drying kinetics model is its ability to represent drying at larger scales, to prove it can be used to represent industrial drying equipment. The modelling developed in this thesis was experimentally tested for both alga species using a pilot scale flighted rotary dryer. The larger scale involves both a larger mass of material, and a larger slab width than lab scale tests in Chapter 5. The model including volume changes (developed in Section 6.2) and including volume and material slab temperature (developed in Section 6.3) were compared to test their ability to represent drying at this larger scale. Drying conditions were also different to those used in Chapter 5, providing a further test of model ability to represent conditions outside those used in initial experimentation.

6.4.1 Equipment

The pilot scale flighted rotary dryer used in testing was an existing drum owned by JCU Macroalgae Facility (Figure 6.11). Dimensions of the drum are 750mm diameter and 2400mm length. Heated air is provided by a hot air blower (Hotwind Premium, Leister, Switzerland), set at a flow rate of 700L/min. Gas conditions inside the drum were assumed to be independent of position in the drum, and equal

to the conditions of the exhaust gas. Exhaust gas conditions were measured using an anemometer (for gas velocity) and a K type thermocouple (for temperature). Exhaust velocity and the known inlet flow rate was used to estimate the average air velocity inside the drum, assuming that all air flow left through the exhaust and that there was even distribution of gas throughout the drum. It was assumed that the bulk density of the macroalga was at its minimum due to the rotary action of the drum loosely distributing the material. Rotation speed of the drum was 3 RPM. Flights are made of two segments each 5cm in length, with a 5° bend between the segments.

a)

b)

Figure 6.13; side (a) and internal (b) view of pilot scale drum.

6.4.2 Methodology

Moisture content against time was measured by removing small samples of algae material (1-2g) from the drum, and immediately fully drying these samples in Sartorius moisture analyser (MA-45) at 110°C. The sample mass removed is assumed to have negligible effects on the drying rate of the remaining material, as the amount is minimal compared to the mass of material loaded (typically greater than 14kg loaded compared with less than 20g total removed). Drying conditions and initial loaded mass are shown in Table 6.10. Gas outlet humidity was initially measured at close to 100% RH, but further measurement of humidity was not possible due to probe malfunction.

Table 6.210; Pilot drying conditions used for both macroalga species.

Macroalgae	Temperature (°C)	Ambient temperature (°C)	Air flow rate (m/s)	Density (kg/m^3)	Material loading (kg)	L (m, rounded)
U. ohnoi	60	40	0.03	33	14.1	0.2
O. intermedium	41	31	0.03	33	15.2	0.2

The material slab width L was estimated from the known material volume in the drum and the width of the chord W as illustrated in Figure 6.12. As an example, the mass of *U. ohnoi* loaded was 14.1 kg. The material is expected to be at the minimum bulk density of 33kg/m^3 due to the drum rotation continually redistributing the material. The volume taken up by the material at this bulk density is then;

$$Volume = \frac{mass}{density} \tag{6.36}$$

$$V = \frac{14.1}{33}$$

$$V = 0.43m^3$$

The area occupied by the algae (A) can be calculated from the volume by dividing by the drum length;

$$A = \frac{0.43}{2.4} = 0.18m^2 \tag{6.37}$$

The value of W was directly measured with a ruler as 0.8m. A reasonable estimate of the average slab length was obtained by assuming that the material in the drum is represented as a rectangular slab with the same width W and cross-sectional area A;

$$L = \frac{A}{W} = 0.2m$$

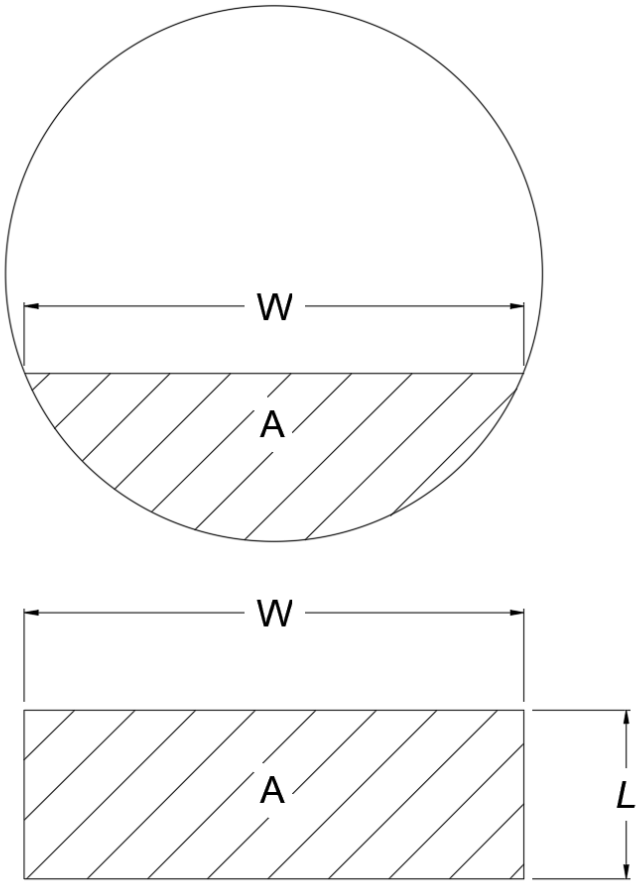

Figure 6.14; Diagram of method used to estimate material slab height in the pilot scale drum.

6.4.3 Results & Discussion

The moisture ratio data for *U. ohnoi* and *O. intermedium* is shown in Tables 6.11 and 6.12 respectively. The measured exhaust temperature at each time is also shown.

Table 6.11; experimental drying rate data and exhaust temperature; U. ohnoi.

Time (minutes)	Moisture Ratio	Exhaust temperature (°C)
0	1	42
90	0.797	50
180	0.554	55
290	0.216	60
390	0.108	60
480	0.079	60

Table 6.12; experimental drying rate data and exhaust temperature; O. intermedium.

Time (minutes)	Moisture Ratio	Exhaust temperature (°C)
0	1	32
60	0.948	37
120	0.944	39
180	0.829	41
240	0.656	41
300	0.571	41
360	0.504	41

The Fick's law drying model used in this thesis is dimensionless with respect to the mass of material being dried. As such, the models presented in Section 6.2 and 6.3 should also be valid for representation of drying in the pilot scale drum if the model assumptions (listed in Section 2.1.2.2) are sufficiently met. The measured temperature against time was used to formulate a linear temperature model by the same methodology in Section 6.3. Model fitting was performed using Equation 6.27, both with and without the inclusion of changing temperature. The diffusivity and model fit was also calculated from the drying conditions using the models developed in Section 6.2 for comparison. Tables 6.13 and 6.14 compares the model fitting results between the three methods. Finally, Figures 6.13 and 6.14 provide a visual comparison between model fit and experimental data.

Table 6.13; Diffusion parameter estimation results for *U. ohnoi*.

Method	D_e (*10^{-8} m2/s)	R^2
L(t) model, parameter estimation (Equation 6.17)	64.1	0.948
L(t) model, D_e from drying conditions (Equations 6.22 and 6.23)	80.6	0.924
L(t) and T(t) model, parameter estimation (Equation 6.34)	(varies)	0.971

Table 6.14; Diffusion parameter estimation results for *O. intermedium*.

Method	D_e (*10^{-8} m2/s)	R^2
L(t) model, parameter estimation (Equation 6.17)	18.3	0.776
L(t) model, D_e from drying conditions (Equations 6.24 and 6.25)	14.7	0.752
L(t) and T(t) model, parameter estimation (Equation 6.34)	(varies)	0.805

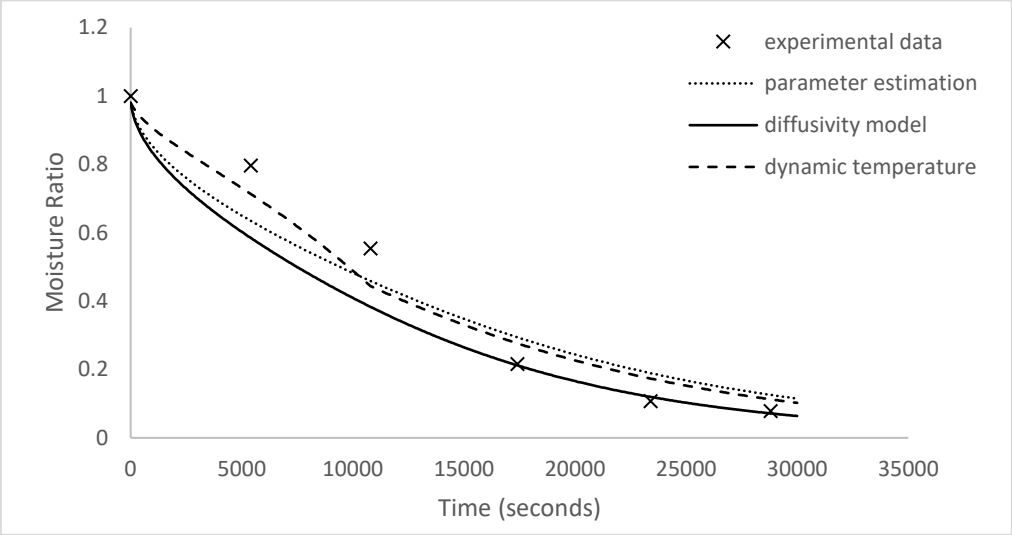

Figure 6.15; *U. ohnoi* pilot scale drying. Comparison of experimental results, parameter estimation, diffusivity from conditions, and dynamic temperature.

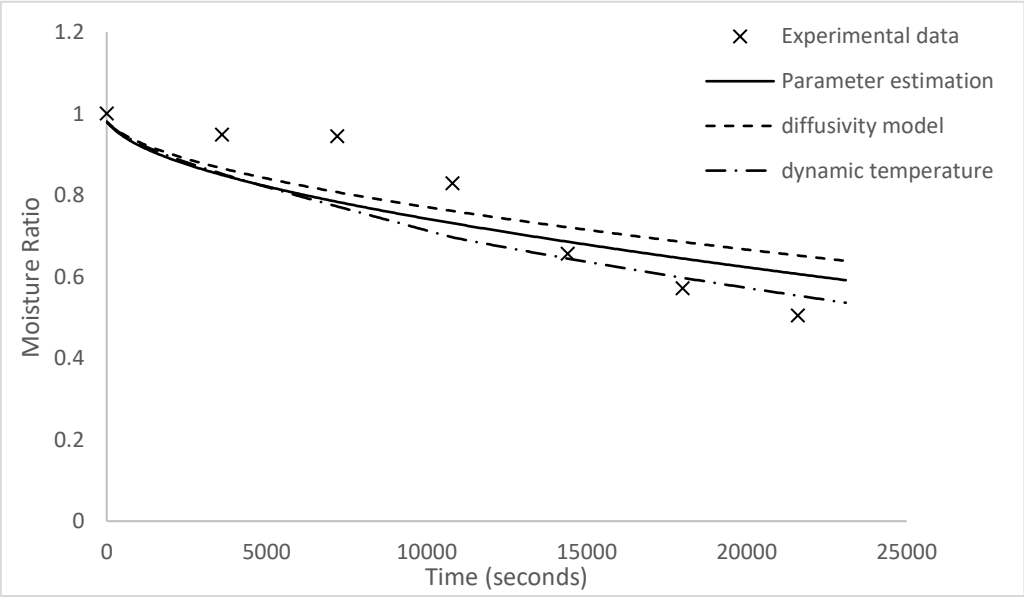

Figure 6.16; *O. intermedium* pilot scale drying. Comparison of experimental results, parameter estimation, diffusivity from conditions, and dynamic temperature.

Modelling fits the data well for *U. ohnoi*, even though conditions are well outside of those in model development, and despite the scale increase. The model as calculated from parameter estimation has acceptable overall fit. The model as calculated from the diffusivity model in Section 6.2 fits very well at the later stages of drying, but worse at the initial period. The model including dynamic temperature changes as developed in Section 6.3 has the best overall fit, and is much better at representing drying during the initial heating period. The heating period time was a significant portion of the measured drying time. This reinforces the conclusion that an accurate understanding of heating period drying becomes more significant as the scale of drying increases. The model fit to *O. intermedium* drying was acceptable. Best fit was with the dynamic temperature model, with R^2 of 0.805. Prediction of diffusivity from drying conditions had slightly lower fit with R^2 of 0.752.

Model fit to experimental data was very similar between parameter estimation and diffusivity calculated from drying conditions when using the L_t model for both species. It can be concluded that the model for diffusivity as a function of drying conditions (Equations 6.20 to 6.23) is sufficiently accurate for the estimation of drying times. As such, it would be of use for equipment design and optimization in providing drying times from equipment design parameters.

The air flow rate through the pilot scale drum was very low. This caused some build-up of humidity inside the drum for both algae species (the measured RH at outlet was close to 100% at the first mass measurement). This invalidates the assumption of air flow being significantly large enough for drying conditions to be unaffected by the transfer of moisture. This is likely another factor in the deviations between experimental data and the models during the initial period, especially for *O. intermedium* where little change in moisture was measured over the first two data points. Meeting the assumption of sufficiently large air flow is likely to be a significant consideration for modelling of drying at industrial scales.

Finding or calculating a 'correct' or equivalent slab width (L) was identified as the biggest gap in applying the F2L model to represent drying of material in a flighted rotary dryer. L is not well defined for materials in the dryer drum, as there are multiple 'states' the material can be in. In this work, the value used for L was estimated from observation of the material in the drum; the slow rotation speed of the drum alongside the amount of material loaded put the majority of material at the bottom of the drum, rather than in flights or airborne and the expected density of the loaded material. In a real rotary dryer, there are likely to be multiple 'sections' where drying is at different rates (Ajayi et al. 2012). For example, material in the airborne phase presents different slab thickness than material in the bottom of the drum. The air flow is likely to be different at differing positions as well due to

channelling through or around falling curtains (Lee et al. 2014). An understanding of the time material spends in different phases and air flow with respect to position could therefore be of use in further work to more accurately characterise drying in this type of equipment.

6.5 Conclusions

This chapter has presented a final model for macroalgae drying, adjusted from the base F2L model to include effects of air velocity, material bulk density, material volume loss and material temperature effects. The intention of these adjustments was to pragmatically account for deviations between the F2L model assumptions and observed drying rates. Testing proved that the model was able to represent drying of biomaterials at a pilot scale well, and at conditions outside those used in model development.

The F2L model was adjusted to include major volume losses noted to occur during drying of the macroalgae. The experimental study of slab width changes during drying noted that the shape of L versus time curves was similar to moisture ratio versus time. The slab widths were converted to a nondimensional value L_D for better comparison to the nondimensional moisture content MR, where L_D represents the remaining percentage difference between the initial and final slab widths. Statistical analysis showed that L_D and MR were correlated and could be considered equivalent. This correlation allows for much easier implementation of shrinkage relations with drying kinetics models, with the final slab width as the only additional measurement required. The inclusion of volume losses in the drying kinetics model was found to improve drying model fit at the initial and final drying stages. These periods were identified in previous chapters as where the F2L model was consistently deviating from experimental data.

The use of estimated slab temperature over the initial heating period rather than drying gas temperature was shown to provide some model accuracy increase for slow drying conditions for both macroalgae species. The significance of this effect was seen to increase as the scale of drying increases. An analytical solution for slab temperatures was developed from similarities between the fundamental heat diffusion and mass diffusion equations. Prediction of heating time via this analytical model correlates well with the best fit of a range of heating times to experimental data, indicating the modelling approach has merit. Further research to evaluate the temperature ratio model to experimental data for slab temperatures as a function of position and time would be desired, especially for pilot or industrial scales of drying.

Finally, the model was demonstrated to well represent drying at a pilot scale for both species of macroalgae. The best fit was shown when relations to represent material volume losses and material temperature were included. Predictive models using D_e from previous chapters had little loss in accuracy compared with D_e values obtained from direct parameter estimation. As such, the models derived in this thesis should be of value in equipment design and optimization through estimation of drying times over a range of conditions. The results from pilot scale drying indicate that adjustments to account for non-isothermal behaviour are important for accurate prediction of drying at larger scales.

Chapter 7

7. Conclusions and Recommendations

7.1 Conclusions

The equilibrium moisture content for both species of macroalgae over typical drying temperature (35, 40, 45, 50, 55°C) and humidity (10 – 60%RH) was experimentally determined. The GAB equation had the best fit to the experimental moisture isotherms, matching general literature conclusions of best models to represent equilibrium moisture. The GAB model is typically considered semi-empirical in the literature. It was noted the model is likely empirical in representing equilibrium moisture of the macroalgae due to interference from dissolution of material components at increased temperatures that are not considered in the model development. These effects resulted in the crossover effects noted in Section 3.2.2, where increased temperatures resulted in increased equilibrium moisture at higher humidity. Complications resulting from material components make it difficult to be able to predict equilibrium moisture functions without experimental data. For example, the assumption of zero equilibrium moisture made for some materials in literature would be incorrect for the macroalgae, but that assessment is not possible without testing. It follows that any potential impacts of assumptions about M_e on drying rates cannot be known without the correct value of M_e. The relation for M_e as a function of surrounding conditions also allows the determination of storage conditions that prevent decay of biomaterials. It is recommended to determine M_e as a function of drying conditions for a new biomaterial.

Thin layer drying rates for the two macroalga were experimentally determined for typical biomass drying temperatures (40, 45, 50, 55, 60°C), comparing results from radiative and convective heating methods. The F2L model was found to well represent experimental data for all conditions and both heating methods. Convective heat driven drying (diffusivity up to $1.5e^{-7}$ m^2/s for *U. ohnoi*, and up to $9e^{-8}$ m^2/s for *O. intermedium*) was faster than radiative heat drying (diffusivity up to $8.8e^{-8}$ m^2/s for *U. ohnoi*, and up to $4.8e^{-8}$ m^2/s for *O. intermedium*) for all temperatures and for both species. All experimental data was found to be in a falling rate period and was therefore determined to meet the assumption of drying limited by internal diffusion, implying that convection heating was not rate limiting. The radiative drying experimental data was used to evaluate the activation energy E_a (41.3kJ/mol for *U. ohnoi*, and 34.1 kJ/mol for *O. intermedium*) and initial values for the model coefficient D_0 for both species. Regression coefficients (R^2) for E_a and D_0 were high, at 0.97 for *U.*

ohnoi and 0.95 for *O. intermedium*. The use of radiative heating equipment (e.g. moisture analyser) to determine E_a and D_0 was found to be a quick and reliable method to estimate these values.

The results of the thin layer drying experiments were used to investigate the number of series terms chosen to represent the F2L model infinite series. It was shown that the number of terms used has no significant effect on parameter estimation for D_e, but does cause changes in the initial model shape (i.e. MR vs t profile). This is best shown at t=0, where MR should be equal to 1 by definition (no drying yet occurred), but one term of the infinite series produces an MR value of 0.81 (rounded) at t=0. Model fitting improves for the initial period of drying as the number of terms used increases. Ten series terms was chosen as a sufficient compromise between accuracy at all times and model complexity.

An experimental apparatus was designed which provided consistent and controlled air flow rates and drying gas temperatures. The known chamber volume allowed for controlled changes in bulk density, sample dimensions, and enabled the impact of density on drying to be determined. Furthermore, in situ mass and volume loss measurements substantially improved the frequency of data collection compared to similar studies reported in the literature, and removed potential errors due to heat losses from periodically removing the material from drying conditions. These measurements were facilitated by the inclusion of a gas flow bypass. The ability to measure volume changes of the material in situ is particularly novel, with other literature examples which included measurement of volume losses performing ex situ analysis.

The experimental apparatus was used to determine drying kinetics over a range of air flow rates (0.4-2.0 m/s) and initial bulk density (33-100kg/m^3) for both species. Increases in air velocity caused a linear increase in drying rate, while increases in material bulk density caused a linear decrease in drying rate. The diffusivity obtained from radiative thin layer drying tests matched well with these results extrapolated to a zero velocity point, which reinforces the validity of values of E_A determined in Chapter 3. Testing showed that drying was in a single falling rate for all conditions tested and therefore air velocity cannot be affecting drying during a constant rate period. Statistical analysis showed that there was no significant interaction effect between air velocity and material density on the drying rate. The relationship for diffusivity as a function of temperature, air velocity and initial bulk density was found to be

$$D_e = \left(18.27 + 11.47 v_g - 0.2996\rho\right)\exp\left(-\frac{43914}{RT}\right)$$

for *U. ohnoi* and

$$D_e = \left(0.05798 + 0.0191 v_g - 0.000787\rho\right)\exp\left(-\frac{31776}{RT}\right)$$

for *O. intermedium*.

These models were shown to have high overall fit to experimental drying data. The bulk densities of material slabs used in kinetics studies are rarely reported and are suspected to be a cause for some part of the variance in diffusivity results between studies of the same material. As such, similar testing should be performed for drying kinetics studies of other loose particulate materials. Several orders of magnitude of difference between reported D_e values can be found in the literature for sugar cane bagasse (Slogrove et al 2017, Vijayaraj et al 2006) and olive bagasse (Montero et al 2011, Friere et al 2001) as examples.

Insight into drying mechanisms provided this work have been used to put forward a theoretical explanation of the mechanisms by which air velocity and bulk density are affecting drying rates. The original theory used in the development of the F2L model describes drying through a solid slab of material, and assumes that drying is limited by internal movement of moisture across the entire slab. This implies that external air flow rate should not affect drying limited by internal diffusion. Although, some results that show this kind of behaviour have been reported in literature, these studies were performed for single layers of separated particles. These examples can well represent a solid slab with the characteristic length of a single particle, but are less suitable for representing more realistic material dimensions used in drying equipment. The data and modelling results obtained in this thesis suggest that 'internal diffusion' occurs in two stages for loose particulate material such as the macroalgae; diffusion through each particle to the particle surface, then a secondary transfer stage through the particulate bed to the bulk gas interaction surface. This second stage is theorized to be affected by changes in air velocity and bulk density through gas penetration breaking the bulk up into smaller blocks. Recommendations on how to prove or disprove the mechanisms outlined in Section 5.3 are discussed in Section 7.2.

Experiments were undertaken to determine whether the inclusion of adjustments to the F2L equation to account for deviations between the real behaviour of the material during drying and model assumptions improved representation. Volume losses during drying were measured in situ via a novel approach using images of the material through a transparent drying chamber and analysed using image analysis software. It was noted that the changes in slab volume over time were similar in shape to moisture losses. A statistical analysis of dimensionless volume loss (L_D) compared with the dimensionless moisture content (MR) proved that volume losses were directly correlated to moisture

content. This allowed for direct calculation of slab volume or width at a given time (L_t) from moisture content data. The model for slab width was included in the F2L model and improved the model fit at the initial and final stages of drying, when compared to the use of a constant slab width. The final models for drying as a function of temperature, air velocity and initial bulk density with included volume is was

$$MR_t = \frac{8}{\pi^2}\sum_{n=0}^{\infty}\frac{1}{(2n+1)^2}\exp\left(-\frac{(2n+1)^2\pi^2 D_e t}{4(L_\infty + MR_{t-\Delta t}L_\Delta)^2}\right)$$

$$D_e = \left(4.597 + 2.79v_g - 0.0726\rho\right)\exp\left(\frac{-41300}{RT}\right)$$

for *U. ohnoi* and

$$MR_t = \frac{8}{\pi^2}\sum_{n=0}^{\infty}\frac{1}{(2n+1)^2}\exp\left(-\frac{(2n+1)^2\pi^2 D_e t}{4(L_\infty + MR_{t-\Delta t}L_\Delta)^2}\right)$$

$$D_e = \left(0.0933 + 0.029v_g - 0.00119\rho\right)\exp\left(\frac{-34100}{RT}\right)$$

for *O. intermedium*. Accuracy at low moisture content is particularly relevant for the design of drying equipment, which depends on accurate prediction of residence times. Consideration of volume losses is recommended for materials that undergo significant shrinkage during the drying process.

An analytical solution for the average slab temperature across time was developed by noting similarities between the fundamental heat conduction and mass diffusion processes. Prediction of heating times for the macroalgae via theoretical modelling match the best fit heating time from a separate empirical approach, providing confidence in underlying reason for model deviation. The inclusion of this heating period in the F2L model further improves model fit across the heating period time. The effects of material heating were demonstrated to be more significant as the scale of drying increases. It is recommended that this effect is investigated and included in drying kinetics modelling of biomaterials to provide good fit at all times, especially for large scales of drying.

Finally, testing was performed to characterise drying of both algae species in a pilot scale rotary dryer, with the aim of determining whether the developed models could independently and accurately predict drying at larger scales. The accuracy of predicting drying rates from drying conditions was high for U. ohnoi (R2 = 0.92) but lower for O. intermedium (R2 = 0.75). The best model fit was obtained when the exhaust gas temperature was used as an estimation of the material temperature, with R2 of 0.97 for U. ohnoi and 0.80 for O. intermedium. It is expected that the loss in accuracy for O. intermedium is due to the substantial clumping effects of the material and variability in pilot scale

drying conditions. The high R2 for U. ohnoi indicates that the model presented in this work is and effective tool to predict drying at industry scale. The drying kinetics models developed in this thesis can estimate drying rates from conditions well, and have been shown to be able to represent drying at pilot scales. As such, these models have merit for use in equipment design by providing prediction of equipment residence times under various gas flow rates. This modelling provides a basis for the design of drying equipment and estimation of energy costs that help evaluate the best path to a low carbon economy.

7.2 Recommendations

The following recommendations are made for further research to improve the understanding of drying kinetics of loose particulate materials, and to determine the validity of the modelling approaches used in the design of industrial scale drying equipment.

- Given the importance of non-isothermal conditions to the early MR versus time profiles, further investigation to determine the validity of the non-isothermal (TR) model would be recommended. This is likely best achieved through determining the value of α independent of drying, then experimentally determining temperature in a slab as a function of time and position, then comparing that data to model predictions. This study will be easier to perform with material that does not shrink during drying to reduce experimental design and modelling complications.
- Further work should be undertaken to more comprehensively investigate the theory and mechanisms for gas velocity effects on drying rate outlined in this thesis. Specifically, the theory that in porous biomaterials gas velocity is changing the effective slab width (L) rather than directly affecting diffusivity (D_e) should be investigated. If the TR model proves to be valid as recommended above, it may be better to utilise temperature as the measured variable for this investigation. In this approach the heat diffsivity (α) is a well-defined variable that can be determined independently of the TR model application (i.e. does not need to be parameter estimated). D_e is almost universally determined using the F2L model, so it may have lumped uncertainty or unknown effects from changes in gas velocity. Study of the mechanism would involve matching drying (or heating) rates at different gas velocities to drying at zero gas velocity and different slab widths. The ultimate aim of this would be to determine a relation for the effective slab width as a function of gas velocity. Measurement of temperature as a function of position and time is more easily implemented than for

moisture content and would allow for the evaluation of the specific effects that are actually occurring with respect to slab width. This model for effective slab width is likely to be different for a given material and particle geometry. As with investigation of the TR model, this investigation is likely best undertaken with a material that does not shrink during drying is more homogenous than the macroalgae used in this thesis. Any relationship for effective slab width and gas velocity determined for temperature should also applied to drying to demonstrate if the relationship is the same.

- Consider whether any pre-treatment methods, such as chopping and cutting, would enhance drying rates of macroalgae, or in the case of *O. intermedium* reduce the variance caused by clumping of the material.
- Solar drying is the current most commonly used drying approach for macroalgae industries, and represents a low energy cost drying method. Similar kinetics modelling should be undertaken to characterise solar drying of macroalgae. Complications that would exist for modelling of solar drying are that there are two different driving forces for drying; solar intensity (that in itself varies depending on the time of day and weather conditions and leading to slow heating times compared to convection heating) and variance in surrounding air temperature.
- Further testing to validate the presented models at pilot or industrial scale should be performed. This would best be achieved through the use of the models to actually design a pilot or full scale equipment rather than testing an existing design. The results could be compared to designs from other methods, or the equipment designs could be implemented and drying rates quantified from its operation. This comparison would be the basis of a techno-economic analysis demonstrating the benefits of the improved model formulation provided in this thesis compared to normal methods of design.
- Techno-economic analysis should be undertaken to determine the best drying methods for a given macroalgae product with respect to energy, carbon emissions and capital costs. This is likely to comprise a comparison between energy intensive drying processes (e.g. convection driven) and low-energy but slower and less controllable drying methods (i.e. solar). Throughput and material consistency are expected to be factors in this evaluation.

Chapter 8

8. References

Ajayi, O.O.; Sheehan, M.E. Application of image analysis to determine design loading in flighted rotary dryers. *Powder Technol.* **2012**, *223*, 123-140.

Alp Akın, N.; Ö., Ali Güngör. Equilibrium moisture content and equations for fitting sorption isotherms of capsicum annuum. *GIDA* **2009,** *34*, 205-211.

Al-Muhtaseb, A.; Mcminn, W.; Magee, T. Moisture sorption isotherms characteristics of food products: a review. *Food Biopr. Process*. **2002**, *80*, 118–128.

Bezzina, G; Sheehan, M; Walker, C. The influence of gas velocity and fibre density on the drying kinetics of bagasse. *In: Proceedings of the 40th Annual Conference of the Australian Society of Sugar Cane Technologists* **2018**, 424-435.

Cárcel, J.; García-Pérez, J.; Riera, E.; Mulet, A. Influence of high intensity ultrasound on drying kinetics of persimmon. *Dry. Technol.* **2007**, *25*, 185–193.

Castine, S.; McKinnon, A.; Paul, N.; Trott, L.; de Nys, R. Wastewater treatment for land-based aquaculture: improvements and value-adding alternatives in model systems from Australia. *Aquacult. Environ. Interact.* **2013**, *4*, 285-300.

Çengel, Y. **2007**. Heat and Mass Transfer: A Practical Approach. McGraw-Hill, United States of America.

Chen, X.; Xie, G. Fingerprints of the drying behaviours of particulate or thin layer food materials established using a reaction engineering model. *Transactions of IChemE Part C: Food and Bioproducts Processing* **1997**, *74*, 213-222.

Chkir, I.; Balti, M.; Ayed, L.; Azzouz, S.; Kechaou, N.; Hamdi, M. Effects of air drying properties on drying kinetics and stability of cactus/brewer's grains mixture fermented with lactic acid bacteria. *Food Bioprod. Process.* **2015,** *94,* 10-19.

Cole, A.; Mata, L.; Paul, N.; de Nys, R. Using CO2 to enhance carbon capture and biomass applications of freshwater macroalgae. *GCB Bioenergy* **2013,** *6*. 10.1111/gcbb.12097.

Cole, A.; Dinburg, Y.; Haynes, B.; He, Y.; Herskowitz, M.; Jazrawi, C.; Landau, M.; Liang, X.; Magnusson, M.; Maschmeyer, T.; Masters, A.; Meiri, N.; Neveux, N.; de Nys, R.; Paul, N.; Rabaev, M.; Vidruk-

Nehemya, R.; Yuen A. From macroalgae to liquid fuel via waste-water remediation, hydrothermal upgrading, carbon dioxide hydrogenation and hydrotreating. *Energy Environ. Sci.* **2016**, *9*, 1828-1840.

Crank, J. **1975**. Mathematics of Diffusion, Oxford University Press, London.

Dissa, O.; Compaore, A.; Tiendrebeogo, E.; Koulidiati, J. An effective moisture diffusivity model deduced from experiment and numerical solution of mass transfer equations for a shrinkable drying slab of microalgae spirulina. *Dry. Technol.* **2014**, *32*, 1231–1244.

Djaeni, M.; Sari, D. Low temperature seaweed drying using dehumidified air. *Procedia Environmental Sciences* **2015**, *23*. 10.1016/j.proenv.2015.01.002.

Elshout, P.; van Zelm, R.; Balkovic, J.; Obersteiner, M.; Schmid, E.; Skalsky, R. Greenhouse-gas payback times for crop-based biofuels. *Nat. Clim. Change* **2015**, *5,* 604-610.

Fick, A. On liquid diffusion, *The London, Edinburgh, and Dublin Philosophical Magazine and Journal of Science* **1855**, *10*, 30-39.

Freire, F.; Figueiredo, A.; Ferrão, P. Modelling high temperature, thin layer, drying kinetics of olive bagasse. *J. Agric. Eng. Res.* **2001,** *78*, 397-406.

Fu, N.; Woo, M.; Lin, S.; Zhou, Z.; Chen, X. Reaction Engineering Approach (REA) to model the drying kinetics of droplets with different initial sizes—experiments and analyses, *Chem. Eng. Sci.* **2011**, *66*, 1738-1747.

Ghadiryanfar, M.; Rosentrater, K.; Keyhani, A.; Omid, M. A review of macroalgae production, with potential applications in biofuels and bioenergy. *Renew. Sust. Energ. Rev.* **2016**, *54*, 473-481.

Goh, C.; Aikawa, T.; Ahl, A.; Ito, K.; Kayo, C.; Kikuchi, Y.; Takahashi, Y.; Furubayashi, T.; Nakata, T.; Kanematsu, Y.; Saito, O.; Yamagata, Y. Rethinking sustainable bioenergy development in Japan: decentralised system supported by local forestry biomass. *Sustain. Sci.* **2019**, *15*, 1461-1471.

Gomez, L.; Steele-King, C.; McQueen-Mason, S. Sustainable liquid biofuels from biomass: the writing's on the walls. *New Phytologist* **2008**, *178*, 473-485.

Greenspan, L. Humidity Set Points of Binary Saturated Aqueous Solutions. *Journal of Research of the National Bureau of Standards - A. Physics and Chemistry* **2008,** *81A*, 89-96.

Gupta, S.; Cox, S.; Abu-Ghannam, N. Effect of different drying temperatures on the moisture and phytochemical constituents of edible Irish brown seaweed. *Food Sci. Technol.* **2011**, *44*, 1266–1272.

Lauren, H.; Lisa, B.; Sheehan, Madoc, S.; Walker, C. Experimental analysis and diffusion modelling of solar drying of macroalgae - Oedogonium sp. *Chem. Eng. Trans.* **2018**, *65*, 427-432.

Lee, A.; Sheehan, M.; Schneider, P.; (2014) Multi-scale process models to enable the embedding of CFD derived functions: curtain drag in flighted rotary dryers. *In: Proceedings of the 10th International Conference on Computational Fluid Dynamics in the Oil and Gas, Metallurgical and Process Industries* **2014**, 1-9.

Hassini, L.; Azzouz, S.; Peczalski, R.; Belghith, A. Estimation of potato moisture diffusivity from convective drying kinetics with correction for shrinkage. *J. Food Eng.* **2007**, *79*, 47–56.

Hernández, J.; Pavón, G.; García, M. Analytical solution of mass transfer equation considering shrinkage for modeling food-drying kinetics, *J. Food Eng.* **2000**. *45*, 1-10.

Inyang, U.; Oboh, I.; Etuk, B. Drying and the Different Techniques. *Int. J. Food Nutr. Saf.* **2017**, *8*, 1-25.

Katekawa, M.; Silva, M. (2006). A review of drying models including shrinkage effects. *Dry. Technol.* **2006**, *24*, 5-20.

Kosky, P.; Balmer, R.; Keat, W.; Wise, G. **2013.** Exploring Engineering: An Introduction to Engineering and Design (3rd Edition), Elsevier, London.

Krokida, M.; Maroulis, Z. Process design of rotary dryers for olive cake. *Dry. Technol.* **2002**, *20*, 771-788.

Kurozawa, L.; Hubinger, M.; Park, K. Glass transition phenomenon on shrinkage of papaya during convective drying. *J. of Food Eng.* **2012**, *108*, 43-50.

Langrish, T. Characteristic drying curves for cellulosic fibres. *Chem. Eng. J.* **2008**, *137,* 677-680.

Lawton, R.; Mata, L.; de Nys, R.; Paul, N. Algal bioremediation of waste waters from land-based aquaculture using Ulva: selecting target species and strains. *PLOS One* **2013,** *8*. 10.1371/journal.pone.0077344.

Lawton, R.; Cole, A.; Roberts, D.; Paul N.; de Nys, R. The industrial ecology of freshwater macroalgae for biomass applications. *Algal Res* **2017,** *24*, 486–491.

Lemus, R.; Pérez, M.; Andrés, A.; Roco, T.; Tello, C.M.; Vega, A. Kinetic study of dehydration and desorption isotherms of red alga Gracilaria. *Food Sci. Technol.* **2008**, *41*, 1592–1599.

Machado, L.; Kinley, R.; Magnusson, M.; de Nys, R.; Tomkins, N. The potential of macroalgae for beef production systems in Northern Australia. *J. Appl. Phycol.* **2015,** *27*, 2001–2005.

Machado, L.; Magnusson, M.; Paul, N.; Kinley, R.; de Nys, R.; Tomkins, N. Dose-response effects of Asparagopsis taxiformis and Oedogonium sp. on in vitro fermentation and methane production. *J. Appl. Phycol.* **2016**, *28,* 1443–1452.

Milledge, J.; Benjamin, S.; Dyer, P.; Harvey, P. (2014). Macroalgae-derived biofuel: a review of methods of energy extraction from seaweed biomass. *Energies* **2014**, *7*, 7194-7222.

Mohamed, L.; Kouhila, M.; Lahsasni, S.; Jamali, A.; Idlimam, A.; Rhazi, M.; Aghfir, M.; Mahrouz, M. Equilibrium moisture content and heat of sorption of Gelidium sesquipedale. *J. Stored Prod. Res.* **2005**, *41*,199-209.

Mohamed, L.; Kane, C.; Kouhila, M.; Jamali, A.; Mahrouz, M.; Kechaou, N. (2007). Thin layer modeling of Gellidium sesquipedale solar drying process. *Energy Convers. Manag.* **2007**, *49*, 940-946.

Montgomery, D. **2013**. Design and Analysis of Experiments. John Wiley and Sons, United States of America.

Moreira, R.; Chenlo, F.; Sineiro, J.; Arufe, S.; Sexto, S. Water sorption isotherms and air drying kinetics of fucus vesiculosus brown seaweed. *J. Food Process. Preserv.* **2017**, *41*, e12997.

Mulet, A; Berna, A; Borras, M; Pinaga, F. Effect of air flow rate on carrot drying. *Dry. Technol.* **1987**, *5*, 245-258.

Murphy, C.; Allen D. Energy-water nexus for mass cultivation of algae. *Environ. Sci. Technol.* **2011**, *45*, 5861-5868.

Musielak, G. Modeling of heat and mass transfer during ultrasound-assisted drying of a packed bed consisting of highly shrinkable material. *Chem. Eng. Res. Des.* **2018**, *129*, 25-33.

Naik, S.; Goud, V.; Rout, P.; Dalai, A. Production of first and second generation biofuels: A comprehensive review. *Renew. Sust. Energ. Rev* **2010**, *14*, 578-597.

Neveux, N.; Yuen, A.; Jazrawi, C.; Magnusson, M.; Haynes, B.; Masters, A.; Montoya, A.; Paul, N.; Maschmeyer, T.; de Nys, R. Biocrude yield and productivity from the hydrothermal liquefaction of marine and freshwater green macroalgae. *Biores. Tech* **2013**, *155C*, 334-341.

Paris Agreement to the United Nations Framework Convention on Climate Change, Dec. 12, 2015, T.I.A.S. No. 16-1104.

Perry, J. **1950**. Chemical Engineer's Handbook. McGraw-Hill, United States of America.

Peters, M., Timmerhaus, K. **1991**. Plant Design and Economics for Chemical Engineers. McGraw-Hill, United States of America.

Raja, R.; Hemaiswarya, S.; Kumar, N.; Sridhar S.; Rengasamy, R. A perspective on the biotechnological potential of microalgae. *Crit. Rev. Microbiol.* **2008**, *34*, 77-88.

Ranz, W.; Marshall, W. Evaporation from drops: Part 1. *Chem. Eng. Prog.* **1952**, *48*, 141-146.

Rastikian, K.; Capart, R.; Benchimol, J. (1999). Modelling of sugar drying in a countercurrent cascading rotary dryer from stationary profiles of temperature and moisture. *J. Food Eng.* **1999**, *41,* 193-201.

Rawat, I.; Kumar, R.; Mutanda, T.; Bux, F. Biodiesel from microalgae: A critical evaluation from laboratory to large scale production. *Appl. Energy* **2013**, *103*, 444-467.

Richardson, J., Harker, J., Backhurst, J. **2002**. Coulson and Richardson's Chemical Engineering Volume 2. Butterworth-Heinmann, Oxford.

Roberts, D.; de Nys, R.; Paul, N. The effect of CO2 on algal growth in industrial waste water for bioenergy and bioremediation applications. *PLOS One* **2013**, *8,* e81631.

Roberts, D.; Cole, A.; Whelan, A.; de Nys, R.; Paul, N. Slow pyrolysis enhances the recovery and reuse of phosphorus and reduces metal leaching from biosolids. *Waste Manage.* **2017**, *64*, 133-139.

Rosa, D.; Cantú-Lozano, D.; Luna-Solano, G.; Polachini, T.; Telis-Romero, J. Mathematical modeling of orange seed drying kinetics. *Ciênc. Agrotecnol.* **2015**, *39*, 291–300.

Ryan, D.; Barnett, S.; MacDonald, V. (1997) *Realistic Rations*. Dairy Research and Development Corporation. https://www.dpi.nsw.gov.au/__data/assets/pdf_file/0018/163332/realistic-rations.pdf

Santacatalina, J.; Soriano, J.; Cárcel, J.; Garcia-Perez, J. Influence of air velocity and temperature on ultrasonically assisted low temperature drying of eggplant. *Food Bioprod. Process*. **2016**, *100*, 282-291.

Scala, K.; Crapiste, G. Drying kinetics and quality changes during drying of red pepper. *Food Sci. Technol.* **2008**, *41*, 789–795.

Schneider, C.; Rasband, W.; Eliceiri, K. NIH Image to ImageJ: 25 years of image analysis. *Nat. Methods* **2012**, *9*, 671-675.

Sherwood, T. The drying of solids–I. *Ind. Eng. Chem.* **1932**, *24*, 307–310.

Show, K.; Lee, D.; Chang, J. Algal biomass dehydration. *Biores. Tech.* **2013**, *135*, 720-729.

Sims R., R. Schaeffer, F. Creutzig, X. Cruz-Núñez, M. D'Agosto, D. Dimitriu, M.J. Figueroa Meza, L. Fulton, S. Kobayashi, O. Lah, A. McKinnon, P. Newman, M. Ouyang, J.J. Schauer, D. Sperling, and G. Tiwari, 2014: Transport. In: *Climate Change 2014: Mitigation of Climate Change. Contribution of Working Group III to the Fifth Assessment Report of the Intergovernmental Panel on Climate Change* [Edenhofer, O., R. Pichs-Madruga, Y. Sokona, E. Farahani, S. Kadner, K. Seyboth, A. Adler, I. Baum, S. Brunner, P. Eickemeier, B. Kriemann, J. Savolainen, S. Schlömer, C. von Stechow, T. Zwickel and J.C. Minx (eds.)]. Cambridge University Press, Cambridge, United Kingdom and New York, NY, USA.

Slogrove, H.; Sheehan, M.; Walker, C. Modelling and experimental determination of the drying kinetics of bagasse fibre. *In: Proceedings of the 39th Annual Conference of the Australian Society of Sugar Cane Technologists* **2017**, 406-416.

Sorda, G.; Banse, M. An overview of biofuel policies across the world. *Energy Policy* **2010**, *38*, 6977-6988.

Sudhakar, K.; Mamat, R.; Samykano, M.; Azmi, W.; Ishak, W.; Yusaf, T. An overview of marine macroalgae as bioresource. *Renew. Sust. Energ. Rev.* **2018**, *91*, 165-179.

Suganya, T.; Varman, M.; Masjuki, H.; Renganathan, S. Macroalgae and microalgae as a potential source for commercial applications along with biofuels production: A biorefinery approach, *Renew. Sust. Energ. Rev.* **2016**, *55*, 909-941.

Tello-Ireland, C.; Lemus-Mondaca, R.; Vega-Gálvez, A.; López, J.; Scala, K. Influence of hot-air temperature on drying kinetics, functional properties, colour, phycobiliproteins, antioxidant capacity, texture and agar yield of alga Gracilaria chilensis. *LWT* **2011**, *44*, 2112-2118.

Uribe, E.; Vega-Gálvez, A.; Vásquez, V.; Lemus-Mondaca, R.; Callejas, L.; Pastén, A. Hot-air drying characteristics and energetic requirement of the edible brown seaweed Durvillaea antarctica. *J. Food Process. Preserv.* **2017**, *41*, e13313.

Vargas, P.; Pereira, N.; Guimarães, A.; Waldman, W.; Pereira, V. Shrinkage and deformation during convective drying of calcium alginate. *LWT* **2018**, *97*, 213-222.

Vega-Gálvez, A.; Ayala-Aponte, A.; Notte, E.; Fuente, L.; Lemus-Mondaca, R. Mathematical modeling of mass transfer during convective dehydration of brown algae Macrocystis pyrifera. *Dry. Technol.* **2008**, *26*, 1610–1616.

Vijayaraj, B.; Saravanan, R.;Renganarayanan, S. (2007). Studies on thin layer drying of bagasse. *Int. J. Energy Res*. **2007**, *31*, 422-437.

Vucko, M.; Cole, A.; Moorhead, J.; Pit, J.; de Nys, R. The freshwater macroalga Oedogonium intermedium can meet the nutritional requirements of the herbivorous fish Ancistrus cirrhosus, *Algal Res.* **2017**, *27*, 21-31.

Xanthopoulos, G.; Yanniotis, S.; Lambrinos, G.R. Water diffusivity and drying kinetics of air drying of figs. *Dry. Technol.* **2009**, *27*, 502–512.

Zeraatkar, A.; Ahmadzadeh, H.; Talebi, A.; Moheimani, N.; McHenry, M. Potential use of algae for heavy metal bioremediation, a critical review. *J. Environ. Manage*. **2016,** *181*, 10.1016/j.jenvman.2016.06.059.

Appendix 1

The following is adapted from work by Crank 1975 (Mathematics of Diffusion), and Sherwood 1929 (Drying of Solids 1).

The Fick's law diffusion equation for one-directional diffusion and constant diffusivity D is

$$\frac{\partial C}{\partial t} = D\frac{\partial^2 C}{\partial x^2} \tag{A.1}$$

Assuming that;

- Flux of moisture is some function of time ($-D\frac{\partial C}{\partial x} = F(t)$)
- Moisture flow is proportional to the concentration gradient between material and surroundings ($\frac{\delta C}{\delta x} + \alpha(C_s - C_0) = 0$)
- The surrounding gas is well mixed ($V\frac{\partial C_x}{\partial t} = D\frac{\partial C}{\partial x}$)

Some solution of the Fick's law differential equation exists of the form

$$C = XT \tag{A.2}$$

Where X is C as a function of *x* alone, and T is C as a function of *t* alone. Substituting this solution into Equation A.1 and rearranging gives;

$$\frac{1}{T}\frac{dT}{dt} = \frac{D}{X}\frac{d^2X}{dx^2}$$

The left side of this equation depends on *t* only, while the right side depends on *x* only. Both sides of the equation must then have a solution where they are equal to the same constant. For ease in the subsequent algebra, this is taken as $-\mu^2 D$. Therefore,

$$\frac{1}{T}\frac{dT}{dt} = -\mu^2 D \tag{A.3}$$

$$\frac{1}{X}\frac{d^2X}{dx^2} = -\mu^2 \tag{A.4}$$

These can be solved by integration;

$$T = e^{-\mu^2 Dt} \tag{A.5}$$

$$X = A \sin \mu x + B \cos \mu x \tag{A.6}$$

Equations A.5 and A.6 can then be substituted in to Equation A.2;

$$C = (A \sin \mu x + B \cos \mu x).\, e^{-\mu^2 Dt} \tag{A.7}$$

Where *A* and *B* are integration constants. Equation A.7 is valid for any value of *A* and *B*.

Equation A.1 is a linear equation. As such, any number of unique solutions of the type of Equation A.7 added together is also a solution of Equation A.1. The most general solution for C is therefore an infinite series of these solutions;

$$C = \sum_{m=1}^{\infty} (A_m \sin \mu_m x + B_m \cos \mu_m x).\, e^{-{\mu_m}^2 Dt} \tag{A.8}$$

A_m, B_m and μ_m can then be chosen to validate the boundary conditions for the given geometry.

For diffusion out of an infinite slab of material of width *L*, the relevant boundary conditions are;

$$C = C_0 \text{ at } 0 < x < L, t = 0 \text{ (even initial distribution of moisture)}$$

$$C = 0 \text{ at } x = 0, x = L, t > 0 \text{ (concentration at gas} - \text{material interface is zero)}$$

The second boundary condition describes a core assumption of the model; it assumes that diffusive moisture transfer is the limiting step in the drying process. Convective mass transfer from the material surface to the surrounding gas is assumed to occur at a sufficiently high rate such that any surface moisture is immediately removed from the system.

At C=0 and x=0, the equation is;

$$0 = \sum_{m=1}^{\infty} (A_m \sin 0 + B_m \cos 0).\, e^{-{\mu_m}^2 Dt}$$

B_m must equal zero to satisfy the boundary.

At C=0 and x=L, the equation is;

$$0 = \sum_{m=1}^{\infty} (A_m \sin \mu_m L + 0).e^{-{\mu_m}^2 Dt}$$

μ_m can be taken as $\frac{m\pi}{L}$ to satisfy this boundary condition; sin mπ will then equal 0 for any value of m. Putting these into Equation A.8, and then placing the resultant equation for C in the initial distribution assumption gives;

$$C_0 = \sum_{m=1}^{\infty} A_m \sin \frac{m\pi x}{L} \text{ at } 0 < x < L, t = 0 \tag{A.9}$$

This can be solved for A_m by multiplying both sides by $\sin \frac{p\pi x}{l}$, and integrating across x using the following relationship;

$$\int_0^L \sin \frac{p\pi x}{L} . \sin \frac{m\pi x}{L} dx = 0 \text{ if } m \neq p$$

$$\int_0^L \sin \frac{p\pi x}{L} . \sin \frac{m\pi x}{L} dx = \frac{1}{2} l \text{ if } m = p$$

Series terms where m is even are equal to zero. A_m can then be written as

$$A_m = \frac{4C_0}{m\pi}, \text{where } m = 1,3,5,7, \ldots.$$

Putting A_m, B_m and μ_m into Equation A.8 gives the following relationship;

$$C = \frac{4C_0}{\pi} \sum_{n=0}^{\infty} \frac{1}{(2n+1)} . \sin\left(\frac{(2n+1)\pi x}{2L}\right) . exp\left(-\frac{(2n+1)^2 \pi^2 Dt}{4L^2}\right)$$

or

$$\Delta = \frac{C}{C_0} = \frac{4}{\pi} \sum_{n=0}^{\infty} \frac{1}{(2n+1)} . \sin\left(\frac{(2n+1)\pi x}{2L}\right) . exp\left(-\frac{(2n+1)^2 \pi^2 Dt}{4L^2}\right) \tag{A.10}$$

Where Δ represents the ratio of free moisture concentration at time *t* and the point *x* to the initial concentration.

For representation of drying, it is more useful to represent the averaged moisture across the material slab at a given time rather than at a given point *x*. This can be calculated by integrating Δ across the slab width *L*, using the notation MR to represent the averaged moisture ratio throughout the material slab.

$$MR = \frac{1}{L}\int_0^L \Delta \, dx$$

$$MR = \frac{4}{\pi L}\int_0^L \left[\sin\left(\frac{\pi x}{2L}\right).exp\left(-\frac{\pi^2 Dt}{4L^2}\right) + \frac{1}{3}\sin\left(\frac{3\pi x}{2L}\right).exp\left(-\frac{9\pi^2 Dt}{4L^2}\right) + \cdots\right] dx$$

$$MR = \frac{4}{\pi L}\left[\frac{2L}{\pi}\left(-cos\left(\frac{\pi x}{2L}\right).exp\left(-\frac{\pi^2 Dt}{4L^2}\right) - \frac{1}{9}cos\left(\frac{3\pi x}{2L}\right).exp\left(-\frac{9\pi^2 Dt}{4L^2}\right) - \cdots\right)\right]_{x=0}^{x=L}$$

At x=L, the terms $cos\frac{\pi L}{2L}$, $cos\frac{3\pi L}{2L}$, … are all equal to zero.

At x=0, the terms $cos\left(\frac{0\pi}{2L}\right)$, $cos\left(\frac{3*0\pi}{2L}\right)$, … are all equal to cos 0 = 1.

Therefore;

$$MR = \frac{4}{\pi L}\left[-\frac{2L}{\pi}\left(-exp\left(-\frac{\pi^2 Dt}{4L^2}\right) - \frac{1}{9}exp\left(-\frac{9\pi^2 Dt}{4L^2}\right) - \cdots\right)\right]$$

Removing common series factors and simplifying;

$$MR = \frac{8}{\pi^2}\left(exp\left(-\frac{\pi^2 Dt}{4L^2}\right) + \frac{1}{9}exp\left(-\frac{9\pi^2 Dt}{4L^2}\right) + \cdots\right)$$

Or as infinite series notation;

$$MR = \frac{M}{M_0} = \frac{8}{\pi^2}\sum_{n=0}^{\infty}\frac{1}{(2n+1)^2}\exp\left(-\frac{(2n+1)^2\pi^2 Dt}{4L^2}\right) \qquad \text{(A.11)}$$

The diffusion constant D is usually instead written as D_e, or the effective diffusivity. This is used to incorporate both external (drying temperature, air velocity, pack density) and internal (pore size,

average pathway lengths, material layer resistances to diffusion) variables that effect the drying of the material as a single variable.

Similar methodology can be used to determine equations for MR for an infinite cylinder of radius r;

$$MR = 4 * \sum_{n=1}^{\infty} \frac{1}{(\varepsilon_n)^2} \exp\left(\frac{(-D_e(\varepsilon_n)^2 t)}{r^2}\right) \quad \text{(A.12)}$$

Where ε_n is the nth root of the zeroth order Bessel function. All drying is assumed to be directly outward from the centre line of the cylinder.

Finally, for a sphere of radius r;

$$MR = \frac{6}{\pi^2} * \sum_{n=1}^{\infty} \frac{1}{n^2} \exp\left(\frac{(-D_e n^2 \pi^2 t)}{r^2}\right) \quad \text{(A.13)}$$

All drying is assumed to be directly outward from the centre point of the sphere.

Appendix 2

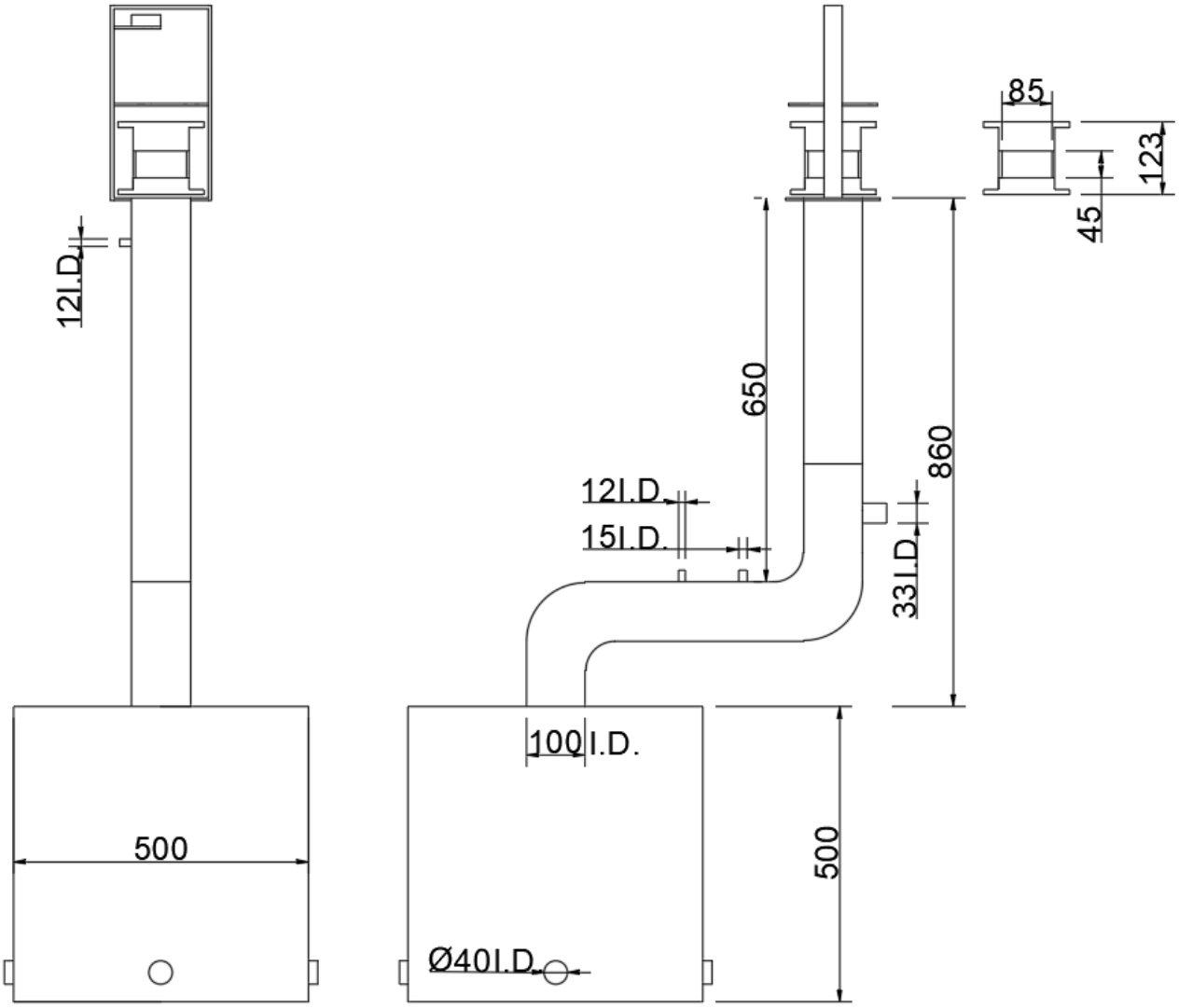

Figure A.1; To scale and dimensioned diagram of convective drying equipment setup.

Appendix 3

Table A.1; Density variance as calculated from the initial mass measurements.

Condition	Measured mass	Calculated density (kg/m^3)	Variance (kg/m^3; average ± standard deviation)
33 kg/m^3	9.99 9.99 9.99 9.99 10.00 10.01 10.02 10.01 10.01 10.01 9.99 10.01 9.99	33.40 33.40 33.40 33.40 33.42 33.46 33.50 33.46 33.46 33.46 33.40 33.46 33.40	33.43±0.037
50 kg/m^3	14.99 15.00 14.97 14.98 14.99 15.00 15.02 14.99	50.11 50.14 50.04 50.08 50.11 50.14 50.21 50.11	50.12±0.050
66 kg/m^3	20.03 19.98 20.03 19.97 19.99 20.00 19.99 20.00 19.99 19.96 20.01 19.99 20.00 20.00 20.00 19.99 19.96 19.99 19.96 19.99 19.99	66.96 66.79 66.96 66.76 66.82 66.86 66.82 66.86 66.82 66.72 66.89 66.82 66.86 66.86 66.86 66.82 66.72 66.82 66.72 66.82 66.82	66.84±0.057

	20.02 20.00 19.99 20.00 19.98 19.99 19.99 19.99 20.01 20.00 19.99 20.00 20.00 20.00 20.00 20.00 20.01 20.04 20.00	66.92 66.86 66.82 66.86 66.79 66.82 66.82 66.82 66.89 66.86 66.82 66.86 66.86 66.86 66.86 66.86 66.89 66.99 66.86	
100 kg/m^3	29.96 29.99 30.00 29.98 30.01 29.99 29.79 30.00 29.98	100.15 100.25 100.29 100.22 100.32 100.25 99.58 100.29 100.22	100.18±0.23